Detailed model for robust feedback design of main steam temperatures in coal fired boilers

Prepared by:

Cheriska Polton

PLTCHE003

Department of Electrical Engineering

University of Cape Town

Academic Supervisor: Prof. Edward Boje

Industrial Mentor: Mr. R. Govindsamy

February 2020

Submitted to the Department of Electrical Engineering at the University of Cape Town in partial fulfilment of the academic requirements for a Master's of Science degree in Electrical Engineering

Key Words: Thermo-fluid model, Quantitative Feedback Control, Valve Position Control, Robust Control

Abstract

Main steam temperatures play a significant role in large coal fired power plant operation. Ideally, main steam temperatures should be accurately controlled to protect the thick wall components against long term overheating and thermal stress while meeting the design conditions at the steam turbine inlet. Although high steam temperatures are beneficial for thermal efficiency, it accelerates creep damage in high temperature components which is detrimental to the life of components. Alternatively, low steam temperatures increase the moisture content at the last stage blades of the turbine, causing the blades to deteriorate and fail.

Control of the outlet steam temperature according to design conditions at variable loads is maintained via a balance between heat input (flue gas temperature and mass flow rate), evaporator outlet steam mass flow and spray water. The present control philosophy accuracy of main steam temperatures at an Eskom coal fired power plant was evaluated and compared to the latest technology and control strategies. Improving and optimizing steam temperature controls ensures design efficiency while maintaining long term plant health.

The level of spatial discretization applied in simplifying the real boiler for modelling purposes was approached at a relatively high level. The intention was to model normal operating conditions and certain transients such as variable heat input and load changes to see its effect on steam temperatures and to be able to evaluate the performance of different temperature control techniques.

The main outcome of this project was to design a robust control system for a dynamic model of the boiler using sets of low order linear models to account for uncertainty. The main concepts, models and theories used in the development of this dissertation include:

1) A detailed thermo-fluid model developed using Flownex to have high fidelity models of the process under varying operating conditions. This model was used to test and evaluate the robust controller design.
2) System Identification in Matlab to construct mathematical models of dynamic systems from measured input-output data and identify linear continuous time transfer functions under all operating conditions [1].
3) Quantitative Feedback Theory (QFT) to design controllers for an attemperator control system at various on-load operating conditions. This design was used understand the engineering requirements and seeks to design fixed gain controllers that will give desired performance under all operating conditions.
4) The design of a valve position controller to increase the heat uptake in a convective pass, thereby improving efficiency: Excessive attemperation in the superheater passes is generally associated with high flue gas temperatures which decrease thermal efficiency. Therefore, robust control of the attemperation system leads to an increase in heat uptake between the flue gas and steam in the boiler, resulting in a reduction in the flue gas temperature leaving the boiler, thus improving efficiency. The robust QFT controllers were set up using the valve position control technique and were used to confirm the improvement of control performance.

The theories mentioned above were used to understand the control performance under varying plant conditions using a standard cascaded arrangement. It incorporated robust control design and engineering requirements such as bandwidth, plant life, spray water and thermodynamic efficiency. The control effort allocated to each superheater-attemperator subsystem in the convective pass was designed as a multi-loop problem.

Declaration

I, *Cheriska Polton*, hereby declare the work contained in this dissertation to be my own. All information which has been gained from various journal articles, text books or other sources has been referenced accordingly. I have not allowed, and will not allow, anyone to copy my work with the intention of passing it off as their own work or part thereof.

Signed by candidate

09 February 2019

Name: Cheriska Polton

Date

Acknowledgements

Firstly, I would most importantly like to thank my academic supervisor, Prof. Edward Boje, for his invaluable guidance, patience and direction throughout my project. His abundance in knowledge and remarkable experience assisted in making this project successful.

I would like to thank my industrial mentor, Mr. Ravendra Govindsamy, for his contribution and guidance to this project.

I am grateful for the continuous support and encouragement from my family and friends throughout my studies.

Thank you to EPPEI and my Eskom line manager, Mrs V. M. Masuku, for allowing me the opportunity to complete my Master's degree full time and funding my studies, for which I am truly grateful for. I am also thankful for my colleagues at Eskom who assisted with plant data and expert advice on the current systems processes.

Lastly, thank you to my fellow colleagues in the ATPROM department at UCT for their expert mechanical advice and involvement in my thesis, as well as the adventurous outdoor experiences we embarked on.

Table of Contents

List of Figures

List of Tables

List of Nomenclature

General symbols

A	Area	m^2
b	Depth	m
B_K	Bounds	-
c_p	Specific Heat	kJ/kg
d	Diameter	m
D_h	Hydraulic Diameter	m
e	Error	-
f	Friction factor	-
F	Correction factor	-
h	Heat transfer coefficient	W/m^2K
H	Height	M
k	Thermal Conductivity	W/mK
K_P	Controller gain	-
L	Length	m
LMTD	Log Mean Temperature Difference	°C
$\dot{m}$	Mass flow rate	kg/s
N	Number of tubes	-
Nu	Nusselt number	-
p	Perimeter	m
P	Pressure	kPa
P(s), G(s), H(s), Y(s), R(s), D(s), P(jω), L(jω), G(jω), H(jω)	Controller Transfer function	-
q	Heat flux	W/m^2
Q	Heat transfer	W
r	Radius	m
Re	Reynolds number	-

s	Mean beam length	m
SA	Surface Area	m^2
T	Temperature	°C or K
t	Thickness	m
U	Overall heat transfer coefficient	W/m^2K
v	Velocity	m/s
w	Width	m
Y	Mass concentration ratio	-

Greek symbols

ε	Emissivity	-
μ	Viscosity	kg/ms
ρ	Density	kg/m^3
σ_o	Stefan-Boltzmann constant	W/m^2K^4
ω	Frequency	rads/s
π	Pi	3.141
ψ	Effectiveness coefficient	-
α	Absorption	-
τ	Time	s
τ_i	Controller reset or integral time	s

Subscripts

100, 97, 70	Transfer function at specific MCR
ash	Ash
Att	Attemperator
bund	Tube bundle
cavity	Space between two Superheater sections
cond	Conduction
conv	Convection
counter	Counter flow
cs	Cross-section
down	Downstream
duct	Duct
ext	External
fg	Flue Gas

flow	Fluid Flow
fluid	Fluid (steam or flue gas)
i	Inner
in	In
int	Internal
L	Longitudinal
max	Maximum
o	Outer
out	Outlet
par	Parallel flow
pass	Superheater pass
platen	Platen superheater
rad	Radiation
s	Steam
Sensor	Sensor or Instrument
SH	Superheater
spray	Spraywater
T	Transverse
t or tube	Tube
up	Upstream
w	Wall

Acronyms and Abbreviations

AH	Air Heater
CFD	Computational Fluid Dynamics
EPPEI	Eskom Power Plant Engineering Institute
FD	Forced Draught
FEGT	Furnace Exit Gas Temperature
FGS	Fuzzy Gain Scheduler
GPC	Generalised Predictive Controller
HP	High Pressure
ID	Induced Draught
ID	Identification
LP	Low Pressure
MBPC	Model-based Predictive Controller
MCR	Maximum Continuous Rating

MIMO	Multiple-Input Multiple-Output
MPC	Multivariable Predictive Controller
MW	Megawatt
OEM	Original Equipment Manufacturer
P	Proportional
PA	Primary Air
PF	Pulverised Fuel
PI	Proportional Integral
PID	Proportional Integral Derivative
PMBC	Process Model-based Control
QFT	Quantitative Feedback Theory
RLS	Recursive Least Squares
SA	Secondary Air
SH	Superheater
SISO	Single-Input Single-Output
SVC	State Variable Control
VPC	Valve Position Control

1. Introduction

Thermal power plants are the largest producers of electricity in South Africa. The overall thermal efficiency of a power plant is defined as the ratio of heat energy (which is converted into electrical energy or saleable energy) to the heating value of coal combusted. It is mainly dependent on the pressure and temperature of the steam entering the turbine, and the pressure in the condenser. According to the Carnot cycle, efficiency can be improved by increasing the main steam temperature entering the turbine as an increase in heat energy results in an increase in the work done by the turbine, leading to an increase in energy output. Steam temperatures in the boiler are affected by changes in feed water temperature and flow rate, excess air, fuel variations and heating surface cleanliness etc.

1.1 Project purpose

One of the most critical variables in coal-fired power plants is the main steam temperature as errors in this can cause extensive damage to the turbine blades and boiler tubes. The increase of disturbances, such as an increase of renewable energy onto the national grid, will increase the risk of thermal cycling as traditional power plants will be required to either cycle their load or operate under low load conditions in order to meet varying load demands [44] [45]. Load cycling leads to a considerable reduction in efficiency and has adverse effects on plant health. Therefore, to minimise the impact that these undesirable conditions have on power generating plants, advanced control strategies are significant in maintaining key controlled variables, such as main steam outlet temperatures, at their desired range.

Although high steam temperature is beneficial for thermal efficiency, it accelerates creep damage and thermal fatigue in high temperature components, which is detrimental to the life of these components. Alternatively, low steam temperatures increase the moisture content (should be <10% [2]) of the last stages of the turbine, which causes the turbine blades to erode and fail and reduces the efficiency of the energy conversion. It is therefore crucial to design a robust control system to meet design steam conditions at the turbine inlet in order to protect thick wall components against long-term overheating and thermal stress and improve efficiency while maintaining long term plant health.

There are many factors that change from the original design over the lifespan of boiler, such as coal quality and modifications to the boiler. It is therefore important to continuously review, adapt and accommodate such conditions by optimising the plant parameters. The biggest influences on steam temperature fluctuations are ash deposition on heat exchanger surfaces, and load and fuel variations. Accurately regulating the steam temperature is key to preventing failures due to high metal temperatures in the superheaters, reheaters and turbine, as well as to reduce the moisture in the last stages of the turbine which leads to erosion [3].

Hypothesis:

1. Highest available bandwidth control of each stage may not be the “best” in terms of plant life and thermodynamic efficiency.
2. As more and more renewable energy is connected onto the grid, conventional base-load thermal plants will be expected to do more load following. Dynamic loading will result in concerns about plant life through thermal stressing of thick wall vessels, control problems with the boiler and risks of not meeting turbine inlet conditions during transient operations. For these new challenges, control systems must be designed to balance fast response with robustness and properly managed inputs in order to enhance plant life.

1.2 Project Aim and Objectives

The steam temperature entering the turbine should be controlled within acceptable design limits to ensure the highest level of efficiency and to mechanically protect the turbine and boiler. The steam conditions are controlled using attemperators, also known as de-superheaters, which are located between superheater stages in the convection pass of the boiler. The aim of this project is to investigate attemperation control at various stages of the convective pass of the boiler at variable and low load conditions and to design a robust control system.

The objective is to analyse the dynamic behaviour affecting the convection pass of a boiler with the addition of a robust main steam attemperation control system. The purpose of the control system, as explained using Figure 1, is to maintain the design temperature setpoint at the superheater outlet $Y(s)$ using advanced control strategies, irrespective of any disturbance input $D(s)$ occurring within the boiler such as load changes, changes in flue gas and steam temperature profiles, and model uncertainty. To achieve this, an input demand signal $R(s)$, defined as the setpoint, is compared to a feedback loop which takes into consideration the system output, and produces an error when the output deviates from the demand signal. The error signal is then fed into the controller $G(s)$ which manipulates the signal $U(s)$ according to the requirements of the boiler plant $P(s)$ in order to meet the desired outlet steam conditions.

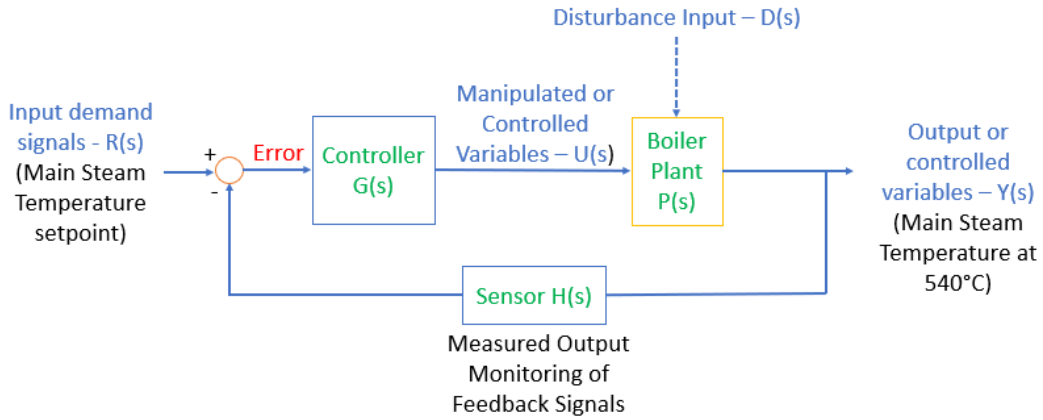

Figure 1: Closed loop control system

The design of a robust attemperation control system was proposed around various stages of the convection pass of the boiler using Quantitative Feedback Theory and Valve Position Control under variable load conditions. The aim is to optimise the control system to improve thermal efficiency by increasing the heat uptake in the convective pass while minimising the risk of tripping the boiler according to the maximum superheater steam temperature boiler protection, minimising maintenance costs and adhering to metal temperature margins. In order to achieve this, the dynamic behaviour of the convective pass was modelled in Flownex at various load and operating conditions. These variants were used to evaluate the effect on steam and flue gas temperatures in the boiler, as well as the performance and validation of various controller design techniques.

1.3 Literature Review

Heat is transferred from the flue gas, which is a by-product of combustion in the boiler furnace, to the fluid in the tube banks, to either convert water into steam in the evaporator, or further increase the steam temperature in the

superheater stages in the convection pass. The heat transfer in the convective pass depends on the layout and geometries of the tube bundles and can be categorised into three types: convection, conduction or radiation. Any change in the boiler load results in a change in the temperature and flow profiles of the steam and flue gas, which directly influences the main steam conditions. Attemperation control assists in regulating the steam temperatures by adjusting to any fluctuations due to disturbances, particularly boiler load, in order to prevent reaching design metal temperature limits. The turbine original equipment manufacturer (OEM) establishes the rate at which the turbine can be brought to full load, and this is usually done in accordance to a steam temperature-time curve. It is therefore key that the steam temperature at the turbine inlet remains constant and is maintained at a specific designed turbine inlet setpoint, irrespective of the load demand, hence the need for main steam outlet temperature regulation. Spray attemperation provides quick acting control for regulating steam temperatures.

For the purpose of process control, the ideal location for superheater attemperation is at the final superheater outlet. Although temperature control at this location would be immediate with no time lag, it could also lead to possible water carryover into the turbine, overheating of previous superheater stages and resulting in loss of efficiency. Therefore, placing attemperation valves between superheater stages addresses this. This allows the attemperation spray to mix with the steam from the previous stages, before it enters the next stage in a uniform temperature profile. Since each superheater stage in the convective pass is designed with different geometries and layouts, the amount of heat transfer to each stage varies, hence the need for multi-stage attemperation systems to be installed between two superheater bank stages to regulate the temperature difference per stage, hence providing improved control dynamics of the system. Besides changes in boiler load due to disturbances, fouling is another characteristic that affects the heat transfer from the flue gas to the steam, as it adds an additional layer between the flue gas and tube wall. Fouling deposits on the superheater tube bundles are dependent on the heating surface cleanliness, location and age of the tubes in the boiler. To account for the uncertainty of these conditions, it is not uncommon to have continuous attemperation to allow for flexibility in controlling the steam temperature.

Oluwande and Boucher [4] researched the implementation of a multivariable model-based predictive controller (MBPC) for superheater steam temperature control. This paper shows that a multivariable controller can achieve tighter control of the superheater temperature through firing and attemperation co-ordination by linking the master pressure and main steam temperature controllers.

Peet [5] patented the utilization of a reliable feed-forward controller to control the superheater outlet temperature of a steam generator. This controller was developed to improve control stability by providing a feed-forward of the spray demand to an attemperator control valve. The feed-forward controller bases its control on boiler load and its corresponding superheater inlet steam temperature. However, this system is limited during dynamic operations when steam temperature varies with load fluctuations.

Molbak [6] evaluates the use of various advanced feedback control strategies which is applied within the Danish power plant industry. These advanced control strategies include:

1. A comparison between conventional control and predictive control.
   A conventional fixed PID cascade controller was compared to an adaptive control strategy which is based on Generalized Predictive Control (GPC) and Recursive Least Squares (RLS) identification methods.
2. A comparison between two model-based strategies such as GPC and a PT_x-based model.
   This comparison shows that the application of these two strategies performs almost identically, with marginal differences due to closed loop bandwidths which result from differences in controller tuning methods.

3. A comparison between Fuzzy control and model-based control.
   A fuzzy PI controller was implemented to handle higher order dynamics and was compared to a PT_x-model. The model-based controller proved to perform better as it uses explicit and accurate process knowledge to deal with faster and larger control actions, whereas the fuzzy controller uses a less accurate and implicit process model.

Molbak also investigated using feed-forward control to measure disturbances before they impact the outlet steam temperature, resulting in further improvements on steam temperature controls.

Prasad, et. al [7] investigated a multivariable control using neural network model-based strategy. Their paper derives a neural network model-based non-linear long-range predictive control algorithm to provide offset-free closed-loop behaviour to deal with modelling errors and disturbances for more efficient control. This control strategy was simulated on a power plant boiler, with the proposed controller resulting in excellent performance over the operating range without online adaption such as self-tuning control. This controller can be applied to various other plants and processes in thermal power plants.

Riggs, et. al [8] used a non-linear dynamic model of a coal-fired drum boiler to compare the application of a nonlinear process model-based control (PMBC) algorithm, which is based on a non-linear approximation model, and a state variable control (SVC) algorithm to a conventional PI controller. Each controller was tuned to produce a "minimum integral absolute error" [8], which was then simulated and tested against a conventional PI controller at 10 different disturbance scenarios. Following these tests and tuning of the controllers, the paper claims that the SVC controller showed little improvements when compared to the PI controller, and the PMBC controller reduced the variability of the steam temperature by a factor of 3 - 5%. The PMBC controller adapts to process gain changes, whereas the PI and SVC controllers use a fixed gain approach. The PI controller was then detuned, and when compared to the tuned PI controller and the two other controllers, the results show a greater variability over longer time. This paper also showed that the non-linear PMBC controller was less sensitive to tuning when compared to the PI controller.

Menkina [9] presented the simulation and methodology for using robust control theory, both decentralised and centralised, for superheater steam temperature control in a once-through boiler. This was based on the theoretical synthesis of a robust H_∞ controller and compared to a standard PID cascade control structure. A conventional cascade P controller structure was applied in the secondary loop and a robust controller was applied in the primary loop for a decentralised temperature control, with a single robust feedback controller used in the feedback loop. The purpose of this paper was to improve temperature regulation through control algorithms while minimising temperature fluctuations. This paper claims that both the standard PID cascade controller and decentralised H_∞ controller demonstrated to be efficient for superheater steam temperature regulation.

Sanchez, et al. [10] presented the design and simulation of a multivariable predictive controller (MPC) and compared the results to a conventional PID controller for superheater steam control. The benefit of using a MPC is that it employs only one controller and has proven to be an alternative to a PID controller as it improves the regulation of superheater steam temperature.

Reddy and Sai [11] evaluated a conventional PID controller with fixed parameters against a fuzzy gain scheduler (FGS) which is an adaptation of a PID controller. FGS is a new rules-based scheme that combines fuzzy logic with gain scheduling of conventional PID controllers, therefore providing a suitable alternative for control. The fuzzy rules

determine the PID controller parameters, which generates a control signal for superheater temperature control. A Mamdani fuzzy inference engine is used in the defuzzification process. This paper shows that PID controllers provide better disturbance rejection. However, FGS allows for a smaller overshoot and faster settling time at the cost of more input effort due to the adaptive variation of the P and D values.

2. System Analysis

2.1 Boiler Overview

Eskom is currently South Africa's largest power generating producer with a total generating capacity of 44 172 MW [14] onto the national grid, supplying about 96% of the country's electricity and approximately 45% of electricity to Africa [13]. Eskom uses various technologies to produce electricity, with coal-fired power stations being the largest contributor of the energy mix. There are currently 15 coal-fired power stations in operation, which supply the majority of the energy onto the national grid.

Steam is generated in a coal fired power plant by converting chemical energy into thermal energy through combustion of fuel in the boiler (mainly pulverised coal under normal operations and fuel oil during start up). Water is heated and converted into steam before entering a steam turbine (thermal energy $\Rightarrow$ mechanical energy) which drives an electrical generator (mechanical energy $\Rightarrow$ electrical energy). The exhaust steam from the low-pressure turbine is then condensed in the condenser, preheated in the LP and HP heaters, before returning to the boiler. This process is known as the Rankine cycle.

The boiler can be categorised into the following main heat exchanger components:

- furnace (water wall and evaporator tubes),
- convection pass heat exchanger tube bundles (superheater, reheater, headers), economiser
- attemperation valves and control system

As shown in Figure 2, the main subsystems supporting these components which feed to the boiler are the mills, burners, air fans, separating vessel, recirculation pumps and soot blowing system. Coal is transported to the mill via conveyor belts were the mill grinds the coal into fine particles called pulverised fuel (PF). With the help of the Primary Air (PA) fan, the PF is heated and transported to the burner for combustion. Secondary air (SA), which is preheated in the Air Heater (AH), is supplied to the burners from the Forced Draught (FD) fan to aid in complete combustion of the PF. Once the stoichiometric conditions are met for complete combustion, the PF and air mixture is combusted, creating a flame in the furnace. The coarse ash formed through combustion falls into the boiler hopper, while the remaining by-products of combustion known as fly ash, rises in the boiler by the flue gas and is collected in the electrostatic precipitator and/or bag filters, aided by the suction pressure created by the Induced Draught (ID) fan.

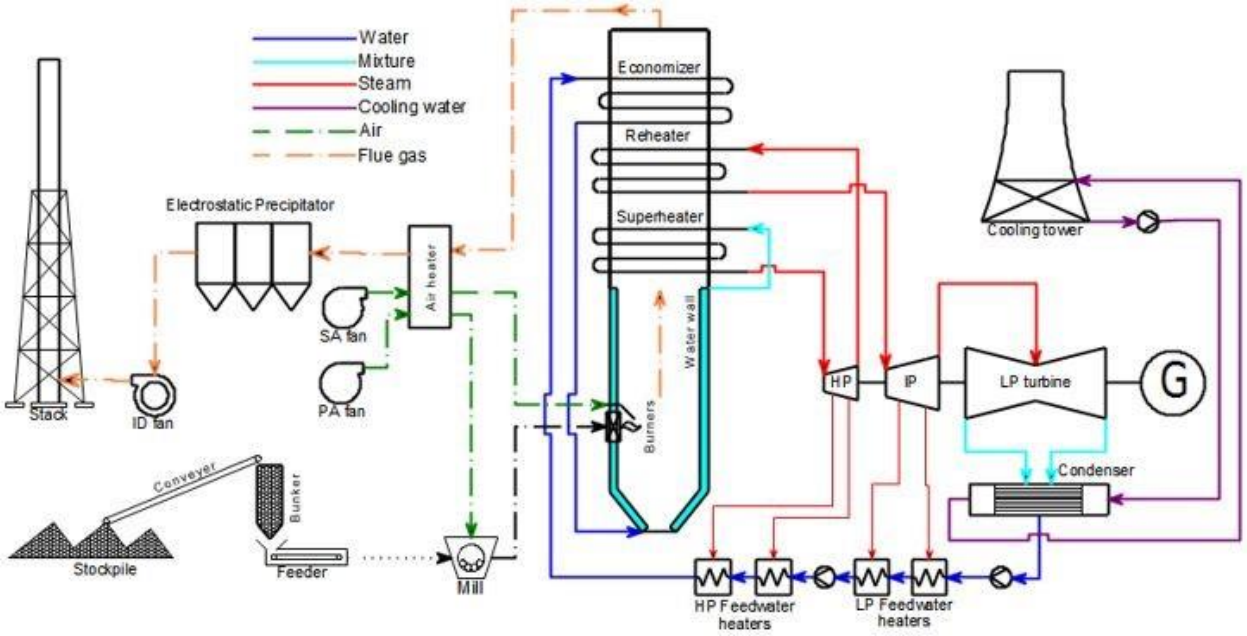

Figure 2: Power plant operation overview [12]

The furnace is a large volume designed for PF combustion and is enclosed by water walls or evaporator tubes that absorb heat energy directly from the flame primarily through radiation. It is important that the furnace is adequately sized to ensure enough heat is transferred from the flue gas in the furnace to the water walls to effectively cool the furnace exit gas temperature (FEGT) to below its ash deformation temperature. This is to prevent excessive heat from entering the platen heat exchanger which is situated closest to the furnace exit, as excessive heat will result in slagging and extremely high metal temperatures. The convection pass consists of the superheaters, reheaters, headers and economiser. As the flue gas rises from the furnace into the convective pass, it superheats the steam in the superheaters, reheats the steam in the reheaters, and preheats the evaporator feed water in the economiser. These components are arranged to efficiently transfer heat energy from the flue gas and generate steam at the required mass flow rate, pressure and temperature in the convective pass [3]. Each heat exchanger tube bundle terminates in a header which mixes and distributes the steam.

Figure 3 illustrates a cross-section of a once-through boiler schematic showing the evaporator and the convective pass which consists of an economiser, superheater and reheater arrangements, as well as:

- Burners which are located at the bottom of the furnace.
- A back pass of the boiler which is represented by duct between the economiser and the air heater where the flue gas exits the boiler.
- The black dotted line between the evaporator and SH1 represents the level at which the flue gas exit temperature is calculated, before entering the convection pass.

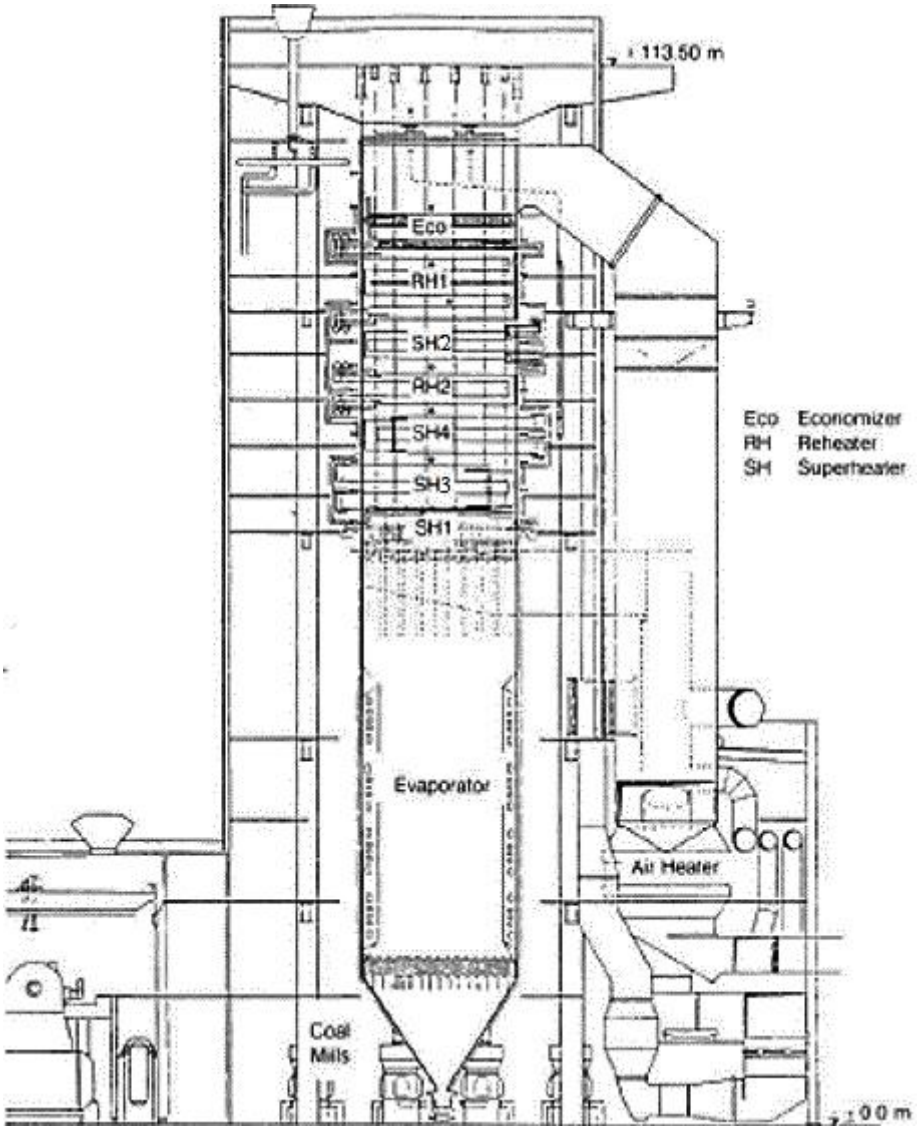

Figure 3: Cross section of a once-through boiler configuration [23]

2.1.1 Boiler Operation

The difference between a once-through boiler and a drum boiler is explained using the Rankine cycle below. The T-s diagram in Figure 4 represents the Rankine cycle which illustrates the parts of the boiler that generate steam, starting from the economiser inlet to the superheater/reheater outlet. The T-s diagram explains the various phases of water and steam at each stage in the boiler with temperature being a function of the specific entropy.

In a subcritical boiler, the pressurised water from the feed pump enters the boiler at the first heat exchanger, the economiser (***A***), where it is preheated. From the T-s diagram below, it can be noted that even though the water increases in heat and temperature when it flows from point (A) to the beginning of the evaporator (***B***), it is still below its boiling point. The preheated water then flows through the evaporator walls, where it absorbs heat energy from the combustion of fuel in the furnace, before entering the drum (in a drum boiler) or separating vessel (in a once-through boiler) (***C***). During this process, the heat energy thermodynamically changes the phase of the fluid from water into a water-steam mixture without increasing the temperature of the water (***horizontal line B-C***). One of the functions of the drum/separating vessel is to separate the water and steam mixture, allowing the steam to enter the convection

pass. The water is recirculated back to the economiser from the separating vessel in a once-through boiler, and from the drum to the evaporator water walls in a drum boiler. The main difference between a drum boiler and a once-through boiler is that the drum is supplied with feed water from the economiser and is required to maintain a constant water level as it continuously supplies the water walls with saturated water, whereas under normal operation in a once-through boiler, all the water is converted into steam in the evaporator, resulting in there being no level in the separating vessel. The steam leaves the drum/separating vessel and enters the second set of heat exchangers, the superheater section (***D***). In this process, the steam is superheated at a constant pressure. The steam then leaves the final superheater at the desired pressure and temperature and enters the high-pressure turbine, converting some of the thermal energy into mechanical energy. Efficiency is generally limited and governed by the laws of thermodynamics [3]. The exhaust steam from the high-pressure turbine (***D - E***) re-enters the boiler at the reheater section (***E***) for further heating at a constant lower pressure, which increases the efficiency of the Rankine cycle and reduces the likelihood of water droplets forming in the low-pressure turbines (***F - G***). The designed station thermal efficiency of the modelled conventional thermal power plant at rated MCR is typically 37.6% [14].

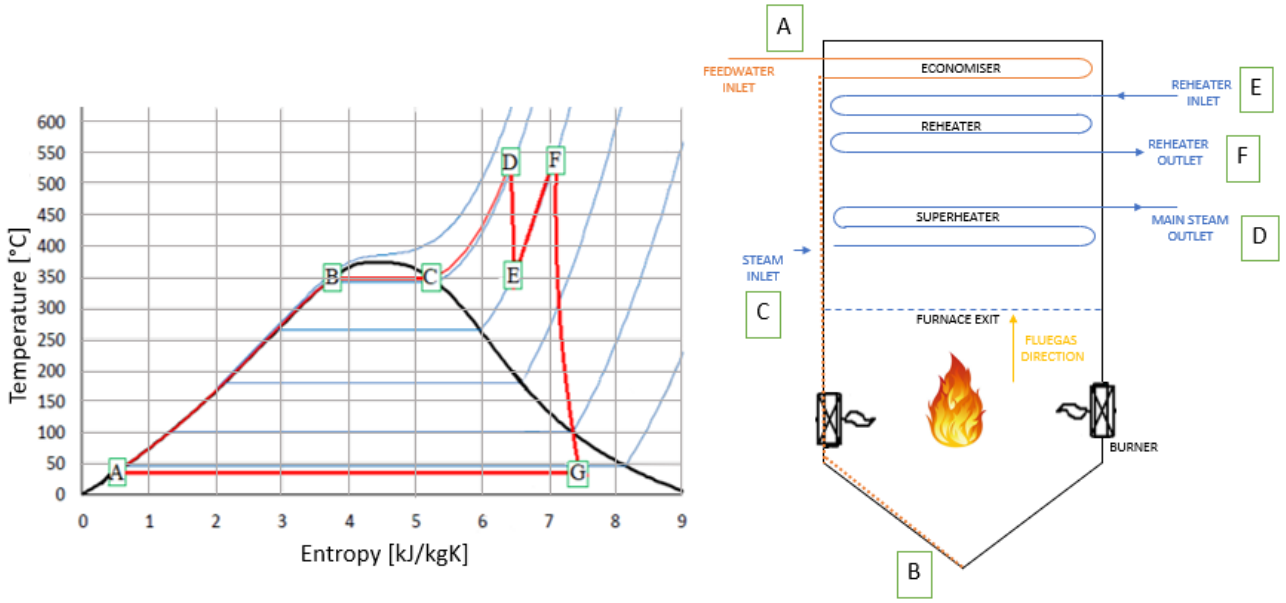

Figure 4: T-s diagram showing heating and phase transformation on water in boiler [15]

Although the main aim of improving boiler efficiency is to minimise coal consumption and maximise steam generation, there are various factors that influence boiler operation and steam temperature regulation. Despite these factors, boiler operation is still required to conform to the required temperature, pressure and environmental regulations [3]. Steam temperatures are mainly affected by the variables introduced by the following and should be compensated in order to maintain constant steam temperatures [3]:

- Slag or ash accumulation (soot blowing cycles)
- Firing rate
- Variable air flow rate
- Feed water temperature
- Fuel variation
- Variable use of saturated steam for auxiliaries
- Attemperation
- Load Variation
- Variation in burner operation

2.1.2 Superheaters

Superheaters are heat exchanges that are installed in series and comprise of inline tube bundles with steam flowing on the inside of the tubes and flue gas flowing over the outside of the tubes, typically in a cross-flow configuration. The main purpose of superheaters is to increase the temperature of the steam entering from the evaporator, resulting in the boiler being more effective and thermodynamically efficient. Superheaters and reheaters minimise the likelihood of saturated steam leaving the boiler. Saturated steam in the turbine leads to condensation due to reduced temperature and pressure, which increases the moisture content in the turbine, resulting in energy loss, excessive blade wear and erosion.

Types of Superheaters: Radiant vs Convective

The dominant mode of heat transfer from the flue gas path is dependent on the location of the superheaters in the convection pass, classifying them as either convective type or radiative type superheaters. Radiant superheaters (platen) are located closest to the furnace exit and are directly exposed to the radiation heat flux from the flame. The platen superheater (Superheater 1) is located to receive heat energy dominantly through thermal radiation from the flue gas leaving the furnace and passing over the tube bundles, with some additional energy from convective heat transfer as the flue gas is at its highest temperature in the convective pass. Convective superheaters are situated after the platen superheater and receive heat energy dominantly through forced external convection, with additional radiation energy from the flue gas passing over the tube bundles due to the flue gas being at a lower temperature in this part of the convective pass. One of the main factors that distinguish between convective and radiant superheaters is the transverse pitch, which is the horizontal distance between two tube rows in a bundle. For tower type once-through boilers, the transverse pitch decreases along the height of the boiler, leading to forced convection being the primary heat transfer mode at higher elevations in the boiler.

Superheater Tube Layout

The superheater heat exchangers were modelled as horizontal convection and radiant superheaters as shown in Figure 5 and are located above the furnace for tower type boilers. These superheaters consist of parallel rows of tubes, terminating in inlet and outlet headers where mixing of steam occurs. In this configuration, all convective superheaters have two passes per superheater tube bundle.

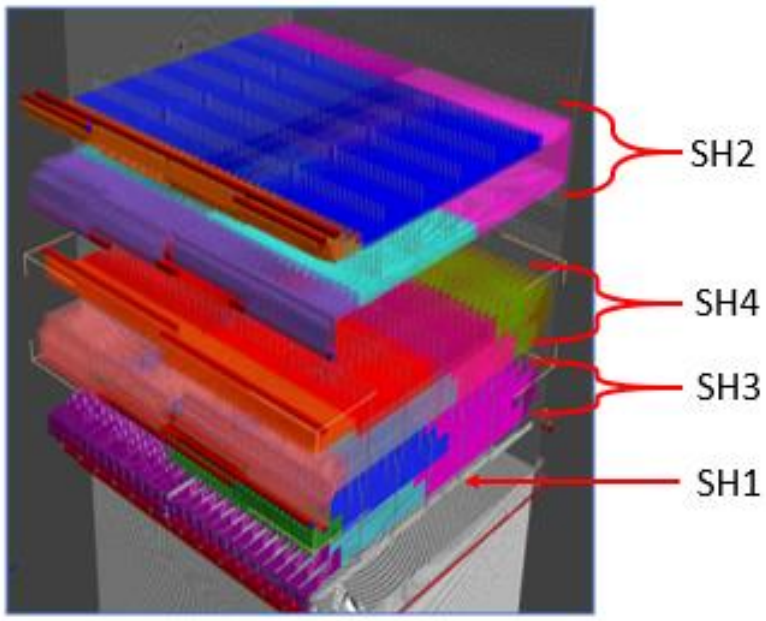

Figure 5: 3D view of a convection pass of a boiler [16]

Figure 6 defines the geometric inline superheater tube spacing corresponding to the transverse/horizontal (S_T) pitch and longitudinal/vertical (S_L) pitch, as well as the number of transverse rows or tube bundles (N_{bund}) and longitudinal rows or parallel tubes (N_{tube}).

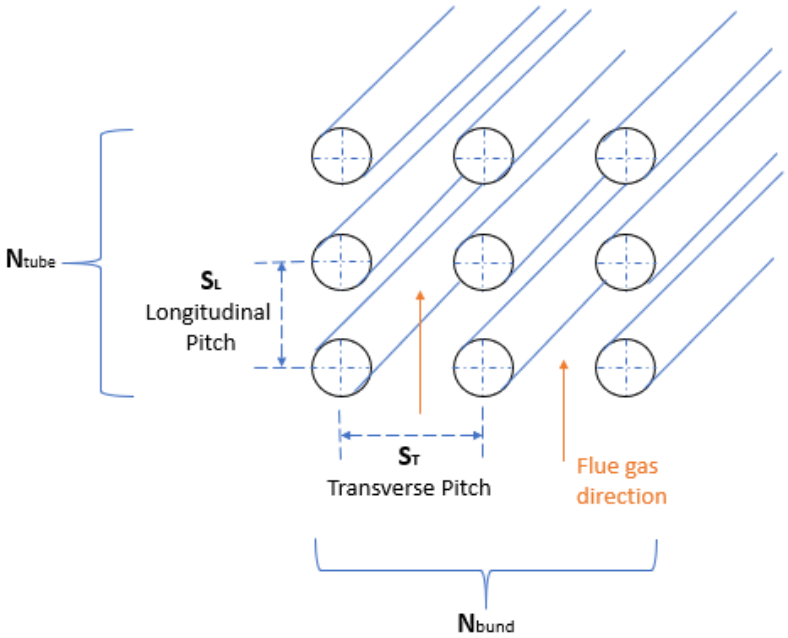

Figure 6: Transverse vs Longitudinal Pitch for in-line superheater tubes

2.1.3 Types of Heat Exchanger Configurations

There are three main types of heat exchanger flow arrangements, namely parallel flow, counter flow and cross flow. Parallel flow refers to an arrangement where both the 'cooler' steam and 'hotter' flue gas enter the heat exchanger at the same end, and flow parallel to each other in the same direction as shown in Figure 7 [17].

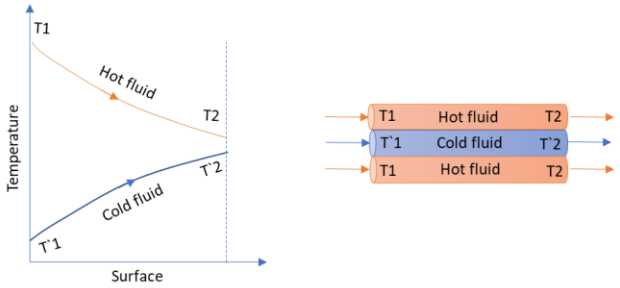

Figure 7: Parallel flow heat exchanger

Counter flow refers to an arrangement where the 'cooler' steam and 'hotter' flue gas enter the heat exchanger at opposite ends, and flow parallel to each other but in opposite directions as shown in Figure 8. Counter flow heat exchangers are the most efficient of the heat exchangers as it has the highest average temperature difference between the two fluids per unit surface area. In other words, the log mean temperature difference is larger for counter flow heat exchangers when compared to parallel and cross flow heat exchangers, resulting in greater heat transfer between the two fluids for counter flow heat exchangers [17].

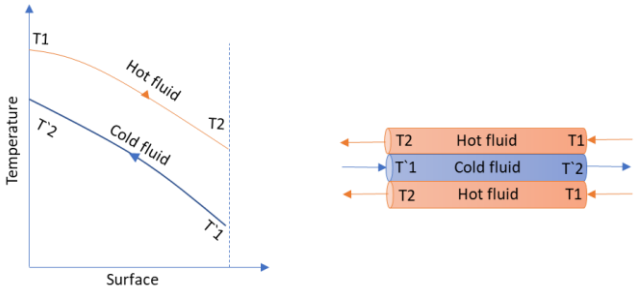

Figure 8: Counter flow heat exchanger

Cross flow occurs when the 'cooler' steam and 'hotter' flue gas flow perpendicular to each other as shown in Figure 9 and Figure 10. This arrangement has an intermediate efficiency between parallel and counter flow exchangers. The heat exchangers modelled uses a cross-counter flow configuration where the steam flows internally through the tubes and flue gas threads over and through the spaces between a bank of tubes at either right angles or counter flow to the steam. Cross flow heat exchangers are thermally more effective than parallel flow heat exchangers [17].

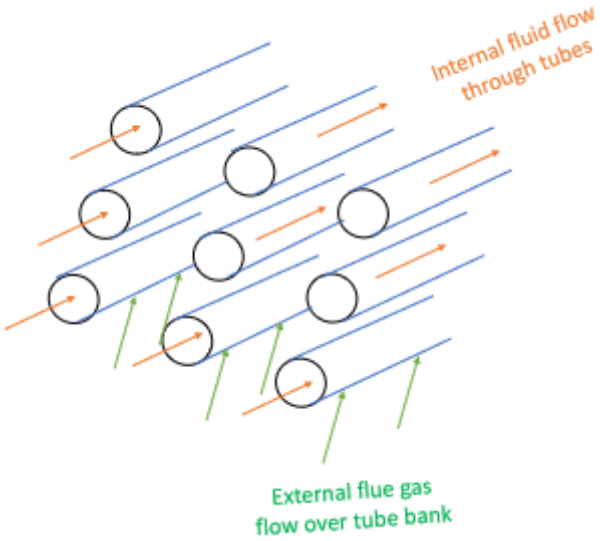

Figure 9: Schematic of in-line tube banks in a cross-flow configuration

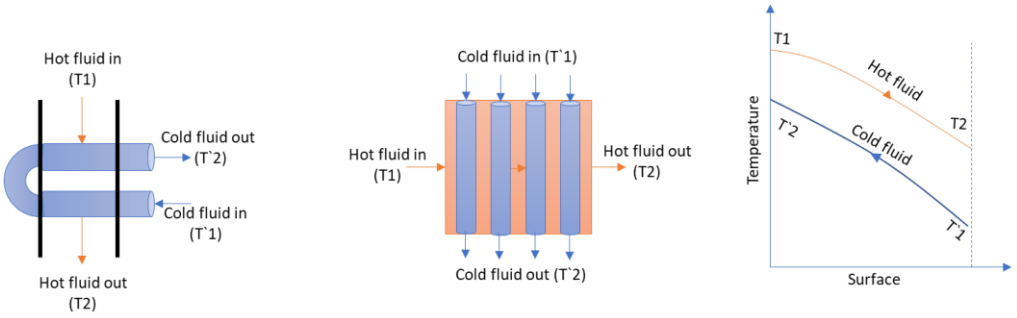

Figure 10: Cross flow heat exchanger

2.1.4 Types of Attemperators

There are various factors that cause boiler operation to be unsteady such as the coal quality and those mentioned in Section 2.1.1 above. It is therefore important, that despite these unpredictable disturbances, the superheater outlet steam temperature remains within acceptable limits as specified by the turbine inlet requirements.

Attemperation methods can be characterised into two types, direct and indirect. The direct type is also known as spray attemperators and are typically used to control or cool down the superheater steam temperature in boilers whereas the indirect type is generally a conventional shell-tube heat exchanger where heat is transferred from a high temperature fluid to a cooler fluid [18]. This dissertation focusses on direct type attemperators and its configuration will therefore be briefly discussed below.

Direct Type Attemperators:

Due to its rapid response, spray attemperation is generally used to dynamically control and cool down high temperature steam flow according to a setpoint. They are specially positioned and designed to spray atomised low temperature steam or feed water at either the Superheater 1 inlet or in the header between two superheater sections while maintaining better control of the metal temperatures and preventing thermal shock in the tubes. Spray water is

tapped off from feed pumps discharge but is at a higher pressure than the steam because of the pressure drop in the intervening tubes of the economiser, evaporator, etc.

Mass and energy balance calculations for attemperators:

The inlet mass flow rates and the enthalpies of the superheated steam and spray water are used to calculate the outlet enthalpy of the attemperator. The mass balance for the control volume is given by:

$$\dot{m}_{Att,out} = \dot{m}_{SH} + \dot{m}_{spray} \tag{2.1}$$

where $\dot{m}_{SH}$ (kg/s) is the outlet steam mass flow rate from the superheater upstream, $\dot{m}_{spray}$ (kg/s) is the spray water mass flow rate, $\dot{m}_{Att,out}$ (kg/s) is the mass flow rate entering the downstream superheater.

The outlet specific enthalpy of the attemperator is calculated (assuming no heat exchange with thermal mass of the thick attemperator walls)

$$h_{Att,out} = \frac{\dot{m}_{SH} \cdot h_{SH,out} + \dot{m}_{spray} \cdot h_{spray}}{\dot{m}_{Att,out}} \tag{2.2}$$

where $h_{Att,out}$ (J/kg) is the attemperator outlet specific enthalpy at $T_{Att,out}[K]$, $h_{SH,out}[J/kg]$ is the specific enthalpy of upstream superheater and $h_{spray}[J/kg]$ is the spray water specific enthalpy.

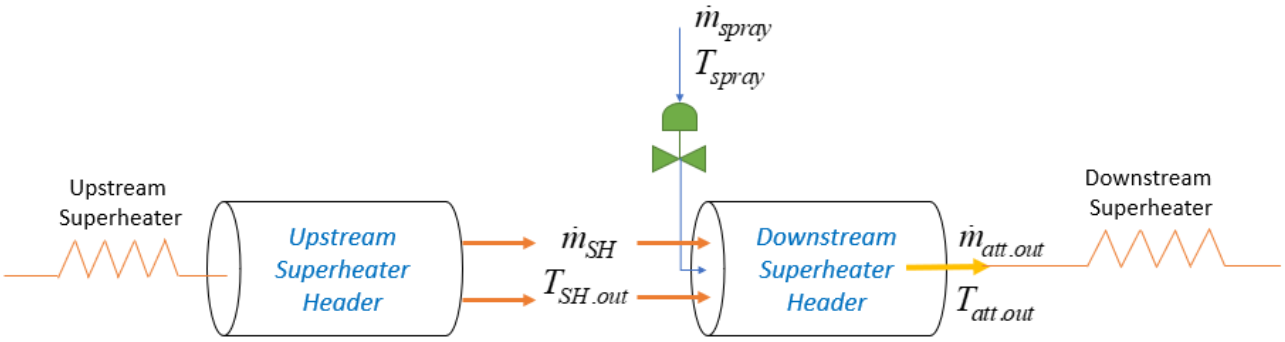

Figure 11: Mass and energy balance for direct type attemperator

3. Heat Exchanger Modelling Approach

This chapter primarily focuses on the theory and practical application of fundamental heat transfer performance calculations of the convection pass in a 600 MW coal fired boiler. Steam generated in the furnace flows to the separating vessel where gas (steam) and liquid (water) are separated, and steam is piped to the inlet of the primary superheater (Superheater 1). The purpose of the superheaters in the convection pass is to heat the high-pressure steam according to the turbine's designed inlet steam conditions. The steam (cooler medium) in the superheater is then heated by the flue gas (hotter medium) passing over the tubes through convection, conduction and radiation. Radiative and convective heat transfer is dependent on the location and configuration of the superheater passes, e.g. Superheater 1, also known as the platen superheater, is located closest to the furnace exit and has the largest transverse pitch, resulting in a larger radiative heater transfer component compared to the subsequent superheaters. It is important to note that even though either radiation or convection is dominant in some heat exchangers, both convection and radiation are always present. Wet steam has adverse effects on the turbine as condensate droplets would increase the wear and failure rate of the turbine blades, thus increasing maintenances cost. It also decreases the energy absorbed in the turbine as less thermal energy is converted into mechanical energy due to the moisture.

This chapter explains the theory and methodology for numerically calculating heat transfer coefficients for convection, conduction and radiation in a once-through power plant boiler in Mathcad using standard correlation formulas. These calculations were then used to model the convective pass of the boiler using the available components in Flownex. The Flownex model was then simulated and the steady state results were extracted, documented and compared to the numerical model.

3.1 Tube geometry

Technical and economic research shows that the most effective method of generating high pressure steam is to heat tubes with relatively small diameters while maintaining a continuous flow of steam through the tubes [3]. Superheaters are made up of heat exchangers which comprise of tubes with fixed lengths, where steam flows inside the tubes and flue gas flows perpendicular to steam (cross flow) on the outside of the tubes.

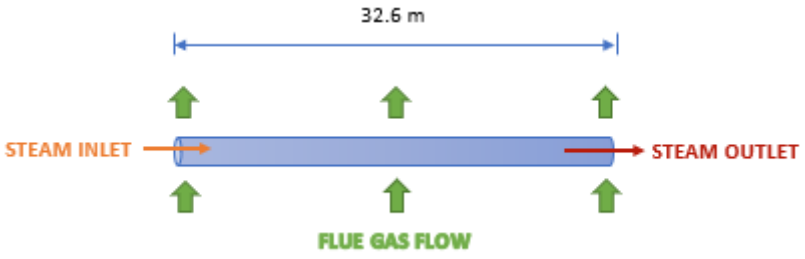

Figure 12: Simplified tube one pass into one finite tube model showing cross flow between flue gas and steam flow

Each individual stage of the convection pass was initially modelled using the Flownex schematic shown in Figure 29 where each component was configured using the associated design operating boundary conditions and geometry parameters. These boundary conditions include the inlet and outlet steam

and flue gas temperatures and mass flow rates, while the geometry parameters include the ducting wall thickness, hydraulic diameters and length. The flue gas flow was modelled as a pipe in Flownex by specifying the area, length and circumference per section. A generic equation for the duct hydraulic diameter is:

$$d_{h,\,fluid} = \frac{4 \cdot A}{p} \tag{3.1}$$

where $d_{h,\,fluid}\ [m]$ is the hydraulic diameter of the respective fluid, $A\ [m^2]$ is the cross sectional area of the flow and $p\ [m]$ is the 'wetted' or inner perimeter of the cross section. Figure 13 is based on Equation (3.1), where the hydraulic diameter for a circular duct is simplified as:

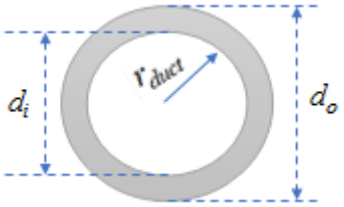

Figure 13: Representation of a tube illustrating the inner and outer diameter and radius

$$d_{h,\,fluid} = \frac{4\pi r_{duct}^{\ 2}}{2\pi r_{duct}} = 2r_{duct} = d_{duct} \tag{3.2}$$

where $r_{duct}[m]$ and $d_i[m]$ or $d_{duct}[m]$ is defined as the inner radius and diameter of the duct respectively. The heat transfer elements were configured using the tube material data, heat transfer coefficients, and inner and outer tube areas for the steam and flue gas streams.

Each superheater arrangement was modelled in Flownex as a two-pass heat exchanger whereas each tube bundle within each pass was simplified into a single tube as shown in Figure 14. It can be noted from this figure that section 'A' was modelled as the first pass, section 'C' was modelled as the second pass, and the length of section 'B' was spilt into half and added to the lengths of sections 'A' and 'C' to account for the complete superheater.

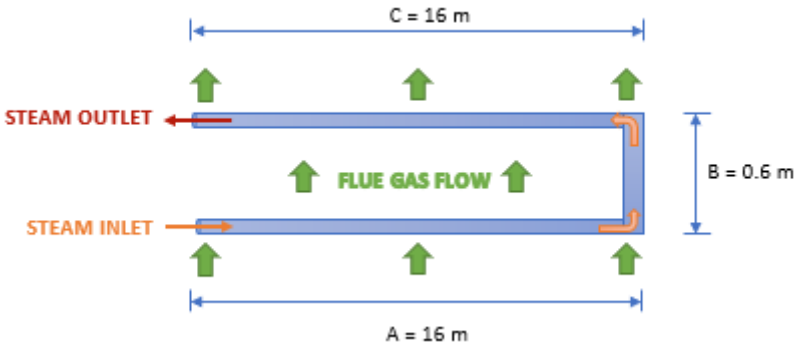

Figure 14: Two pass tube showing cross flow between the flue gas and steam flow

3.1.1 Tube Discretisation

The flue gas flowing over the tubes in the convective pass has a varied temperature distribution over the length of the tube. This required that the tube length be discretised into smaller tube length sections in order to correctly capture the temperature profile as shown in Figure 15. For illustrative purposes, this example shows that the tube length per pass (e.g. 16 m) has been discretised into five increments. Flownex automatically subdivides the total length of the tube according to the value entered in the '*specified number of increments*' input, ensuring each segment is of equal length. Each steam tube in the Flownex model was discretised into 16 segments in order to try and fully capture the flue gas temperature distribution and to accurately achieve the desired outlet steam temperature.

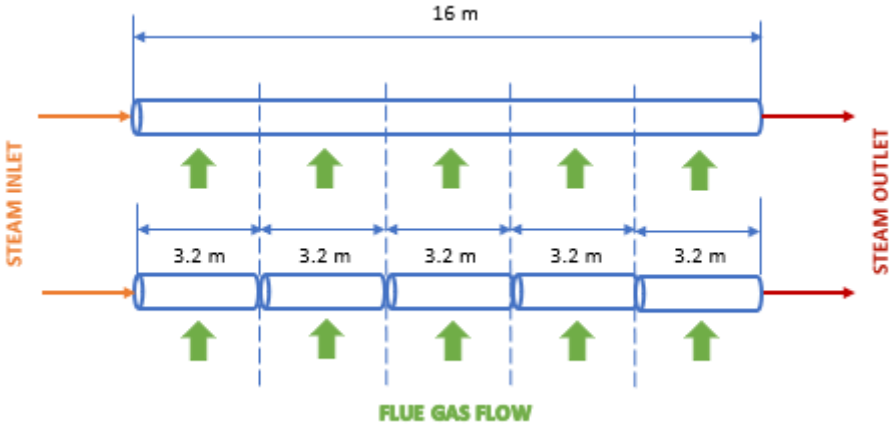

Figure 15: Discretisation of a 16 m tube into 5 equal sections

3.1.2 Heat Exchanger Bundle

The heat exchangers modelled as superheaters are made up of multiple bundles, where each bundle consists of a number of tubes, each terminating in inlet and outlet headers. Figure 16 illustrates an example of four two-pass tubes which make up one bundle.

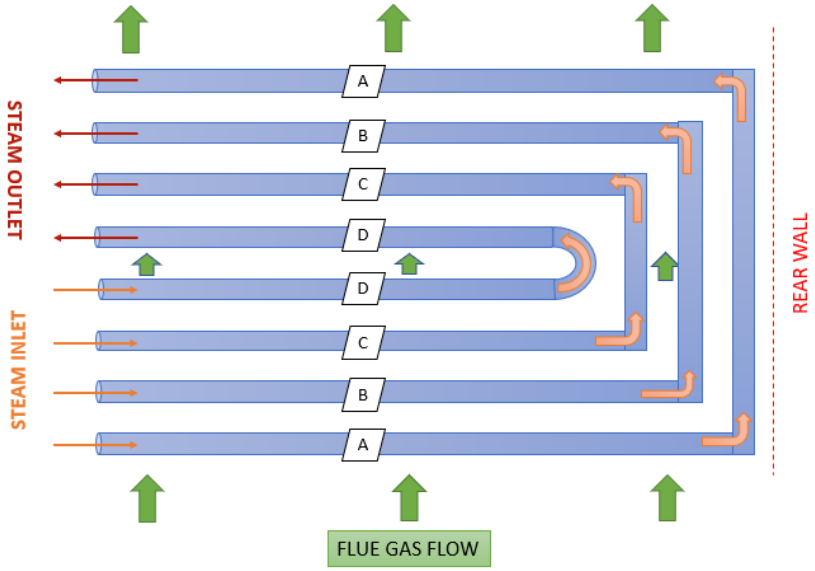

Figure 16: Two-pass tube bundle showing cross flow between steam and flue gas flow

For simplification purposes, each tube bundle per section was modelled as one pipe in Flownex by specifying the number of pipes in parallel as shown in Figure 14. This ensures that all individual tubes have equal flow in the same direction without over complicating the model (although in real boilers, the mass flow rate varies per tube). Although the tube bundles are simplified into one tube, specifying the *'number of tubes in parallel'* as an input in Flownex allows for the tube geometry to be modelled as one tube in the bundle. The value entered in *'number of parallel tubes' input* was calculated as the number of bundles multiplied by the number of tubes per bundle.

3.2 Superheater Heat Transfer Geometry Definition

The geometries for the tower-type boiler convection pass can be split into two sections, the flue gas flow passage and the steam flow passage.

3.2.1 Flue Gas Flow Geometry:

Flue gas flows transversely over a tube bundle in the convection pass of the once-through boiler, therefore the cross-sectional area is required to calculate the external heat transfer coefficient. The flue gas cross-sectional area, $A_{cs.fg}\ \left[m^2\right]$, is a function of the length $L_{boiler}\ [m]$ and width $w_{boiler}\ [m]$ of the boiler section, length of the tube in that section $L_{tube}\ [m]$, outside diameter of the tube $d_o\ [m]$, and number of transverse tube bundle rows per superheater section N_{bund}:

$$A_{cs.fg} = L_{boiler} \cdot w_{boiler} - d_o \cdot L_{tube} \cdot N_{bund} \tag{3.3}$$

The external heat transfer surface area, $A_{s.fg}\ \left[m^2\right]$, is calculated as the total superheater section area exposed to the flue gas:

$$A_{s.fg} = \pi \cdot d_o \cdot N_{bund} \cdot N_{tube} \cdot L_{tube} \tag{3.4}$$

where N_{tube} is the number of parallel tubes per superheater section.

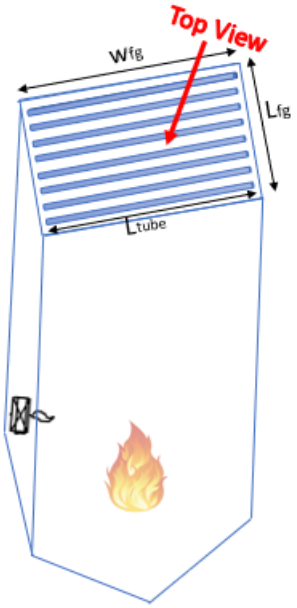

Figure 17: Isometric view of boiler

3.2.2 Steam Flow Geometry

In thermal calculations, the cross-sectional area, $A_{cs.st}\ \left[m^2\right]$, for internal heat transfer is calculated as:

$$A_{cs.st} = \pi \cdot \frac{d_i^{\,2}}{4} \cdot N_{tube} \cdot N_{bund} \tag{3.5}$$

where $d_i\ [m]$ is the inner tube diameter. The internal heat transfer surface area $A_{s.st}\ \left[m^2\right]$ is calculated as the total area that is exposed to the steam:

$$A_{s.st} = \pi \cdot d_i \cdot N_{bund} \cdot N_{tube} \cdot L_{tube} \tag{3.6}$$

3.2.3 Platen Superheater

The method of calculating the heat transfer area for platen superheaters varies from convective superheater in a tower-type boiler due to its unique and complicated layout and configuration arrangement. The heat transfer area for the platen superheater is calculated as the exposed planar area which is created by the tube bundles. The external and internal heat transfer surface area for a platen superheater is calculated using equation (3.4) and equation (3.6) respectively, with L_{tube} being the average length of the platen tubes per bundle [18].

3.3 Heat Transfer Theory

According to Incropera [17], the definition of heat transfer is the thermal energy in transit due to a spatial temperature difference. Analysing the typical heat transfer around a superheater tube in Figure 18, there are three general heat transfer modes which occur:

1. From the flue gas to the outer tube wall surface $(T_{fg} - T_{wo})$:
    - External convection
    - Radiation
2. Between the outer tube wall surface to the inner tube wall surface $(T_{wo} - T_{wi})$:
    - Conduction
3. From the inner tube wall surface to the steam $(T_{wi} - T_{st})$:
    - Internal convection

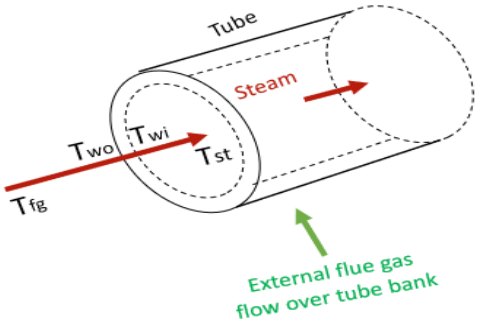

Figure 18: Heat transfer between flue gas and steam in tube

Figure 19 represents an illustration of the flue gas heat distribution and flow path in a once-through type boiler. It shows that the flue gas is the hottest (orange) around the burner/furnace section where the fireball is present and cools down significantly (blue) in the back-pass of the boiler. This is mainly due to the heat exchange between the flue gas and the steam in the convection pass of the boiler.

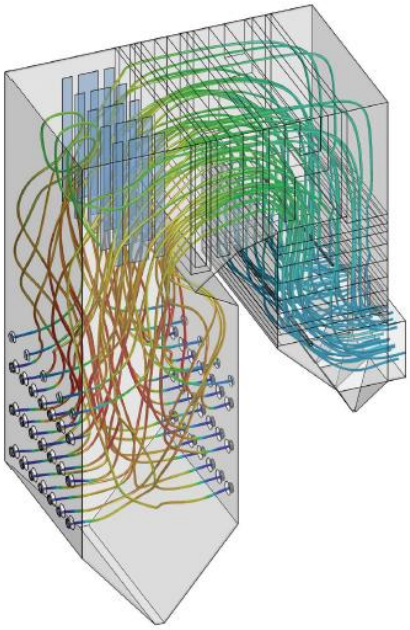

Figure 19: Illustration of the flue gas flow and temperature in a boiler [3]

3.3.1 CONDUCTION:

Conduction is the heat transfer in the tube material that occurs between the external tube surface and internal tube surface. According to Fourier's Law, the transient conductive heat transfer equation for the heat transfer rate depends on the thermal conductivity of the material $k\ [W/m\cdot K]$, the length of the material $x[m]$, the surface area of the tube A and the difference in temperature between the two surfaces:

$$q_x = -kA\frac{dT}{dx} = -kA\frac{T_o - T_i}{\Delta x} \tag{3.7}$$

Fouling on the surface of the tube material is mainly due to the build-up of deposits such as ash and slagging on the external tube surface and scaling on the internal tube surface. Fouling has a negative effect on thermal conductivity, and therefore efficiency, as it adds an extra poorly conducting layer to the tube surface, thereby increasing the effective thickness of the tube and increasing the heat transfer resistance from the flue gas to steam. Slag is a consequence of when the flue gas temperature increases above the ash fusion temperature and scaling is a byproduct of a chemical reaction the steam has with tube material. Soot blowing helps reduce the build-up of ash and slag. To approximate the effect of fouling, the overall heat transfer coefficient can be adjusted for clean tubes with a coefficient of effectiveness ($\Psi_{fouling}$) of 0.65 [19].

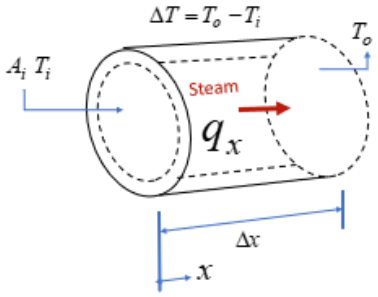

Figure 20: Conduction heat transfer diagram

3.3.2 CONVECTION:

Convection refers to the transfer of heat between a solid surface and a fluid moving over the surface. It includes the effects of energy transfer for both diffusion (random motion of fluid particles) and advection (bulk fluid motion) [17]. This implies that fluid motion improves heat transfer, while no motion results in the heat transfer being purely conduction. Unlike conduction, the calculation of heat transfer rates is relatively complex as it is dependent on the details relating to flow characteristics and patterns such as discussed below.

The Nusselt number $\left(Nu_{fluid}\right)$ is a dimensionless number which indicates the measure of the convective heat transfer rate through a boundary layer. It is usually defined as a function of the convective heat transfer coefficient (HTC) h_{conv}, the length of the tube $L\ [m]$ and the thermal conductivity of the respective fluid $k_{fluid}\ \left[W/m\cdot K\right]$:

$$Nu_{fluid} = \frac{h_{conv}\cdot L}{k_{fluid}} \tag{3.9}$$

As mentioned previously, the superheater thermo-fluid model was spilt into two convective heat transfer sections, namely internal and external convection, which is explained in detail in the following subsections. Internal convection was modelled as the temperature difference between the inner tube surface and the steam, and external convection was modelled as the temperature difference between the flue gas and the outer tube surface (see Figure 18).

Convective heat transfer can be further classified into two terms, forced and natural/free convection. Forced convection refers to the forced flow of fluid around a tube surface and is generally related to the Reynolds number. Natural or free convection refers to the flow of fluid driven by buoyancy forces due to temperature differences and is related to the Grashoff number [15]. Comparing the Reynolds number characteristics mentioned below to Table 8 and Table 9, the convective heat transfer used in this project can be categorised as forced convection. It can be noted that the fluid in this project refers to either the steam inside the tubes or the flue gas flow over the outside of the tubes and fluid temperature is evaluated at the mean temperature of the fluid in the control volume.

For forced convection, the Nusselt number can be correlated to the following Reynolds $\left(\mathrm{Re}\right)$ and Prandtl $\left(\mathrm{Pr}\right)$ number for the given geometry and flow conditions of the tube:

$$Nu_{conv,\mathrm{int}} = \phi\left(\mathrm{Re},\mathrm{Pr}\right) \tag{3.10}$$

The Reynolds number is a dimensionless number which represents the ratio of inertia to viscous forces in a fluid. It is defined as a function of density $\rho\left[kg/m^3\right]$, velocity $v\,[m/s]$, $d_{h,\,fluid}\,[m]$ and dynamic viscosity $\mu_{fluid}\,\left[kg/m\cdot s\right]$:

$$\mathrm{Re} = \frac{\rho \cdot v \cdot d_{h,\,fluid}}{\mu_{fluid}} \tag{3.11}$$

The Reynolds number helps determine the flow characteristic in a pipe [20]:

- For laminar flow, the Reynolds number is $\mathrm{Re} < 2300$, corresponding to low velocity and high viscosity in the tube.
- For turbulent flow, the Reynolds number is $5000 \le \mathrm{Re} \le 10^8$, corresponding to high velocity and low viscosity in the tube.
- When the Reynolds number is in the region of $2300 < \mathrm{Re} < 5000$, the flow is stated as being in a transition region.

The Prandtl number is also a dimensionless number and is a measure of the relative effectiveness between momentum and energy transport by diffusion in the velocity and thermal boundary layers [17]. It can be defined as a function of specific heat $c_p\,\left[J/kg\cdot K\right]$, viscosity $\mu_{fluid}\,\left[kg/m\cdot s\right]$ and thermal conductivity $k_{fluid}\,\left[W/m\cdot K\right]$ of the fluid:

$$\mathrm{Pr} = \frac{c_p \cdot \mu_{fluid}}{k_{fluid}} \tag{3.12}$$

The convective heat transfer coefficient for both internal and external conditions can therefore be calculated using Equation (3.9) as:

$$h_{conv} = \frac{Nu_{conv} \cdot k_{fluid}}{d_{h,\,fluid}} \tag{3.13}$$

Internal Convection Heat Transfer Coefficient Calculation

Total heat transfer between the internal tube surface and steam is done via internal convection. The following represents the heat transfer correlation used for calculating the internal convective heat transfer in the convective pass of the boiler.

Dittus Boelter Correlation [21]:

The Nusselt number for a fully developed turbulent flow between the wall surface and steam path was calculated using the Dittus Boelter correlation:

$$Nu_{conv,\mathrm{int}} = 0.023\,\mathrm{Re}^{0.8}\,\mathrm{Pr}^{n} \tag{3.14}$$

where the Reynolds and Prandtl numbers are evaluated at the mean temperature of the steam in the tube. According to Table 1, $n = 0.4$, since the steam is being heated due to convective heat transfer definition.

Table 1: Dittus Boelter variable description

	n
Cooling fluid	0.3
Heating fluid	0.4

This correlation is valid for the following ranges:

$$\begin{bmatrix} \mathrm{Re} > 1000 \\ 0.7 \le \mathrm{Pr} \le 160 \end{bmatrix}$$

The following table summarises the equations, limitations and accuracy of other internal turbulent flow heat transfer correlations:

Table 2: Summary of internal convection heat transfer correlations [17]

Correlation	Nusselt Number Equation	Reynolds Number	Prandtl Number	Accuracy
Gnielinski	$Nu_{conv,\mathrm{int}} = \dfrac{\left(\frac{f}{8}\right)(\mathrm{Re}-1000)\,\mathrm{Pr}}{1+12.7\left(\frac{f}{8}\right)^{0,5}\left(\mathrm{Pr}^{2/3}-1\right)}$ where $f = \left(0,79\ln(\mathrm{Re})-1,64\right)^{-2}$	$3000 \le \mathrm{Re} \le 5\times10^{6}$	$0.5 \le \mathrm{Pr} \le 2000$	10%
Sieder-Tate	$Nu_{conv,\mathrm{int}} = 0.027\,\mathrm{Re}^{\frac{4}{5}}\,\mathrm{Pr}^{\frac{1}{3}}\left(\frac{\mu}{\mu_s}\right)^{0.14}$	$\mathrm{Re} \ge 10000$	$0.7 \le \mathrm{Pr} \le 16700$	25%

External Convective Heat Transfer Coefficient

Total heat transfer from flue gas to the external tube surface is done via external convection and gas radiation. The heat exchangers were set up in a cross-flow configuration where the flue gas flow is perpendicular to the steam in the tubes. Several empirical correlations were developed for external heat transfer coefficients for tube bundles arranged in-line, however, the Zukauskus method will be explained as this was selected for the design. The heat transfer coefficient is greatly influenced by the flow pattern across a tube.

Zukauskus Method [22]:

The average heat transfer coefficient for the entire tube bank was proposed by Zukauskus [16] in the form:

$$Nu_{ext} = C_1 \, \mathrm{Re}_{D,\max}^{m} \, \mathrm{Pr}^{n} \left(\frac{\mathrm{Pr}}{\mathrm{Pr}_s} \right)^{1/4} \tag{3.15}$$

Provided that the following conditions are met:

$$\begin{bmatrix} N_{tube} \geq 20 \\ 0.7 \leq \mathrm{Pr} \leq 500 \\ 10 \leq \mathrm{Re}_{D,\max} \leq 2 \times 10^{6} \end{bmatrix}$$

where N_{tube} is the number of tube rows which must be greater than or equal to 20, and all other properties except Pr_s are evaluated at the arithmetic mean of the fluid inlet and outlet temperatures. Prandtl number, Pr_s, contains a subscript *s* and is evaluated at the uniform external tube wall surface temperature [21]. The following table illustrates the Nusselt number coefficients using the Zukauskus correlation for cross flow over tube banks which are arranged in-line:

Table 3: Nusselt number coefficients using the Zukauskus correlation [22]

Reynolds Number	C_1	**m**	**n**
$0-100$	0.9	0.4	0.36
$100-1000$	0.52	0.5	0.36
$1000-2\times10^{5}$	0.27	0.63	0.36
$2\times10^{5}-2\times10^{6}$	0.033	0.8	0.4

The Prandtl number Pr_s contains a subscript which indicates that it is evaluated at. This correlation depends on the Reynolds number $\left(\mathrm{Re}_{D,\max} = \rho V_{\max} D/\mu\right)$ which is based on the maximum fluid velocity through the tube banks that occurs at the minimum flow area between the tubes. From the conservation of mass, the maximum velocity $V_{\max}\left[m/s\right]$ can then be calculated using the following equation where $V_{open}\left[m/s\right]$ is the open duct velocity of the flue gas, s_T is the transverse tube pitch between elements and $d_o\ [m]$ is the tube outer diameter:

$$V_{\max} = \frac{s_T}{s_T - d_o}\left(V_{open}\right) \tag{3.16}$$

Other external heat transfer convection correlations that can be used for cross flow configurations are:

Table 4: Other external convectional heat transfer correlations for in-line tube banks

<table>
<tr><th>Correlation</th><th>Nusselt Number Equation</th><th>Re Range</th><th>Pr Range</th></tr>
<tr><td>Churchill and Bernstein [17]</td><td>$$Nu = 0.3 + \frac{0.62\,\mathrm{Re}^{1/2}\,\mathrm{Pr}^{1/3}}{\left[1+\left(\frac{0.4}{\mathrm{Pr}}\right)^{2/3}\right]^{1/4}}\left[1+\left(\frac{\mathrm{Re}}{282000}\right)^{5/8}\right]^{4/5}$$</td><td>$\mathrm{Re} < 10\,000$</td><td>$\mathrm{Pr} > 0.2$</td></tr>
<tr><td>Hilpert [17]</td><td>$$Nu = C_2\,\mathrm{Re}^{n}\,\mathrm{Pr}^{1/3}$$<table><tr><th>Reynolds number</th><th>C_2</th><th>n</th></tr><tr><td>0.4 – 4</td><td>0.989</td><td>0.33</td></tr><tr><td>4 – 40</td><td>0.911</td><td>0.385</td></tr><tr><td>40 – 4000</td><td>0.683</td><td>0.466</td></tr><tr><td>4000 – 40 000</td><td>0.193</td><td>0.618</td></tr><tr><td>40 000 – 400 000</td><td>0.027</td><td>0.805</td></tr></table></td><td>$0.4 \le \mathrm{Re} \le 400\,000$</td><td>$\mathrm{Pr} \ge 0.7$</td></tr>
<tr><td>Kuznetsov [18][23]</td><td>$$Nu = c_s\,c_n\,\mathrm{Re}^{0.65}\,\mathrm{Pr}^{0.33}$$ where $$c_s = 0.2\left[1+\left(2\frac{s_T}{d_o}-3\right)\left(1-\frac{s_L}{d_o}\right)^3\right]^{-2}$$ $$c_n = 0.2 \text{ if } \frac{s_T}{d_o} \le 1.5 \text{ or } \frac{s_L}{d_o} \ge 2$$ If $n < 10$ then $c_n = 0.91 + 0.0125(n-2)$ If $n \ge 10$ then $c_n = 1.0$</td><td>$1500 \le \mathrm{Re} \le 1.5\times10^5$</td><td></td></tr>
</table>

3.3.3 RADIATION:

The constituents of flue gas in a boiler (such as water vapour, carbon dioxide, carbon monoxide and sulphur dioxide) absorb and emit substantial amounts of radiant heat. Ash has a high impact on radiant heat transfer. This radiative energy is dependent on the constituent's temperatures, pressures and the geometries of the gas volume. Radiative heat transfer is defined as the transfer of heat energy between two mediums using electromagnetic waves, and can be separated into two types when incident on the convective pass:

1. Direct radiation
2. Gas radiation

Direct radiation is an example of the radiation emitted from the furnace gases directly onto the radiant superheater, whereas gas radiation is an example of the radiation emitted from the flue gas in the heat exchanger control volume to the external surface of the component. Both types of radiation were modelled in Flownex, however this section focuses on the gas radiation calculation as it forms bulk of the radiative heat flux in the convective pass. The total heat transfer from the flue gas to the external tube surface is a summation of the external convective heat transfer coefficient and the gas radiative heat transfer where $h_{combined,ext}\ \left[W/m^2K\right]$ and is calculated as follows:

$$h_{combined,ext} = h_{conv,ext} + h'_{rad} \tag{3.17}$$

The flue gas volume is cooled due to the loss of the heat energy transferred to the superheater tube walls.

Gas radiation heat transfer coefficient calculation [24]**:**

The tri-atomic gases and fly ash volume surrounding the superheater components contribute to the total radiative heat transfer. The effective radiation thickness for horizontal tube bundle superheaters is determined by

$$s_{SH} = C_3 \frac{V_F}{A_w} = C_3 \cdot \frac{d_o}{4} \cdot \left(\frac{4}{\pi} \frac{s_T \cdot s_L}{{d_o}^2} - 1 \right) \tag{3.18}$$

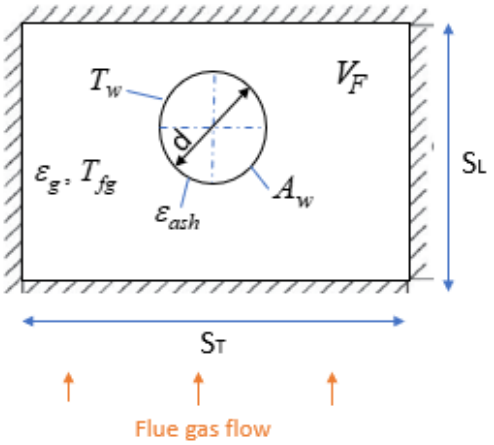

Figure 21: Control volume of a tube in a bank [24]

where $s_{SH}\ \left[m\right]$ represents the geometric mean beam length of the non-platen tube bundle, V_F is the enclosure volume, A_w is the surface area of the superheater walls, $d_o\ \left[m\right]$ is the tube outside diameter, $s_L\ \left[m\right]$ is the longitudinal pitch of the superheater elements and $s_T\ \left[m\right]$ is the transverse pitch between elements and shown in Figure 6. The value of C_3 is generally less than 4.0, where $C_3 = 3.6$ can typically be used as a standard for most conditions [24]. The radiative heat transfer rate in the superheater is calculated in the form of Newton's Law of cooling as [25]:

$$\dot{Q}_{fg,rad} = \frac{\varepsilon_{ash} + 1}{2} \sigma_0 \, \varepsilon_g \left(T^4_{fg,SH} - T^4_{SH,w} \right) \tag{3.19}$$

where $\sigma_0 = 5.67 \times 10^{-8} \left[W/m^2 K^4 \right]$ is the Stephan Boltzmann constant, $T_{fg,SH} \left[K \right]$ is the average superheater flue gas temperature, $T_{SH,w} \left[K \right]$ is the superheater tube wall temperature and ε_{ash} is the ash deposit emissivity of the ash deposit on the external surface of the tubes. For a slag screen, the ε_{ash} = 0.68 and for any other tube surface, ε_{ash} = 0.8. ε_g is the flue gas emissivity which changes with temperature and is calculated using Equation (3.20) [24][23]

$$\varepsilon_g = 1 - e^{-k_{SH} \cdot P_{furnace} \cdot s_{SH}} \tag{3.20}$$

where $P_{furnace} \left[MPa \right]$ is the absolute pressure of the furnace flue gas. Gas contaminates such as soot and ash is accounted for in $k_{SH} \left[1/m \cdot MPa \right]$ as it is the effective gas absorption coefficient [23]:

$$k_{SH} = k_g \cdot r_{SH} + k_{fa} \cdot Y_{Ash} \tag{3.21}$$

where Y_{ash} is the mass concentration of ash and slag particles (fly ash) in the flue gas and r_{SH} denotes the tri-atomic gas volume fraction of water vapour, carbon dioxide and sulphur dioxide in the superheater pass. The ash and slag particle (fly ash) concentration absorption coefficient is calculated as $k_{fa} \left[1/m \cdot MPa \right]$ [19]:

$$k_{fa} = \frac{48350 \rho_{fg}}{\left(T_{fg,SH,out}^2 \cdot d_{fa}^2 \right)^{1/3}} \tag{3.22}$$

where $\rho_{fg} \left[kg/m^3 \right]$ is the flue gas density at normal conditions and the average ash particle diameter for pulverised coal in a tubular ball mill is $d_{fa} = 13 \mu m$ [18]. The radiant absorption due to tri-atomic gases is given by $k_g \left[1/m \cdot MPa \right]$, where r_{H2O} is the volumetric fraction of water vapour in the flue gas:

$$k_g = 10 \left[\frac{0.78 + 1.6 r_{H2O}}{\left(10 P_{furnace} \cdot s_{SH} \right)^{0.5}} - 0.1 \right] \left(1 - 0.37 \frac{T_{fg,SH,out}}{1000} \right) \tag{3.23}$$

The heat transfer coefficient for radiation can then be expressed as a function of the radiative heat transfer rate:

$$h_{rad} = \frac{\dot{Q}_{fg,rad}}{T_{fg,SH} - T_{SH,w}} \tag{3.24}$$

Therefore, by substituting Equation (3.19) into (3.24), the radiation heat transfer between the flue gas and the external surface is calculated using the following formula suggested by Hottel and Sarofim for solid fuels [23] [24]:

$$h_{rad} = \sigma_0 \cdot \frac{\varepsilon_{ash} + 1}{2} \cdot \varepsilon_g \cdot \left[\frac{{T_{fg,SH}}^4 - {T_{SH,w}}^4}{T_{fg,SH} - T_{SH,w}} \right] \tag{3.25}$$

Other radiation heat transfer equations between the gas and wall have been cited in literature [24]:

$$h_{rad} = \sigma_0 \cdot \frac{\varepsilon_{ash}}{1-(1-\varepsilon_{ash})\cdot(1-\alpha_{rad})} \cdot \left[\frac{\varepsilon_g \cdot {T_{fg,SH}}^4 - \alpha_{rad} \cdot {T_{SH,w}}^4}{T_{fg,SH} - T_{SH,w}} \right] \tag{3.26}$$

However, Equation (3.26) is only valid if the gas temperature, density and concentration remains constant. Equation (3.25) is the most widely used for coal fired boilers and was used to calculate the radiative heat transfer coefficient in this dissertation.

There exists a cavity both upstream (before) and downstream (after) of each superheater component. The cavity located upstream has a higher flue gas temperature, $T_{fg,cavity}\ [K]$, when compared to the cavity downstream of the heat exchanger, therefore the upstream gas volume radiates heat to the heat exchanger external surface. To account for this, the gas radiation transfer coefficient is calculated as [23]:

$$h'_{rad} = h_{rad} \left[1 + A_{gas} \cdot \left(\frac{T_{fg,cavity}}{1000} \right)^{0{\cdot}25} \cdot \left(\frac{L_R}{L_B} \right)^{0{\cdot}07} \right] \tag{3.27}$$

where A_{gas} is the empirical constant whereby $A_{gas} = 0.4$ for bituminous coal and anthracite and $A_{gas} = 0.5$ for lignite, $L_R\ [m]$ is the depth of the upstream empty cavity and $L_B\ [m]$ is the width of the tube bundles downstream [23].

3.3.4 Overall Heat Transfer

The overall heat transfer rate, $\dot{Q}_{SH}\ [W]$, between the flue gas and the steam in the superheater occurs through convection and radiation and is calculated using Newton's law of cooling as:

$$\dot{Q}_{SH} = UA\Delta T_{LMTD} \tag{3.28}$$

where $U\ \left[W/m^2K\right]$ is the overall heat transfer coefficient for the heat exchanger, $A\ \left[m^2\right]$ is the external heat exchanger surface area and $\Delta T_{LMTD}\ [K]$ is the log mean temperature difference (LMTD) between the flue gas and the steam which is defined below. The LMTD method is used to analyse the heat exchanger and was used for this project since the inlet and outlet temperatures and mass flow rates were known or could be calculated using an energy balance. The three flow configurations are parallel flow, counter flow and cross-flow heat exchangers as explained in Section 2.1.3.

For counter flow arrangement, the 'hotter' and 'cooler' fluids enter the heat exchanger at opposite ends of the heating surface and therefore flow in opposite directions over the surface as shown in Figure 8, allowing the outlet temperature of the 'cooler' fluid to exceed the outlet temperature of the 'hotter' fluid in some cases. However, the outlet temperature of the 'cooler' fluid can never exceed the inlet temperature of the 'hotter' fluid due to the second law of thermodynamics. Since the LMTD of a counter flow heat exchanger is larger than that of a parallel flow heat exchanger, a smaller heat exchanger surface area is required to achieve the required heat transfer rate.

$$\Delta T_{counter} = \frac{\left(T_{fg,in} - T_{s,out}\right) - \left(T_{fg,out} - T_{s,in}\right)}{\ln\left(\frac{T_{fg,in} - T_{s,out}}{T_{fg,out} - T_{s,in}}\right)} \tag{3.29}$$

where $T_{fg,in}\ [K]$ is the flue gas inlet temperature, $T_{s,in}\ [K]$ is the inlet steam temperature, $T_{fg,out}\ [K]$ is the outlet flue gas temperature and $T_{s,out}\ [K]$ is the outlet steam temperature.

In parallel flow configurations, both the steam and flue gas enter at the same end of the heating surface as shown in Figure 7 and flow in parallel paths over the heating surface.

$$\Delta T_{par} = \frac{\left(T_{fg,in} - T_{s,in}\right) - \left(T_{fg,out} - T_{s,out}\right)}{\ln\left(\frac{T_{fg,in} - T_{s,in}}{T_{fg,out} - T_{s,out}}\right)} \tag{3.30}$$

The LMTD calculation for cross-flow configurations, where the two fluids flow perpendicular to each other as shown in Figure 10, is similar to the counter flow LMTD Equation (3.29), with the addition of a correction factor (F) to measure the deviation between the two configurations [22]. This factor can be obtained from Figure 22, which illustrates a single pass cross-flow heat exchanger where both fluids remain unmixed [22].

$$\Delta T_{cross} = F \cdot \frac{\left(T_{fg,in} - T_{s,out}\right) - \left(T_{fg,out} - T_{s,in}\right)}{\ln\left(\frac{T_{fg,in} - T_{s,out}}{T_{fg,out} - T_{s,in}}\right)} \tag{3.31}$$

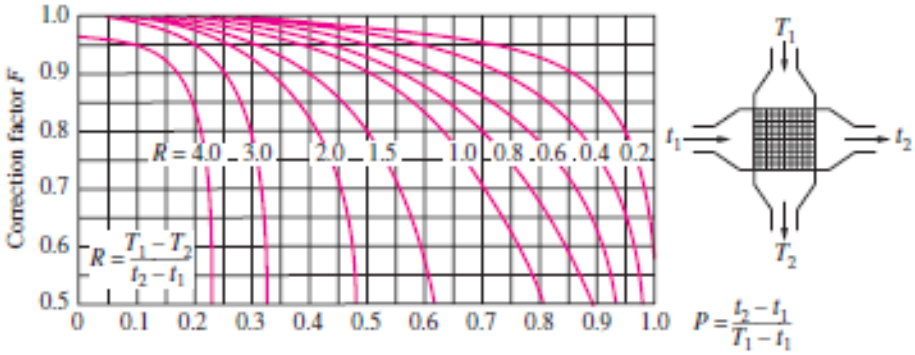

Figure 22: Single cross flow configuration showing correction factor [22]

Using the Dittus Boelter correlation in Equation (3.14), the internal forced convection heat transfer coefficient was calculated as:

$$h_{conv,\text{int}} = Nu_{conv,\text{int}} \frac{k_{fluid}}{d_i} = 0.023 \,\text{Re}^{0.8}\,\text{Pr}^{0.4} \cdot \frac{k_{fluid}}{d_i} \tag{3.32}$$

The Nusselt number, which was calculated using the Zukauskus correlation as shown in Equation (3.15), was used to calculate the external convection heat transfer coefficient for in-line tube bundles:

$$h_{conv,ext} = Nu_{conv,ext}\frac{k_{fluid}}{d_o} = 0.27\cdot \mathrm{Re}^{0.63}\cdot \mathrm{Pr}^{0.36}\left(\frac{\mathrm{Pr}}{\mathrm{Pr}_s}\right)^{1/4}\cdot\frac{k_{fluid}}{d_o} \tag{3.33}$$

The overall heat transfer coefficient $U\left[W/m^2K\right]$ for a generic exchanger is simplified as

$$U = \frac{\psi_{hx}}{\frac{1}{h_{combined,ext}} + \frac{1}{h_{conv,\mathrm{int}}}} \tag{3.34}$$

where the thermal resistance is negligible, and the fouling resistance is approximated by adjusting the overall heat transfer for tube surface cleanliness with an effectiveness coefficient $\left(\psi_{hx}\right)$. The unitless effectiveness factor is the heat transfer ratio between the fouled tubes and the clean tubes. The effectiveness of heat exchangers deteriorates over time due to the build-up of solid deposits on the heat exchanger surface, leading to fouling. This poorly conducting layer creates an additional resistance which has a negative impact on the heat transfer rate. It is therefore important to account for the fouling when calculating the overall heat transfer from the flue gas to the steam. For inline superheaters with an anthracite or semi-anthracite burning boiler, the cleanliness factor is $\psi_{hx} = 0.6$ and bituminous or brown coal uses $\psi_{hx} = 0.65$ [25].

3.4 Thermo-fluid Design Methodology

The convective pass modelling design process was initiated by numerically calculating the heat transfer components using C-schedule boiler design data [26] in Mathcad, which were later used to validate the Flownex model. Mathematical modelling of a thermo-fluid system can be characterised into two basic approaches:

1. Modelling the behaviour of a system which includes network flow models with heat transfer correlations.
2. Using fundamental physics of the system to model the behaviour. This can be done through Computational Fluid Dynamics (CFD) models.

Network flow models depend on flow and geometry measurements per component, with the use of correlations to analyse the heat transfer in the component. These types of models are easily adaptable when compared to the second approach. However, the second approach is beyond the scope of this project as it requires detailed information regarding the behaviour of flow.

The flue gas temperature entering the convective pass was calculated using theoretical fundamentals, which was initially calculated using coal properties such as the as received ultimate analysis of coal. Using Mathcad and C-Schedule data [26], the theoretical air and coal constituents were then calculated in order to calculate the flue gas composition and mass fractions at each boiler component as shown in Table 5. Using the fuel heating value and heat load calculations, the total mass flow rate of fuel required per air ratio was calculated for complete combustion. This was a requirement for calculating the adiabatic flame temperatures and finally, the furnace exit temperature. Once the FEGT was calculated, the convection pass components could be determined.

Table 5: Flue gas composition

Flue Gas component	Gas composition (%) by mass	Mole fraction (%)
CO_2	21.1	14.2
H_2O	5.5	9.0
SO_2	0.3	0.2
N_2	69.6	73.4
O_2	3.5	3.2
Total	**100**	**100**

Detailed boiler drawings were examined to determine the geometries and layout of each superheater section. C-schedule design data [26] included design values for the superheater flue gas temperatures, pressures and mass flows, heat uptake per superheater section, overall superheater area and tube pitch, as well as attemperator temperatures and mass flows. Once the geometries and layout were defined, the convective and radiative heat transfer correlations were calculated using the equations defined above. These were then used to calculate the overall heat transfer coefficient per superheater section. For simplicity, the physical properties of the convection pass were integrated into a series of lumped, single flow heat exchangers. Although the control of reheat steam is beyond the scope of this dissertation, the second reheater stage was included in the model to accommodate for the relevant flue gas temperatures in the boiler.

The numerical model was then used to model the thermo-fluid system using Flownex®, which is a simulation software package used to develop a dynamic thermo-fluid process model of the convection pass [20]. Each superheater section was systematically modelled, and once the inlet and outlet conditions were met for each section, a complete convective pass was modelled by connecting the individual superheater sections together. This enabled the fluid properties to be defined only at the inlet and outlet of the convective pass for both the steam and flue gas streams. Table 6 simplifies the theoretical fundamental methodology used to calculate the overall heat transfer coefficient.

Table 6: Overall heat transfer coefficient calculation summary

<table>
<tr><th colspan="2">CONVECTION PASS GEOMETRY INPUT:</th></tr>
<tr><th>FLUE GAS</th><th>STEAM</th></tr>
<tr><td>INPUTS:
Boiler dimensions:
Boiler width: w_{boiler}
Boiler breath: L_{boiler}
Superheater tube geometry:
Outer tube diameter: d_o
Number of bundles: N_{bund}</td><td>INPUTS:
Superheater tube geometry:
Wall thickness: t_w
Inner tube diameter: $d_i = d_o - 2 \cdot t_w$
No. of tubes per bundle: N_{tube}
Length of tube: L_{tube}</td></tr>
<tr><td>CALCULATION:
• Area of boiler: $A_{boiler} = w_{boiler} \cdot L_{boiler}$
• Boiler perimeter: $P_{boiler} = 2(w_{boiler} + L_{boiler})$
• Flow area: $A_{cs.fg} = A_{boiler} - d_o \cdot L_{tube} \cdot N_{bund}$ (3.3)
• Surface area: $A_{s.fg} = \pi \cdot d_o \cdot N_{tube} \cdot N_{bund} \cdot L_{tube}$ (3.4)</td><td>CALCULATION:
• Flow area: $A_{flow.st} = \pi \cdot (d_i/2)^2$
• Cross-sectional area: $A_{cs.st} = A_{flow.st} \cdot N_{tube} \cdot N_{bund}$ (3.5)
• Surface area: $A_{s.st} = \pi \cdot d_i \cdot N_{tube} \cdot N_{bund} \cdot L_{tube}$ (3.6)</td></tr>
<tr><th colspan="2">SUPERHEATER CONVECTION HEAT TRANSFER COEFFICIENT:</th></tr>
<tr><th>FLUE GAS</th><th>STEAM</th></tr>
<tr><td>INPUTS:
Inlet temperature: $T_{fg.in}$</td><td>INPUTS:
Inlet temperature: $T_{st.in}$</td></tr>
</table>

Outlet temperature: $T_{fg.out}$ Furnace pressure: $P_{furnace}$ Mass flow: $\dot{m}_{fg}$	Outlet temperature: $T_{st.out}$ Outlet pressure: $P_{st.out}$ Mass flow: $\dot{m}_{st}$
CALCULATION: • Average temp: $T_{fg.avg} = \left(T_{fg.in} + T_{fg.out}\right)/2$ • Flue gas properties (calculated using flue gas tables): Density: ρ_{fg} Viscosity: μ_{fg} Thermal conductivity: k_{fg} Specific heat capacity: $c_{p.fg}$ • Velocity: $v_{fg} = \dfrac{\dot{m}_{fg}}{\rho_{fg} \cdot A_{flow.fg}}$ • Reynolds number: $\mathrm{Re}_{fg} = \dfrac{\rho_{fg} \cdot v_{fg} \cdot d_o}{\mu_{fg}}$ (3.11) • Prandtl number: $\mathrm{Pr}_{fg} = \dfrac{c_{p.fg} \cdot \mu_{fg}}{k_{fg}}$ (3.12) • Nusselt number (Zukauskus): (Using the estimated wall temperature, T_{wall}, from Equation (3.35), calculate $k_{fg.w}$, $\mu_{fg.w}$, $cp_{fg.w}$, $\mathrm{Pr}_{fg.w}$) $Nu_{conv,ext} = 0.27 \cdot \mathrm{Re}_{fg}^{0.63} \cdot \mathrm{Pr}_{fg}^{0.36} \cdot \left[\left(\dfrac{\mathrm{Pr}_{fg}}{\mathrm{Pr}_{fg.w}}\right)^{0.25}\right]$ (3.15)	**CALCULATION:** • Average temp: $T_{st.avg} = \left(T_{st.in} + T_{st.out}\right)/2$ • Steam properties (calculated using steam tables): Density: ρ_{st} Viscosity: μ_{st} Thermal conductivity: k_{st} Prandtl Number: Pr_{st} • Velocity: $v_{st} = \dfrac{\dot{m}_{st}}{\rho_{st} \cdot A_{cs.st}}$ • Reynolds number: $\mathrm{Re}_{st} = \dfrac{\rho_{st} \cdot v_{st} \cdot d_i}{\mu_{st}}$ (3.11) • Nusselt number (Dittus Boelter): $Nu_{conv,\mathrm{int}} = 0.023 \cdot \mathrm{Re}_{st}^{0.8} \cdot \mathrm{Pr}_{st}^{0.4}$ (3.14) • Heat transfer coefficient: $h_{conv,\mathrm{int}} = \dfrac{Nu_{conv,\mathrm{int}} \cdot k_{st}}{d_i}$ (3.32)

• Heat transfer coefficient: $h_{conv,ext} = \frac{Nu_{conv,ext} \cdot k_{fg}}{d_o}$ (3.33)	
SUPERHEATER RADIATION HEAT TRANSFER:	
Inputs	**Calculations**
Transverse Pitch: s_T Longitudinal Pitch: s_L Mole fraction of water vapour and tri-atomic gases: X_{H2O}, X_{CO2}, X_{SO2} Stephan Boltzmann Constant: σ_o Tube wall fouling emissivity: ε_{ash} Fuel correction coefficient: A_{fuel} Width of superheater section: b_{sh} Cavity length: L_{cavity} Mass concentration of ash in fly as composition: Y_{ash} Volume fraction of water vapour: $r_{H2O} = X_{H2O}$ Volume fraction of tri-atomic gas: $r_{SH} = \left(X_{H2O} + X_{SO2} + X_{CO2}\right)$	• Radiation thickness: $s_{SH} = 3.6\frac{d_o}{4} \cdot \left(\frac{4}{\pi}\frac{s_T \cdot s_L}{{d_o}^2} - 1\right)$ (3.18) • Radiant absorption due to tri-atomic gases: $k_g = 10\left[\frac{0.78 + 1.6 \cdot r_{H2O}}{\left(10 \cdot P_{furnace} \cdot s_H\right)^{0.5}} - 0.1\right]\left(1 - 0.37\frac{T_{fg,SH,out}}{1000}\right)$ (3.23) • Ash and slag particle concentration absorption coefficient: $k_{fa} = \frac{48350 \cdot \rho_{fg}}{\left(T_{fg,SH,out}^2 \cdot d_{fa}^2\right)^{1/3}}$ (3.22) • Gas absorption coefficient: $k_{SH} = k_g \cdot r_{SH} + k_{fa} \cdot Y_{Ash}$ (3.21) • Flue gas emissivity: $\varepsilon_g = 1 - e^{-k_{SH} \cdot P_{furnace} \cdot s_{SH}}$ (3.20) • Heat transfer coefficient: $h_{rad} = \sigma_0 \cdot \frac{\varepsilon_{ash} + 1}{2} \cdot \varepsilon_g \cdot \left[\frac{{T_{fg,SH}}^4 - {T_{SH,w}}^4}{T_{fg,SH} - T_{SH,w}}\right]$ (3.25) • Corrected heat transfer coefficient: $h'_{rad} = h_{rad}\left[1 + A_{fuel} \cdot \left(\frac{T_{fg,cavity}}{1000}\right)^{0.25} \cdot \left(\frac{L_{cavity}}{b_{sh}}\right)^{0.07}\right]$ (3.27)

OVERALL HEAT TRANSFER COEFFICIENT (HTC):	
$$U = \frac{\psi_{hx}}{\frac{1}{h_{combined,ext}} + \frac{1}{h_{conv,\text{int}}}} = \frac{0.65}{\frac{1}{h_{conv,ext} + h'_{rad}} + \frac{1}{h_{conv,\text{int}}}}$$	(3.34)[1]
LOG MEAN TEMPERATURE DIFFERENCE:	
$$\Delta T_{LMTD} = \frac{\left(T_{fg,in} - T_{s,out}\right) - \left(T_{fg,out} - T_{s,in}\right)}{\ln\left(\frac{T_{fg,in} - T_{s,out}}{T_{fg,out} - T_{s,in}}\right)}$$	(3.31)
OVERALL HEAT TRANSFER RATE:	
$$\dot{Q}_{SH} = U \cdot A_{s.fg} \cdot \Delta T_{LMTD}$$	(3.28)
WALL TEMPERAURE CHECK:	
$$T_{wall} = T_{fg.avg} - \dot{Q}_{SH}\left(\frac{1}{h_{combined,ext} \cdot A_{s.fg}}\right)$$	(3.35)

[1] It can be noted that $U_i \cdot A_i = U_o \cdot A_o$, however, $U_i \neq U_o$ since $A_i \neq A_o$ in steady state

3.4.1 Heat Exchanger Model Methodology in Flownex

This section of the dissertation details the methodology for modelling the convection pass of a once-through Benson type boiler in Flownex. Figure 23 illustrates two different configurations and flow paths, with the figure on the left (Plant A) showing four superheaters and two reheaters and the figure on the right (Plant B) showing three superheaters and two reheaters in the convection pass. These figures also present the various locations of the two attemperator valves for each plant. Steam, which is generated in the evaporator flows through the separating vessel and enters the convection pass at Superheater 1, which is a platen superheater located in the radiant zone of the boiler. Steam exits the boiler at the final superheater (Superheater 3 in Plant B and Superheater 4 in Plant A) and flows to the HP turbine. Flue gas flows from the furnace, through the convection pass towards the boiler roof and out the back pass of the boiler, resulting in cross-parallel flow heat exchanger with respect to the steam. This is due to the steam ('cooler' fluid) in the tubes flowing in a horizontal direction and the flue gas ('hotter' fluid) flowing perpendicular to the tubes as explained in Section 2.1.3.

A numerical model was initially developed in Mathcad for Plant A and was validated against actual boiler plant data. The numerical model parameters where then used to design a thermo-fluid model in Flownex, which was a representation of an actual boiler plant. One of the aims of this project was to investigate cooling down majority of the steam and flue gas temperatures higher up in the boiler rather than at the inlet of the final superheater, which is situated lower down in the convective pass. This was investigated to determine whether this concept increases the heat uptake in the convection pass, and therefore efficiency of the boiler. Therefore, once the thermo-fluid model for Plant A proved valid against actual boiler data, Plant A was converted into Plant B using the geometric parameters from Plant A and setup as shown in Figure 23. Plant B was finally used for research and investigation purposes. The main reason Plant B was configured using a cross-counter flow arrangement was to investigate Valve Position Control systems (discussed in Section 5.6) for attemperation, although other arrangements may be thermodynamically more beneficial for mechanical reasons.

The main differences between the two superheater arrangements in Figure 23 is the location of the attemperator valves and the inclusion of the platen superheater in Plant B, which was included in the Plant B model to account for furnace radiation.

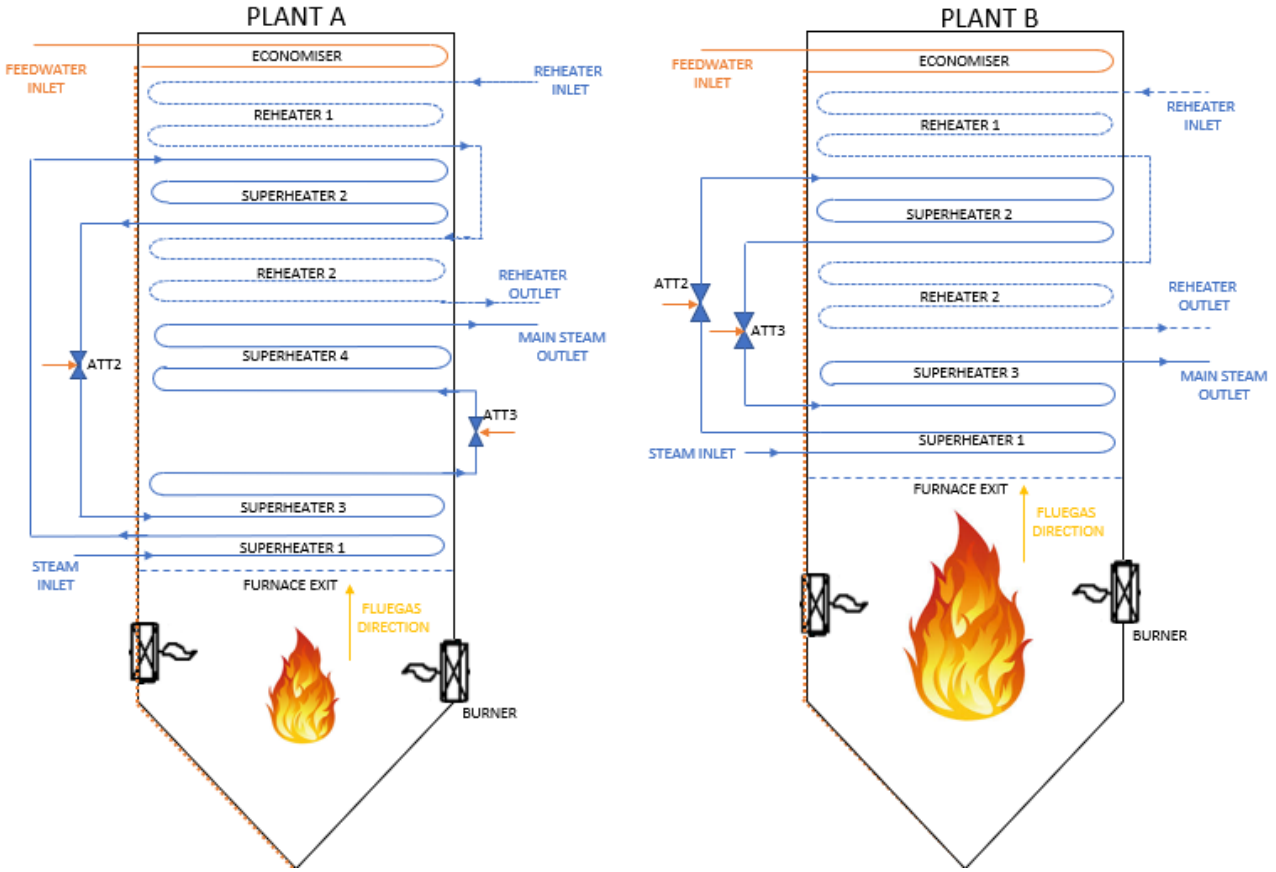

Figure 23: A simplified Benson boiler component configuration (Plant A and Plant B)

To understand the thermo-fluid design process using Flownex, a simple parallel flow heat transfer component, empirical 'flue gas path' component and steam pipe with initial boundary conditions were modelled as shown in Figure 24. A simulation was conducted by increasing the flue gas temperature at 10s and observing an increase in the outlet steam temperature. The heat is transferred from the flue gas, through the tube wall material, to the steam according to the heat transfer coefficient and surface area.

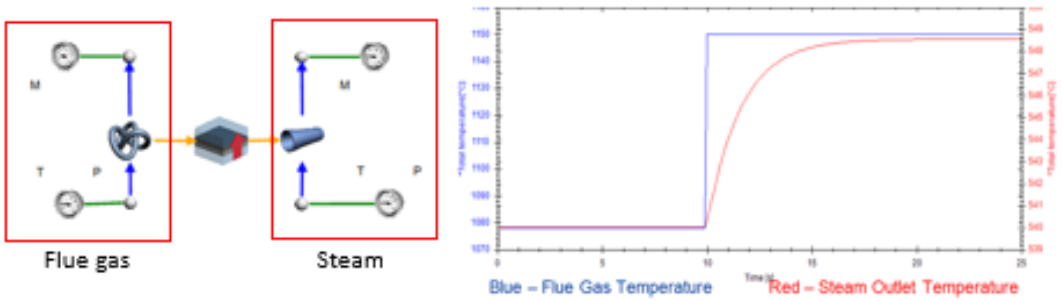

Figure 24: One Pass thermo-fluid model showing step in flue gas temperatures effect on outlet steam temperature

The following describes the input parameters required per component in a Flownex model, where upstream refers to the flue gas (FG) path and downstream refers to the steam (St) path:

Table 7: Flownex component input data

Pipe	**Heat Transfer component**	
Steam (St) Path	**Convection Upstream (FG)**	**Conduction**
Inner diameter d_i	Heat transfer coefficient (HTC) using script $h_{combined,ext}$	Upstream surface area $A_{s.fg}$
Wall thickness t_w	**Convection Downstream (St)**	Tube thickness t_w
Length of pipe L_{tube}	HTC correlation selection (Dittus Boelter) $h_{conv,\text{int}}$	Length of tube L_{tube}
Number of discretisation	Cross sectional area $A_{cs.st}$	Downstream surface area $A_{s.st}$
Number in parallel tubes N_{tube}	Hydraulic diameter d_i	**Material Data -** [27] Chromium-Molybdenum Steel
Flue Gas (FG) Path	Zero flow Nusselt number: 4.364	Capacitance $C_{material} = \rho_{material} \cdot c_{p.material} = 7840\,kg/m^3 * 0.622\,kJ/kgK = 4876\,kJ/m^3K$
Height of tube bundle L_{SH}	Transitional Reynolds number: 2300	Conductivity in element direction (35 W/m*K)
Perimeter of furnace P_{boiler}	Laminar Nusselt number: 4	Conductivity in cross direction (35 W/m*K)
Area of flue gas flow $A_{cs,fg}$	Dittus Boelter coefficients $n = 0.4$	

Once the Flownex components were defined, the model was systematically developed until a full convection pass was modelled. The next step was to include an attemperator control valve and a simple tight local loop PI controller to the one pass model to explore its applicability as shown in Figure 25. The PI controller was initially tuned using the Ziegler Nichols rules (see Section 5.4) for a quick, initial controller, testing purposes. The figure on the right illustrates the behaviour of the steam temperature and attemperation control valve as the flue gas temperature increases. It is noted that the steam temperature increases due to the increase in flue gas temperature, and gradually starts to decrease and settle at its setpoint condition as the attemperation control valve opens. The valve opening was setup to be linear to the attemperator mass flow rate and behaved as a first order system. The example below exemplifies a tight local loop controller which was setup to locally control its individual superheater attemperator valve to achieve its local outlet temperature setpoint, however real boilers have cascade control around attemperator valves or has flow control to reduce effects of valve non-linearity. The real boiler (Plant A) cascade control also includes a local controller per attemperator system within the convective pass, where each local controller cascades backwards from the final superheater in order to control the final temperature, while locally controlling its individual superheater outlet temperature according to its setpoint (see Section 5.5).

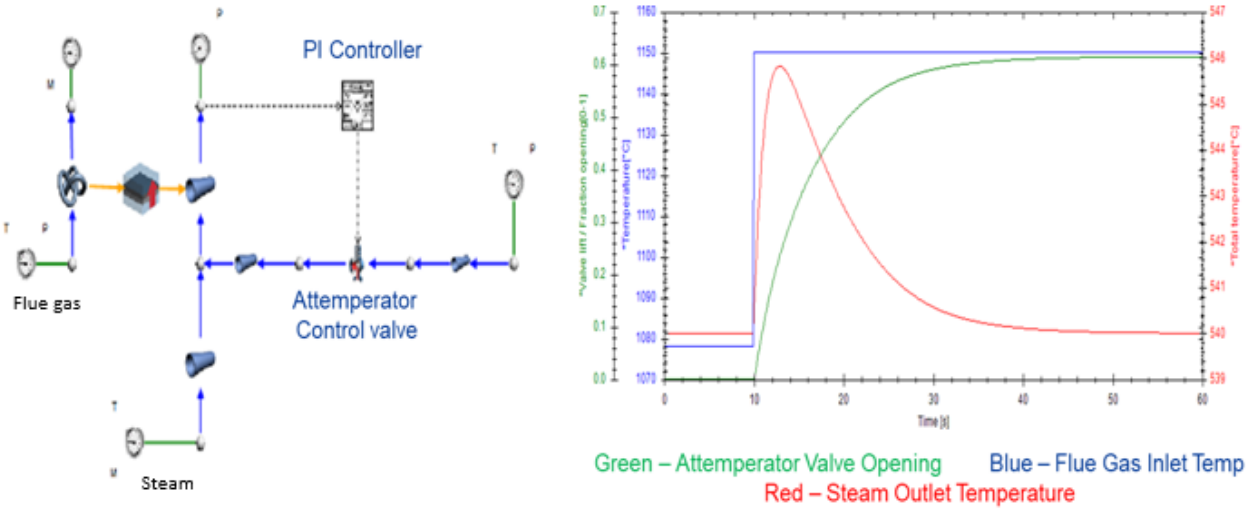

Figure 25: One pass superheater with PI controller and Attemperator valve configuration

Once the behaviour of the simple one pass thermo-fluid model was acceptable, the model was adjusted to include a two-pass configuration as shown in Figure 26, with its simulation result shown on the right. Figure 27 illustrates a comparison between the one pass thermo-fluid model and the two pass thermo-fluid model. From this figure, it can be noted that the two-pass model is more detailed due to its spatial distribution as it solves the underlying partial differential equation with better or higher resolution [43]. By dividing the pipe length and adding shorter pipes together increases the order and the model becomes more accurate, as seen at the initial disturbance point.

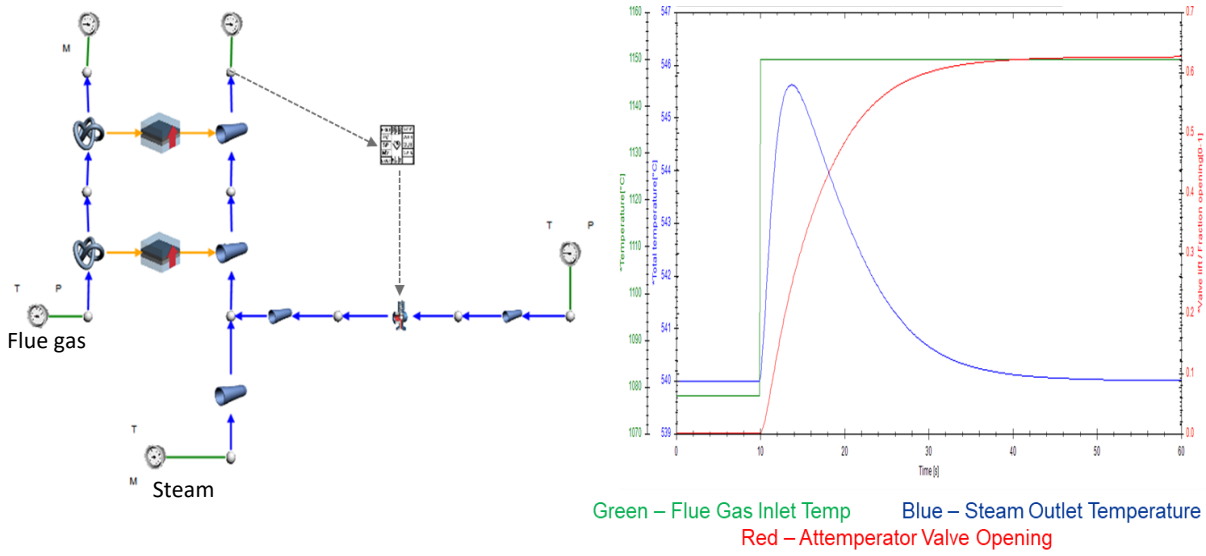

Figure 26: Two pass thermo-fluid model showing increase in flue gas temperature effect on outlet steam temperature

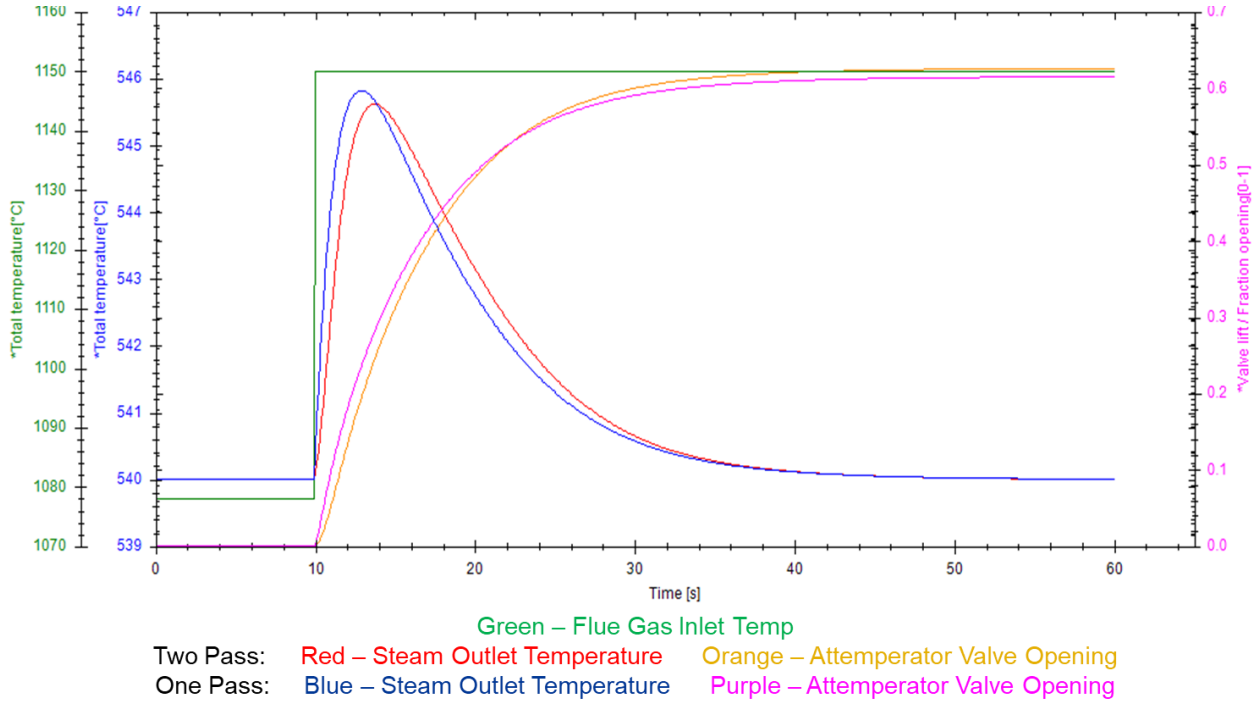

Figure 27: Comparison between one pass and two pass thermo-fluid model

A simple two pass superheater configuration was used to understand the control performance of a standard cascaded controller arrangement under varying plant conditions, where the output of the outer loop controller is the setpoint for the inner loop controller. This model included a relatively high-level approach in a cross-flow configuration. From the simulation results, it is noted that only the outer loop responds to disturbances. The faster dynamics of the inner loop minimises negative effects of the process uncertainty and any disturbance affecting the inner loop is corrected by the inner loop controller before it has an influence on the outer loop. This is explained in more detail using Figure 28 and in Section 5.3. The 'bump' midway of the simulated graph describes the contrasting behaviour between the two controllers as the signals tend to slowly change after this bump, providing steadier control of the steam temperature. This is due to the faster inner loop controller and overshoot effect that the flue gas has on the outlet temperature.

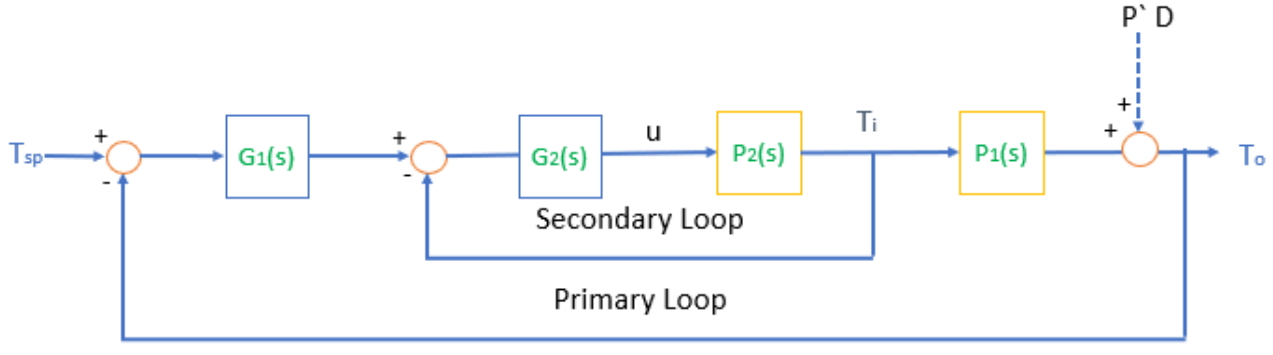

Figure 28: Cascade control system

$$T_{u/D} = \frac{G_1 G_2 P'}{1 + G_2 P_2 + G_1 G_2 P_1 P_2} = \frac{G_1 P'}{1 + G_1 P_1} \frac{1}{P_2} \text{ if} \tag{3.36}$$

$$T_o = {G_2 P_2}/{1 + G_2 P_2} \approx 1$$

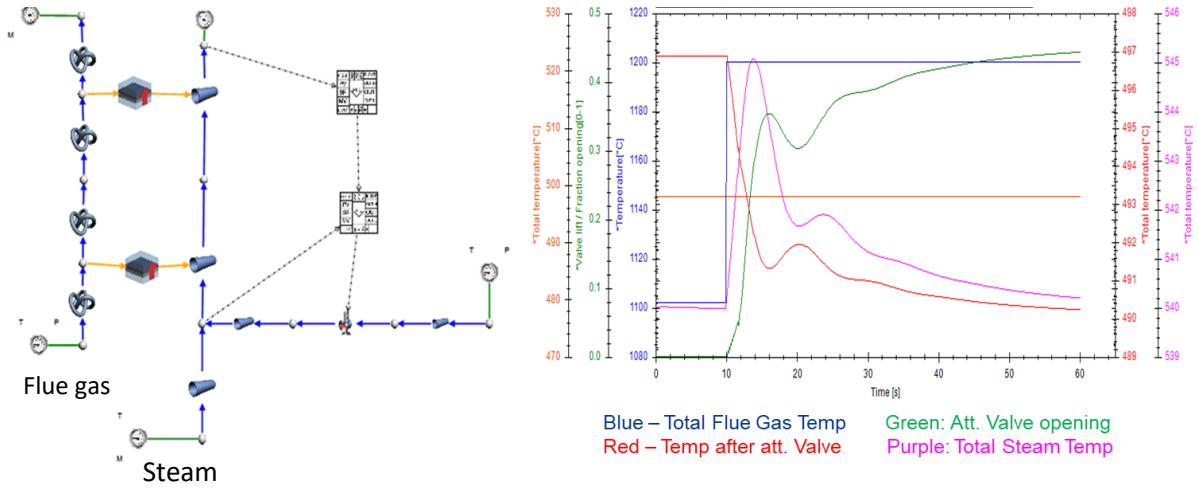

Figure 29: Cascade controller configuration showing effects of increase in flue gas temperatures

Once the Flownex components were explored using arbitrary values, a final convection pass was modelled using the variables calculated in the numerical Mathcad calculations describes above. Each superheater pass was initially modelled using boundary values for each section, and once proved viable, each section was connected sequentially to form a full convective pass design as shown in Figure 30. This final model was used to conduct tests using the various control techniques discussed in Section 1.

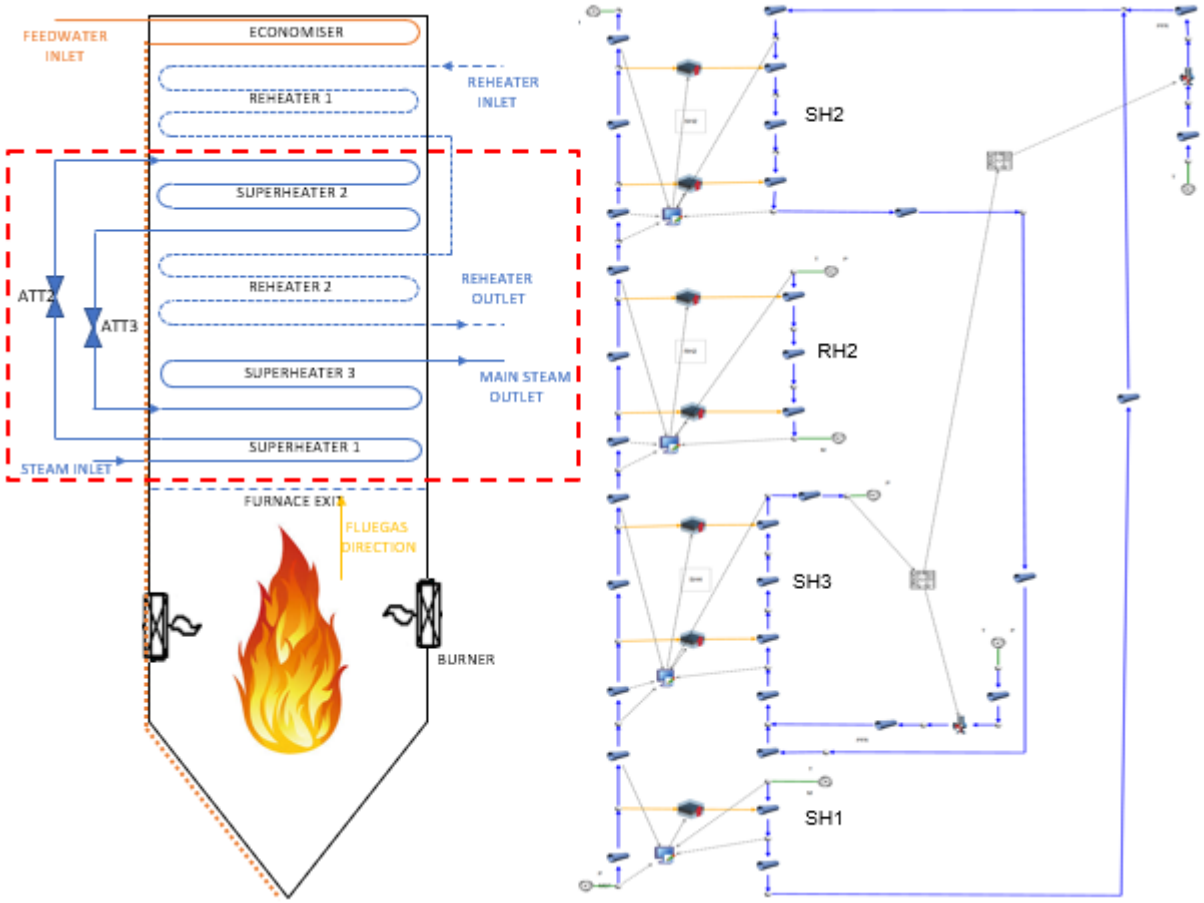

Figure 30: Final Flownex model of Plant B

From this model, it was noted that at higher loads, the temperature of the steam leaving the platen superheater is at its lowest. This is due to there being a higher steam mass flow rate at higher loads which reduces the effects of the radiant energy absorbed per kg. For convective superheaters, heat transfer is highest at higher loads because of the effect that mass flow has on the Reynolds and Nusselt numbers and finally on the heat transfer coefficient. This results in higher steam temperatures exiting each superheater as more heat energy is absorbed.

One of the requirements to adhere to while adjusting the parameters from Plant A to Plant B was the attemperator outlet temperature. It is required that this temperature stay 10°C above the saturation temperature at the attemperation pressure to ensure that there is sufficient temperature potential to convert all water droplets into superheated steam as entrained water droplets lead to water side erosion in the superheater [3].

Figure 31 summarises the methodology used to model the convection and radiation heat transfer components in Mathcad and Flownex®.

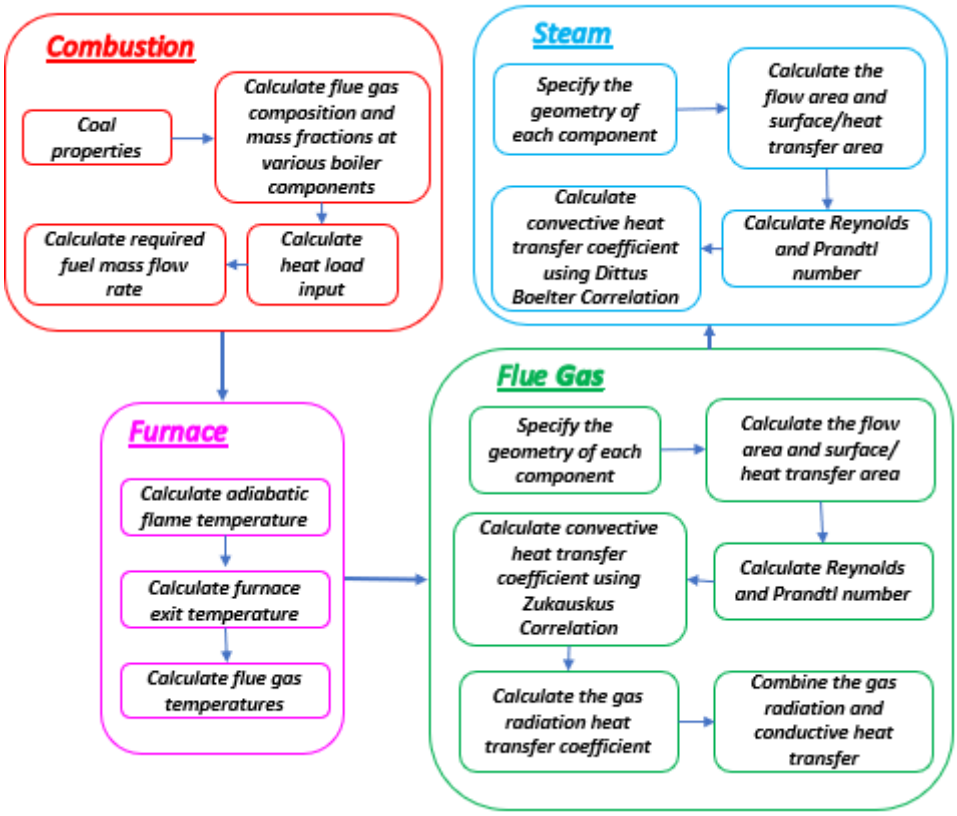

Figure 31: Summary of Flownex® methodology

3.5 Heat Transfer Results using Final Flownex Model (Plant B)

Table 8 compares the results for calculated and simulated data for the internal heat transfer convection coefficients between the wall surface and the steam for 100% MCR. The results show that the calculated results differ slightly from the simulated results, proving validity. It can be noted that the heat transfer coefficient is at its highest for the superheaters closest to the furnace, when compared to superheaters closer to the roof of the boiler.

Table 8: Plant B calculated and simulated values for internal convection heat transfer between wall surface and steam for 100% MCR

100% MCR Calculated Values									
	$d_i\,[mm]$	$\rho\left[kg/m^3\right]$	$v[m/s]$	$k[W/mK]$	$\mu[kg/ms]$	Re	Pr	Nu	$h\left[W/m^2K\right]$
SH2	29	75.3	12.7	0.1	$2.7\text{x}10^{-5}$	$1.0\text{x}10^{6}$	1.3	1626	4836.8
SH3	29	53.3	20.0	0.1	$2.98\text{x}10^{-5}$	$1.0\text{x}10^{6}$	1.1	1529	4415.7
SH1	34.5	84.5	24.9	0.1	$2.6\text{x}10^{-5}$	$2.8\text{x}10^{6}$	1.4	3798	9865.7
Simulated Values for 100% MCR									
SH2	29	66.5	12.7	0.1	$2.7\text{x}10^{-5}$	$0.9\text{x}10^{6}$	1.2	1453.3	4071.4
SH3	29	54.9	18.9	0.1	$3.0\text{x}10^{-5}$	$1.0\text{x}10^{6}$	1.1	1429.9	4179.2
SH1	34.5	75.7	30.2	0.1	$2.6\text{x}10^{-5}$	$2.8\text{x}10^{6}$	1.3	3696.4	9453.3

The values presented in Table 9 represent the simulated internal convection parameter values for 97% MCR and 70% MCR. The results show that the heat transfer coefficients are much smaller at 70% MCR when compared to 97% MCR. Superheater 1 has a 69.7% higher heat transfer coefficient than Superheater 2 for both 97% MCR and 70% MCR. The heat transfer coefficient for 97% MCR is 56.7% higher than that of 70% MCR.

Table 9: Plant B simulated values for internal convection heat transfer between wall surface and steam for 97% MCR and 70% MCR

	$\rho\left[kg/m^3\right]$	$v\left[m/s\right]$	$k\left[W/mK\right]$	$\mu\left[kg/ms\right]$	Re	Pr	Nu	$h\left[W/m^2K\right]$
97% MCR								
SH2	65.9	12.4	0.1	$2.7\text{x}10^{-5}$	$0.9\text{x}10^{6}$	1.2	1410.8	3944.1
SH3	54.6	18.5	0.1	$3.0\text{x}10^{-5}$	$0.9\text{x}10^{6}$	1.1	1989.7	4068.4
SH1	73.8	13.3	0.1	$2.6\text{x}10^{-5}$	$1.2\text{x}10^{6}$	1.3	3598.9	9081.6
70% MCR								
SH2	64.6	9.1	0.1	$2.7\text{x}10^{-5}$	$0.6\text{x}10^{6}$	1.2	1085.8	3012.4
SH3	54.2	13.4	0.1	$3.0\text{x}10^{-5}$	$0.7\text{x}10^{6}$	1.1	1072.5	3128.8
SH1	72.0	9.9	0.1	$2.6\text{x}10^{-5}$	$0.9\text{x}10^{6}$	1.3	2778.8	6928.2

Table 10 shows results for calculated and simulated data for the external heat transfer convection coefficients between the flue gas and wall surface for 100% MCR. Comparing the calculated to the simulated results shows slight differences between the Reynolds and Nusselt numbers, resulting in an average of 4% difference in the heat transfer coefficients. The results show that the radiative heat transfer coefficient for Superheater 1 and Superheater 3 dominates by more than 63%, whereas the convective heat transfer coefficient for Superheater 2 dominates by 54.4%. This is due to the high flue gas and low steam temperatures closer to the furnace flame, and cooler flue gas temperatures higher up in the convective pass.

Table 10: Plant B calculated and simulated values for external heat transfer between flue gas and wall surface for 100% MCR

	$d_o\left[mm\right]$	$\rho\left[kg/m^3\right]$	$v\left[m/s\right]$	$k\left[W/mK\right]$	$\mu\left[kg/ms\right]$	$c_p\left[kJ/kgK\right]$	Re	Pr	Nu	$h_{conv}\left[W/m^2K\right]$	$h'_{rad}\left[W/m^2K\right]$
Calculated Value for 100% MCR											
SH2	38	0.3	7.5	0.1	$4.3\text{x}10^{-5}$	1.2	1975.1	0.8	29.2	54.1	51.1
SH3	38	0.2	8.6	0.1	$5.0\text{x}10^{-5}$	1.3	1567.1	0.8	25.4	56.4	96.8
SH1	44.5	0.2	10.8	0.1	$5.5\text{x}10^{-5}$	1.3	1773.6	0.8	27.5	59.3	113.0
Simulated Values for 100% MCR											
SH2	38	0.3	7.5	0.1	$4.4\text{x}10^{-5}$	1.3	1910.6	0.8	28.5	55.7	53.6
SH3	38	0.2	8.5	0.1	$4.9\text{x}10^{-5}$	1.3	1513.5	0.8	24.7	58.1	104.9
SH1	44.5	0.2	10.8	0.1	$5.5\text{x}10^{-5}$	1.3	1803.8	0.8	27.5	59.3	117.5

Table 11 presents the simulated values for 97% MCR and 70% MCR. The convection heat transfer coefficient for 97% MCR is approximately 23.5% higher than that of 70% MCR, while the radiative heat transfer coefficient for 97% MCR is approximately 8.6% higher than that of 70% MCR. The dominating heat transfer coefficient for Superheater 1 and Superheater 3 is radiation, with a 64 – 70% lead over convection. However, for Superheater 2, convective heat transfer is slightly higher (50.7%) than radiation for 97% MCR, while radiative heat transfer leads by 52.7% for 70% MCR.

Table 11: Plant B simulated values for external heat transfer between flue gas and wall surface for 97% MCR and 70% MCR

	$\rho\left[kg/m^3\right]$	$v\left[m/s\right]$	$k\left[W/mK\right]$	$\mu\left[kg/ms\right]$	$c_p\left[kJ/kgK\right]$	Re	Pr	Nu	$h_{conv}\left[W/m^2K\right]$	$h'_{rad}\left[W/m^2K\right]$
97% MCR										
SH2	0.3	7.5	0.1	$4.4x10^{-5}$	1.3	1859.9	0.8	28.0	54.5	53.2
SH3	0.2	8.7	0.1	$5.1x10^{-5}$	1.3	1473.1	0.8	24.2	56.8	102.5
SH1	0.2	10.2	0.1	$5.4x10^{-5}$	1.3	1754.8	0.8	27.0	58.0	116.8
70% MCR										
SH2	0.3	5.2	0.1	$4.5x10^{-5}$	1.3	1459.8	0.8	24.0	43.9	49.0
SH3	0.2	6.1	0.1	$4.9x10^{-5}$	1.3	1154.2	0.8	20.8	46.0	93.9
SH1	0.2	7.1	0.1	$5.2x10^{-5}$	1.3	1369.7	0.8	23.1	47.1	107.9

3.6 Plant A Steady State Results

(*Plant A was used in this section since actual boiler data was available for comparison)

Table 12 compares the heat uptake of a real coal-fired boiler (C-Schedules [26]) to the simulated (Flownex) and calculated (Mathcad) results of the heat uptake for the final Flownex model at 100% MCR. This table shows that the result of the final Flownex model differs slightly from the real coal-fired boiler. There is a -1.5 – 6% difference between the real boiler and calculated results, and a -11 – 10.6% difference between the real boiler and simulated results for 100% MCR. From the real boiler heat uptake data, it can be noted that the radiant superheater (Superheater 3) contributes 40.9%, Superheater 4 contributes 38.9% and Superheater 2 contributes 20.1% of heat uptake.

Table 12: Heat uptake [Q`] at steady state for a real boiler (Plant A) vs simulated and calculated results for 100% MCR

	$\dot{Q}_{real}\ [MW]$	$\dot{Q}_{simulated}\ [MW]$	$\dot{Q}_{calculated}\ [MW]$
SH2	57.3	64.1	53.6
SH4	110.6	106.8	107.3
SH3	116.5	130.9	118.3

Table 13 compares the external radiative heat uptake between radiation vs external convective heat uptake for 100% and 70% MCR (Plant A). It shows that radiation dominates for superheaters located closer to the furnace by 66.1% for Superheater 3 and 63.2% for Superheater 4, while convection dominates by 51.5% for superheaters located further away from the furnace (Superheater 2). However, for the heat uptake measured for 70% MCR, it is noted that radiation dominates for all three superheaters by between 54 – 69% of the total heat uptake.

Table 13: Heat uptake for radiation vs convection for 100% and 70% MCR (Plant A) at Steady State

	100% MCR		**70% MCR**	
	$\dot{Q}_{radiation}\ [MW]$	$\dot{Q}_{convection}\ [MW]$	$\dot{Q}_{radiation}\ [MW]$	$\dot{Q}_{convection}\ [MW]$
SH2	13.3	14.1	13.0	10.8
SH4	36.2	21.1	26.5	13.4
SH3	40.2	20.6	31.5	13.9

4. Quantitative Feedback Theory

Attemperation control is the regulation of steam temperatures during on-load operation by spraying high purity water fed from the boiler feed pumps into an interconnecting steam pipe located between two superheater stages. Multistage attemperation allows spray control at multiple superheater stages. It works on the philosophy that the first stage attemperator operates initially, where the maximum spray water flow depends in the differential temperature between the spray water and steam mixture and the saturation temperature. If the outlet temperature increases with the initial attemperator fully open, the subsequent attemperators are activated.

Isaac Horowitz [28] [29] combined the revolutionary work established by Hendrik Bode, who introduced frequency-based design fundamentals, with plant model uncertainty, which later advanced into what is presently known as Quantitative Feedback Theory (QFT) [30][31]. This chapter describes the design and methodology of a single-input single-output (SISO) controller around the final superheater and follows the QFT procedure shown in Figure 32. The main objective of using QFT methodology is to design a low-order controller with minimum bandwidth to meet user defined control requirements over the whole range of plant operating conditions. Data, such as valve positions and temperatures, were extracted through several simulations using the developed Flownex® model which initiated the QFT process. This design provides a benchmark for evaluating a valve position control system proposed in Section 5.6.

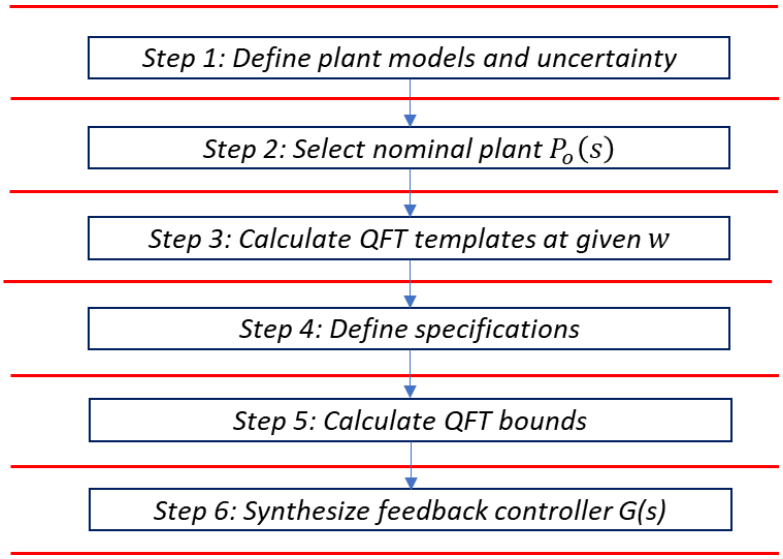

Figure 32: QFT design methodology [32]

4.1 Types of Control Methods

In control terminology for attemperation control, the actual main steam outlet temperature is referred to as the *output*. The desired main steam temperature value is referred to as the *setpoint* and the attemperation valve adjustment value for maintaining the main steam outlet temperature at the required setpoint is referred to as the *manipulated* or *control variable*. Disruptive influences such as load variations resulting in steam and flue gas temperature and mass flow fluctuations, fuel variations, and heating surface cleanliness are referred to as *disturbance*

inputs or parameter uncertainty. The controller compares the actual temperature *output* to the *setpoint* temperature and adjusts the attemperator spray water valve (*manipulated variable*) to ensure that the *output* matches the *setpoint* desired value. The following sections discuss various control systems used for attemperation control in a boiler.

4.1.1 Open Loop Controller

The simplest form of control systems is the open loop controller known as a feedforward controller illustrated in Figure 33. In this controller, the *output* temperature is not monitored, therefore the *manipulated variable* is adjusted using the *input* temperature demand signal only. This type of control generally uses a control curve expressing the attemperation valve adjustment value as a function of the boiler demand conditions. The limitation with using this type of control system is that the control curve is only accurate if the boiler conditions remain constant at the values when the initial calibration was completed. Conditions such as fouling or valve friction will offset the initial calibration.

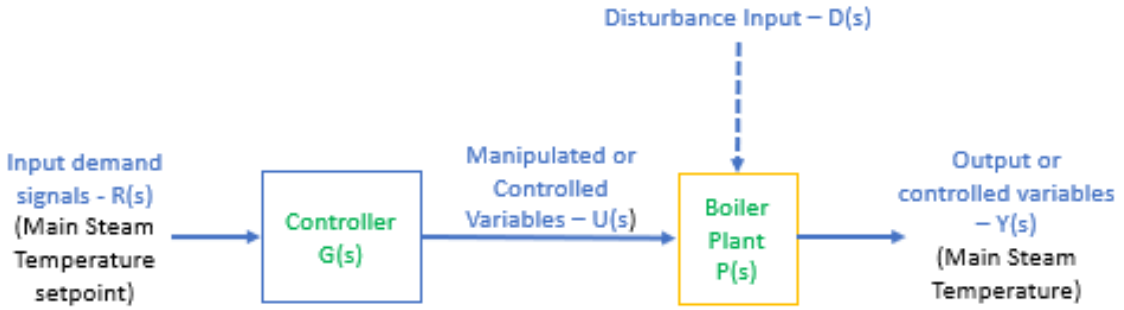

Figure 33: Open loop control system

4.1.2 Closed Loop Control

When the requirements of the control system cannot be met by an open loop system, a closed loop or feedback control is used as shown in Figure 1. In this control loop, the *output* temperature is measured and compared to the *setpoint*, with the difference between these two signals resulting in an *error* signal to try and reduce the difference to zero.

There are three types of feedback control topologies used commonly in industrial systems:

1. **Proportional Gain (P) Control**

$$G_P(s) = K_P \tag{4.1}$$

   In this method, the deviation or error of the output steam temperature to its setpoint is either proportional or inversely proportional to the *manipulated variable*, depending on the controller arrangement.

2. **Proportional Gain - Integral Time (PI) Control**

$$G_{PI}(s) = K_P + \frac{K_I}{s} = K_P\left(1 + \frac{1}{T_i \cdot s}\right) \tag{4.2}$$

This eliminates the offset by adding integral control to the proportional gain. As the name implies, integral or reset control is the repetitive integration of the error over time, thereby shifting or resetting the proportional action to allow for the *manipulated variable* to function at a new operating point.

3. Proportional-Integral-Derivative (PID) Control

$$G_{PID}(s) = K_P + \frac{K_I}{s} + K_D s = K_P\left(1 + \frac{1}{T_i \cdot s} + T_d \cdot s\right) \tag{4.3}$$

To further improve the stability and response of the system, derivative action is added. It is a function of the rate at which the output steam temperature deviates from its setpoint.

The following four characteristics describe how PID parameters affect system dynamics for closed loop systems [42]:

1. **Rise time:** The initial time it takes for the output to increase from 0 to 60% of its desired output setpoint.
2. **Overshoot:** Refers to the percentage by which the peak value exceeds the steady state value.
3. **Settling time:** The time it takes for the plant to reach steady state.
4. **Steady state error:** Refers to the amount by which the actual steady state error differs from the desired output.

By increasing each of the controller dynamics affects the system dynamics as summarised below:

Table 14: Effects of changing controller parameters has on system dynamics [33]

Response	Rise Time	Overshoot	Settling Time	Steady State Error
K_P	Decrease	Increase	No change	Decrease
K_I	Decrease	Increase	Increase	Eliminate
K_D	No change	Decrease	Decrease	No change

4.2 Robust Control Design

The key to successful control engineering projects is based on a reliable and high-performance control system design. The presence of uncertainty in a model challenges the design in practical circumstances as it is required to meet all control specifications for every plant within the uncertainty range, not just a single plant with fixed parameters. Model uncertainty is generally a consequence of unknown dynamics, inaccuracies in parameter estimation, changes in operating point, fouling conditions, errors in sensors and actuators, system non-linearities and plant disturbance input [32]. According to Borghesani [30], the two general control methodologies for dealing with the effects of uncertainty are:

(i) *Adaptive control* which is used to identify plant parameters on-line and this information is used to "tune" the controller.

(ii) *Robust control* which uses a single fixed controller to design the "worst case" approach of a plant with uncertainty. Although the controller is fixed within the robust control design paradigm, like adaptive control, there is scope for using gain scheduling, e.g. on MCR or on mass flow, to reduce the effect of uncertainty in the plant dynamics or to modify performance requirements with changing plant capability.

QFT is a robust control technique that uses integrated theory to emphasizes the use of feedback design for computing parameters for a controller while satisfying performance control specifications. QFT works on the foundation where feedback is required for plant uncertainty reduction and specifically when there are uncertain inputs (disturbances) that influence normal plant operations. It is a powerful control system design tool used to understand and improve the system dynamics, controllability and optimization by integrating model uncertainty, performance specifications and control design. Garcia-Sanz [32] describes QFT as a multi-objective frequency domain control engineering methodology that deals with various performance specifications such as stability, disturbance rejection, reference tracking and noise rejection simultaneously. The main characteristics of the designed controller is to reduce the effect of the uncertainties to an acceptable level by balancing the trade-off between controller complexity and order, cost of feedback such as bandwidths and gains, performance specifications, stability, and plant uncertainty for each frequency specified. An inverse Nichols chart is used to loop shape the frequency response according to the defined specifications.

Robust controllers were designed using QFT for Attemperators 2 and 3 to regulate the main steam temperature at 540°C. Figure 34 illustrates a one-degree-of-freedom closed loop system as using feedback allows for the desired output behaviour of the system to be specified. In Figure 34, *P*(*s*) is the uncertain plant (including actuator dynamics), *G*(*s*) is the closed loop controller and *H*(*s*) represents the dynamics of the sensor (typically, there will be some thermal inertia in measuring steam temperature due to the dynamics of the thermal well the sensor is in). The objective is to design a controller for *G*(*s*) and ensure the output *Y*(*s*) accurately tracks the input/reference demand *R*(*s*) while rejecting the disturbance *D*(*s*). The following equation is a general form of the overall first order system transfer function in which the controller needs to cater for.

$$\frac{Y(s)}{R(s)} = \frac{G(s)P(s)}{1+G(s)P(s)} = \frac{G(s)P(s)}{1+G(s)H(s)A(s)} \tag{4.4}$$

where s represents the Laplace variable. It was assumed that the sensor time constant is $\tau_{sensor} = 10s$ and that the valve time constant is $\tau_{actuator} = 10s$:

$$H(s) = \frac{1}{s \cdot \tau_{sensor} + 1} \quad \text{and} \quad A(s) = \frac{1}{s \cdot \tau_{actuator} + 1} \tag{4.5}$$

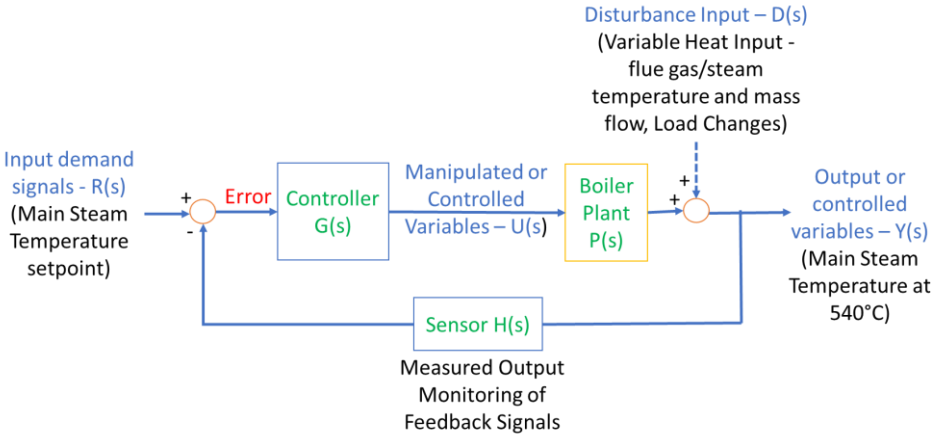

Figure 34: Feedback control system

4.2.1 Attemperator 3 SISO PI Controller Design

This section describes QFT methodology used for designing a robust SISO PI controller by conceptualizing and executing the design steps shown in Figure 32. The initial step is to define the system's open-loop model transfer function as this includes uncertainty, before generating plant templates which represent the plant's frequency response. These templates then allow QFT to generate bounds at the chosen design frequencies by converting the closed-loop magnitude specifications and phase constraints for a chosen nominal plant. The nominal plant, which is an open-loop function, is then loop shaped on an inverse Nichols chart to satisfy its bounds while achieving closed loop stability. An example code used in Matlab is shown in APPENDIX A.

Step 1: Define plant models and uncertainty

The design process began by defining the plant or system using open-loop dynamics, which can either be fixed, or include plant uncertainty. In order to fully understand the potential and limitations of a system, an extensive model of open-loop plant dynamics is required to design a reliable control system to meet specifications.

Pre-processing data:

Various disturbances were simulated in the Flownex Plant B model by changing the Attemperator 3 valve position at each defined MCR (100%, 97% and 70%) and monitoring its respective dynamic effects on the input and output temperature profiles of the final superheater. This data was then compiled and exported to MATLAB®, where the raw datasets were pre-processed to remove unwanted data and signal offsets (using the *mean* command), ensuring an efficient analysis to be conducted. The cleaned data was then used to identify the transfer functions for each dataset using the System Identification (ID) Toolbox, which constructs mathematical models of dynamic systems from defined input-output data using a nonlinear least squares algorithm [1]. This was done using the *iddata* command, which is a standard command for managing data in the System ID Toolbox as it creates a data object to encapsulate the input/output datasets and sample time. A total of 6 disturbances to the system were simulated, with the change in Attemperator 3 valve position defined as the input and the corresponding change in output steam temperature defined as the output. The dataset consisted of 3001 samples, with a sample time of 0.1 seconds and a total measurement time of 5 minutes. A model that captures the dynamics of a plant is a function of the input $(u(s))$ to output $(y(s))$ transfer functions in the Laplace domain $P(s)$. Figure 35 illustrates the time plot of the input (u1)

vs output (y1) of the processed dataset exported to the System ID Toolbox. For a practical plant design, other operating conditions would need to be added to the plant set to capture the uncertainty envelope of the plant.

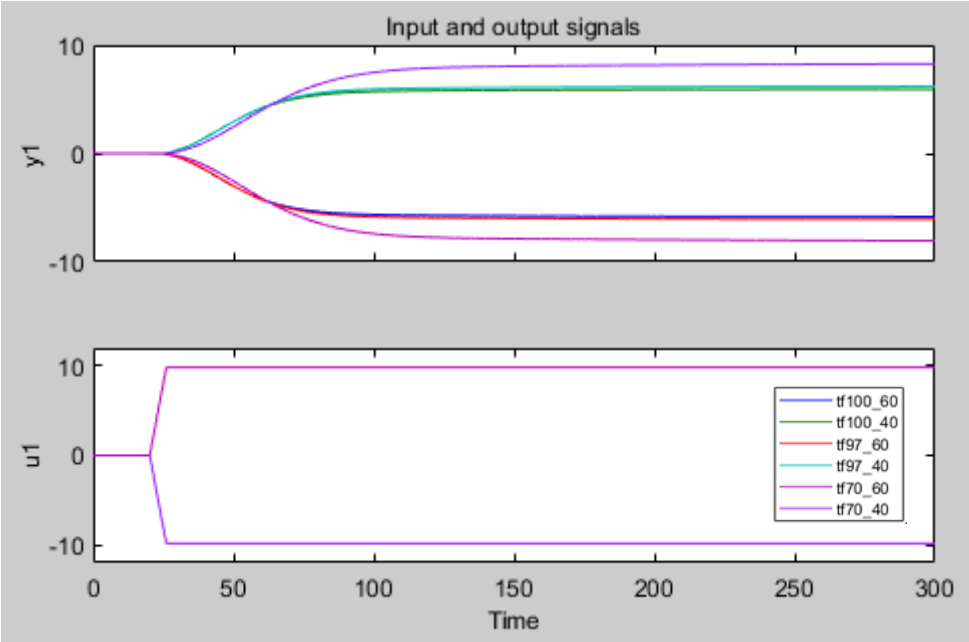

Figure 35: Output steam temperature (y1) vs input valve position (u1) dataset time plot over different MCR values

The following equations are the second order transfer functions modelled using system identification for a 10% change in valve position at the mentioned loads vs. output temperature (%/°C). These open loop transfer functions define the plant models with uncertainty. Each transfer function was identified as continuous time transfer functions, with two poles (located on the left side of the complex plane) and one zero and a fit to estimation data at ± 97%, which implies model stability.

Table 15: Transfer function [%/°C] defined using System Identification Toolbox

MCR (%)	Transfer function for a 10% increase in valve position	Transfer function for a 10% decrease in valve position
100	$P_{100\_60}(s)=\frac{0.0071s-0.0028}{s^2+0.1292s+0.0048}$ (4.6)	$P_{100\_40}(s)=\frac{0.007s-0.0027}{s^2+0.1267s+0.0045}$ (4.7)
97	$P_{97\_60}(s)=\frac{0.0073s-0.0028}{s^2+0.125s+0.0045}$ (4.8)	$P_{97\_40}(s)=\frac{0.0073s-0.0027}{s^2+0.1227s+0.0043}$ (4.9)
70	$P_{70\_60}(s)=\frac{0.0092s-0.0021}{s^2+0.0923s+0.0026}$ (4.10)	$P_{70\_40}(s)=\frac{0.009s-0.002}{s^2+0.0894s+0.0024}$ (4.11)

It can be noted from Figure 36 that the identified models have non-minimum phase behaviour as a result of process delay. This causes the underlying distributed parameter system to search for a finite order linear model. The non-minimum phase behaviour imposes technical limits on the feedback bandwidth and input limitations which also impose practical performance limits on the control design.

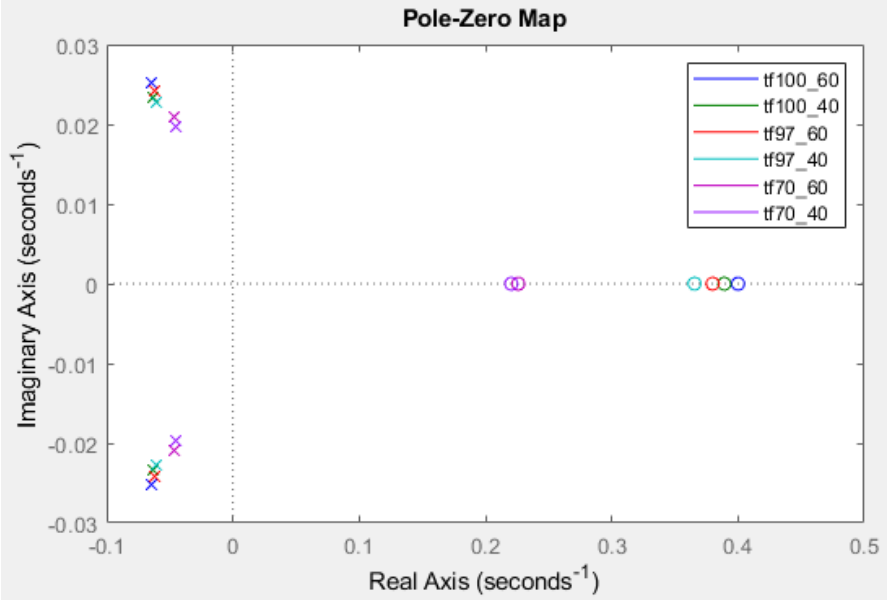

Figure 36: Zero and Poles plot for selected transfer functions[2]

Once the transfer functions are defined and analysed in the System ID Toolbox, a list of the model parameters and associated uncertainties were analysed using the *getpvec(SYS)* command. These parameters were then used to design the QFT controller for all plant cases.

Step 2: Select a nominal plant

In QFT design, time domain specifications are converted into frequency domain specifications by substituting $s = j\omega$, therefore the *nominal* plant, $P_o(j\omega)$, is an arbitrary, fixed plant within model uncertainty. Any plant can be selected as the nominal open loop frequency response $L_o(j\omega) = P_o(j\omega) \cdot G(j\omega)$, and is defined using the *nompt* command in Matlab. The nominal plant chosen for this design was *nompt = 5*, which translates into $P_o(j\omega) = P_{97\_60}(j\omega)$ as presented in equation (4.8).

Step 3: Templates

Plant templates are derived from the magnitude and phase plot of the parametrically uncertain plant set of transfer functions $P(j\omega)$ projected onto the inverse Nichols chart. Templates are a collection of the plant's uncertain

[2] Imaginary axis scale is much smaller than real axis

frequency response at a selected design frequency, ω_i, and characterise the plant parameter's uncertainty region at that frequency. Templates are required for calculating the bounds. Prior to obtaining the templates, an array of frequencies needs to be selected from inspection of the bode plot for each plant within the uncertainty. For frequency analysis, $s = j\omega$ is substituted into equations (4.6) - (4.11) to obtain the sinusoidal transfer function, where $\omega[rads/s]$ represents the frequency response set of the uncertain plant [30]. From Figure 37, the low pass design frequency array selected to adequately cover the system were based on the performance bandwidth and templates shape and were chosen as $\omega = [0.0003, 0.001, 0.01, 0.02, 0.03, 0.04, 0.06, 0.08, 0.1]\ rad/s$, resulting in 9 uncertain templates. Since bounds change as the shape of the template change for the same specification [30], the chosen frequencies were focussed around the area where the shape of the template varied significantly in Figure 38. It is important to select ω_i according to frequencies required for the design, i.e. low frequencies for performance, mid frequencies for gain cross-over and high frequencies for robust stability. The uncertainty region is marked with translucent lines, one on either side of the nominal model curve with the same colour as the curve.

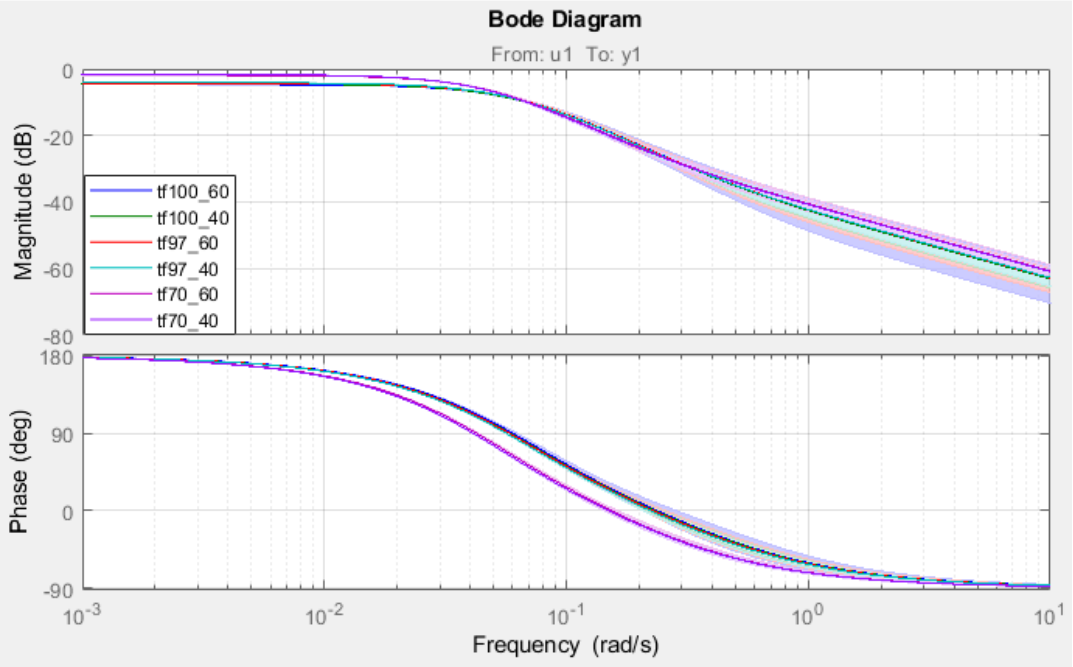

Figure 37: Magnitude (dB) and phase Bode plot showing confidence region for all plant sets

The plant templates are then plotted for each plant set with its uncertainties as shown in Figure 38, using the following command: $plottmpl(w, P, nompt) = plottmpl(\omega, P, 5)$. It can be noted from this figure that at low frequencies, the templates appear as vertical lines, and become wider and more spaced out at middle frequencies, and generally become vertical again at high frequencies. This helps specify on the range of design frequencies.

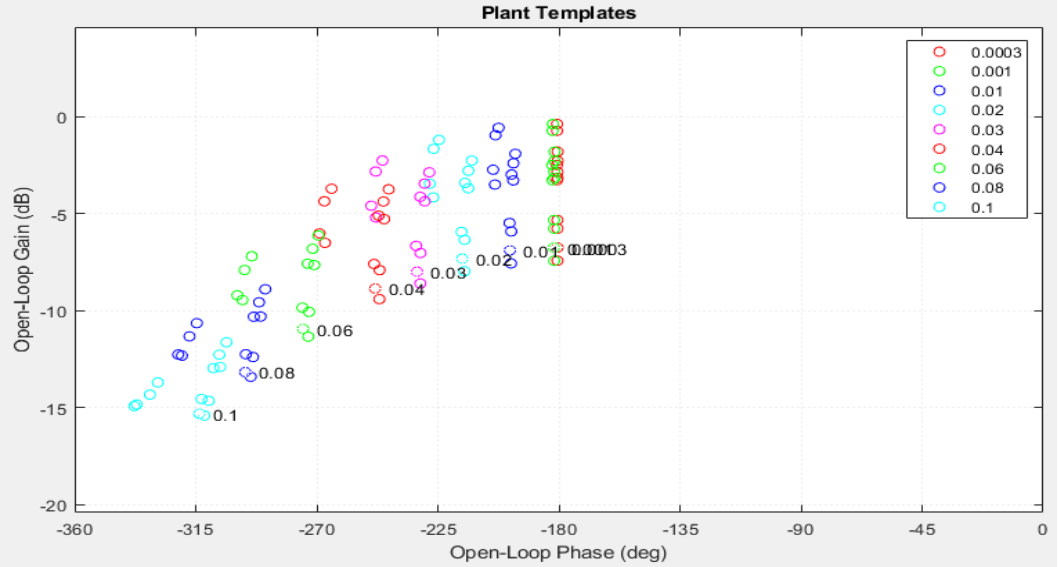

Figure 38: Plant templates for all plant sets

Step 4: Performance specifications

Once the templates are defined at the respective frequencies, the nominal open-loop function in QFT is used to transform the closed-loop magnitude specification into magnitude and phase constraints, which are known as QFT bounds. In general, each specification is expressed as:

$$\left|T_k\left(j\omega_i\right)\right| \le \delta_k\left(\omega_i\right) = Ws_i \tag{4.12}$$

Table 16 defines the closed-loop performance specifications, where the sensitivity weight, Ws_i, defines the specification required for the transfer function magnitude, where $ptype = i$ describes the required specification. It is noted that when calculating the controller bounds, $F = 1$ (pre-filter).

Table 16: Single-loop specification types [30]

Specification	Application Example	*ptype* notation
$\left\|F\dfrac{PGH}{1+PGH}\right\| \le Ws_1$	Gain and phase margins (with sensor dynamics)	1
$\left\|F\dfrac{1}{1+PGH}\right\| \le Ws_2$	Sensitivity reduction	2
$\left\|F\dfrac{P}{1+PGH}\right\| \le Ws_3$	Disturbance rejection at plant input	3
$\left\|F\dfrac{G}{1+PGH}\right\| \le Ws_4$	Control effort minimisation	4

$\left\lvert F\frac{GH}{1+PGH}\right\rvert \le Ws_5$	Control effort (with sensor dynamics)	5
$\left\lvert F\frac{PG}{1+PGH}\right\rvert \le Ws_6$	Tracking bandwidth (with sensor dynamics)	6
$Ws_{7a} \le \left\lvert F\frac{PG}{1+PGH}\right\rvert \le Ws_{7b}$	Classical 2-DOF QFT tracking problem	7
$\left\lvert F\frac{H}{1+PGH}\right\rvert \le Ws_8$	Rejection of disturbances at plant output (with sensor dynamics)	8
$\left\lvert F\frac{PH}{1+PGH}\right\rvert \le Ws_9$	Rejection of plant input disturbances (with sensor dynamics)	9

Step5: Bounds

QFT integrates model uncertainty and control specifications into a set of curves called *bounds*. The bounds provide the magnitude and phase constraints in which the closed loop system lie outside the bounds such that the desired process performance specifications are attained. It can be noted that there is a bound $B_k(\omega_i)$ for each frequency defined by ω and for each performance specification. Each bound, which is equivalent to the bound for $G(j\omega)$, shifts vertically according to $\left\lvert P_o(j\omega)\right\rvert$ and shifts horizontally by $\angle P_o(j\omega)$. The generic function used for computing the single-loop bounds is: $bdb = sisobnds(ptype, w, Ws, P, R, nompt) = sisobnds(2, \omega, W2, P, 0, 5)$, where the performance weight is $W2 = 10.^{\wedge}\left([6, -20, 6, 6, 6, 6, 6, 6]/20\right)$. The argument *loc* was omitted from the *bdb* command as its default value is *loc = 1*, indicating that the controller is located in the forward path *G*(*s*), rather than in the feedback path *H*(*s*), where in this case *loc* = 0. The argument *R* in the *bdb* command is only used for instances where a disk radius is applicable, therefore *R=0*. The bounds are then plotted using the following command *plotbnds(bdb)*, as shown in Figure 39.

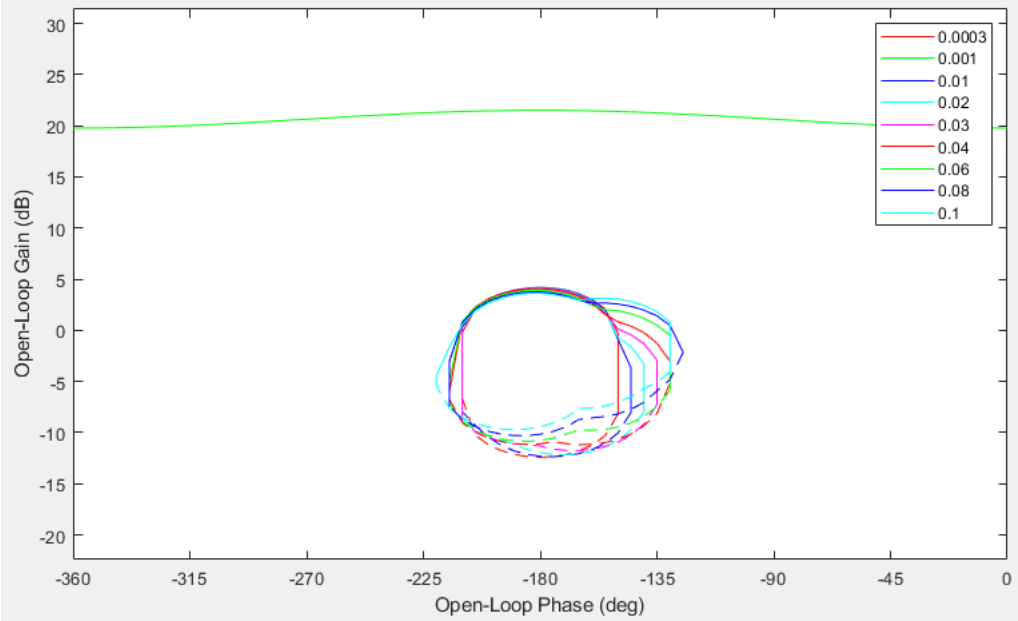

Figure 39: Attemperator 3 Bounds

If there are tracking specifications, these could be above and below bounds on the magnitude of (1) or tracking error bounds compared to model behaviour. For the purpose of illustration here, we are only considering regulation via bounds on the closed loop sensitivity [32]:

$$zero\ steady\ state\ error \tag{4.13}$$

$$\left|T_2(j\omega)\right| = \left|\frac{1}{1+L(j\omega)}\right| \le -20\text{dB},\ \ \omega \le 0.001\text{rads/s} \tag{4.14}$$

$$\left|T_2(j\omega)\right| = \left|\frac{1}{1+L(j\omega)}\right| \le 6\text{dB},\ \forall\,\omega \tag{4.15}$$

Transfer of disturbances (flue gas temperature and mass flow rate changes) are generally $P'/(1+L)$ where P' represents the open loop effect. The disturbance $d_o(j\omega)$ affects the output of the plant $y(j\omega)$ through the transfer function $T_2(j\omega)$, and is limited by the sensitivity specification:

$$\left|T_2(j\omega)\right| = \left|\frac{y(j\omega)}{d_o(j\omega)}\right| = \left|\frac{e(j\omega)}{d_o(j\omega)}\right| = \left|\frac{e(j\omega)}{r(j\omega)}\right|$$

The sensitivity specification was defined for middle to low frequencies as it rejects the disturbances that directly affect the output of the plant, which is the objective of the controller. By rejecting the high-frequency disturbances reduces the potential of having mechanical fatigue problems. (This is a short-cut to PI and PID design which is quite typical in practice – a robust stability margin was designed and maximized the low-frequency performance with steady state error with a low order controller within this constraint. More detailed control specifications can be accommodated easily.)

Step 6: Loop shaping

After computing the performance and stability bounds, the next step is to design, or loop shape the nominal plant to meet its bounds. The open loop robust stability bounds for all frequencies ω can be seen in Figure 39. Once the bounds are plotted on the Nichols chart, the controller $G(s)$ is designed by loop shaping the nominal plant to satisfy the nominal bounds. However, if the nominal plant satisfies the nominal bounds, the design specifications will be satisfied for all plant cases. The nominal plant is only required for loop shaping since the various plant uncertainties and specifications have been integrated into the QFT bounds. The following command is used in Matlab to perform the loop shaping design: $lpshape(\omega, bnd, P(1,1,5))$.

It is important that the nominal plant is loop shaped to the correct area for each frequency. Loop shaping includes shaping the frequency response of the nominal loop such that the magnitude and phase of $L_o(j\omega)$ lies outside the robust performance bounds for each ω. The solid lines in Figure 40 denotes that L_o is to 'lie on or above' and a dashed lines denotes that L_o is to 'lie on or below' the bound of that frequency. Horowitz explained that an optimum controller design, with respect to minimal high frequency controller gain, is when $L_o(j\omega)$ is placed on top of each bound $B_k(\omega)$ for each frequency ω [32]. This provides the minimum possible controller magnitude (cost of feedback) at each frequency ω [32]. The objective of loop shaping is to obtain closed-loop stability. This is done by moving each small circle which represents a specific frequency within ω until it meets its respective bound condition. This can be done by following the loop shaping procedure below.

1. The objective is to design a controller on the inverse Nichols chart from low to high frequency so that each frequency ω_i lies on, above or below its corresponding bound.
2. Choose a sign for the proportional gain of $G(s)$, where a sign depends on the sign of the plant $P_o(s)$. The gain was tuned with a negative sign to allow $L_o(s)$ to meet the lower frequency bound since the plant produces a negative error for attemperation.
3. An integrator was added to accommodate for zero steady state error for step reference input.
4. Starting from the low frequency, a real zero (z) was added to move $L_o(s)$ to the right, and two real poles (p) were added to move $L_o(s)$ to the left of the Nichols chart and account for the sensor and valve dynamics.

The controller designed for this plant in shown in Figure 40 and follows the standard gain (k) – zero (z) structure:

$$G_{PI}(s) = \frac{k \cdot \left((s/z_1)+1\right)}{s} = \frac{-0.02412 \cdot \left((s/0.03714)+1\right)}{s} \tag{4.16}$$

where $k = -0.02412$ and $z_1 = 0.03714$. Once the loop shaping criteria is met, a PI controller was designed in standard form where K_P is the proportional gain term and T_i is the integral time constant:

$$T_i = \frac{1}{z_1} = \frac{1}{0.03714} = 26.93s \tag{4.17}$$

$$K_P = k \cdot T_i = -0.0241 \cdot 26.93 = -0.65 \tag{4.18}$$

Therefore, the overall PI controller for Attemperator 3 valve is:

$$G_{PI}(s) = K_P \cdot \left(1 + \frac{1}{T_i \cdot s}\right) = -0.65 \cdot \left(1 + \frac{1}{26.93s}\right) \tag{4.19}$$

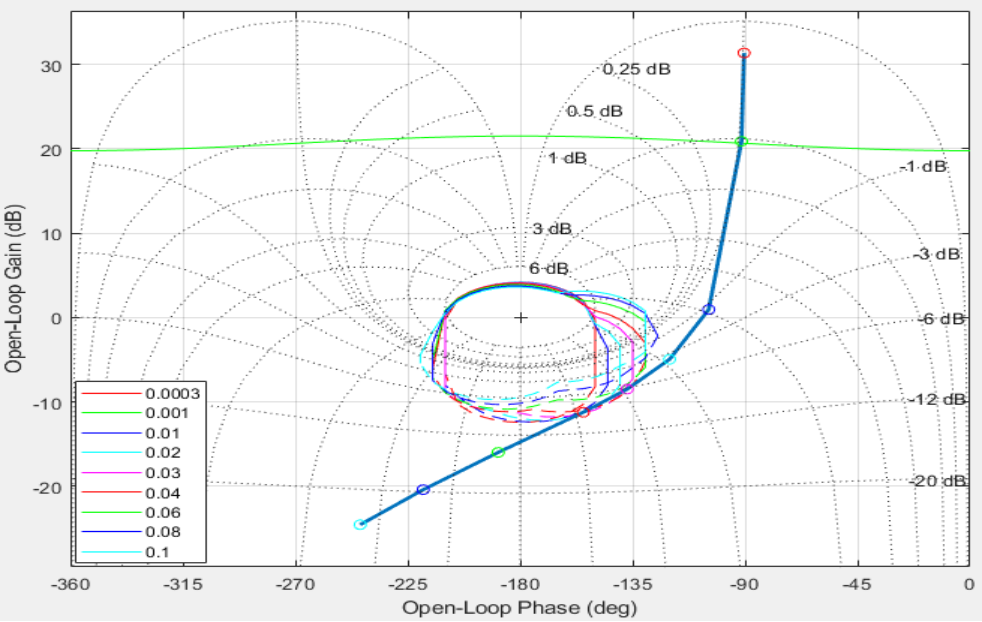

Figure 40: Loop shaping of $L_o(s)$ for Attemperator 3 valve

Equation (4.20) represents the Attemperator 3 controller settings currently used in Plant A. It is noted that equation (4.19) has a smaller proportional gain and a slightly larger integral term when compared to equation (4.20), resulting in a smaller change in output per change in error.

$$G_{att3} = -0.9 \cdot \left(1 + \frac{1}{22s}\right) \tag{4.20}$$

Figure 41 represents the open loop nominal bode plot, L_o, showing magnitude phase, and its respective gain margin and phase margin at their crossover frequencies. The result indicates that for system L_o, a gain variation of over 14.7dB at the gain crossover frequency of 0.0546 rads/s would cause the system to be unstable. Figure 42 represents the closed loop bode plots for $1/(1+L_o)$ and $L_o/(1+L_o)$, showing its magnitude only

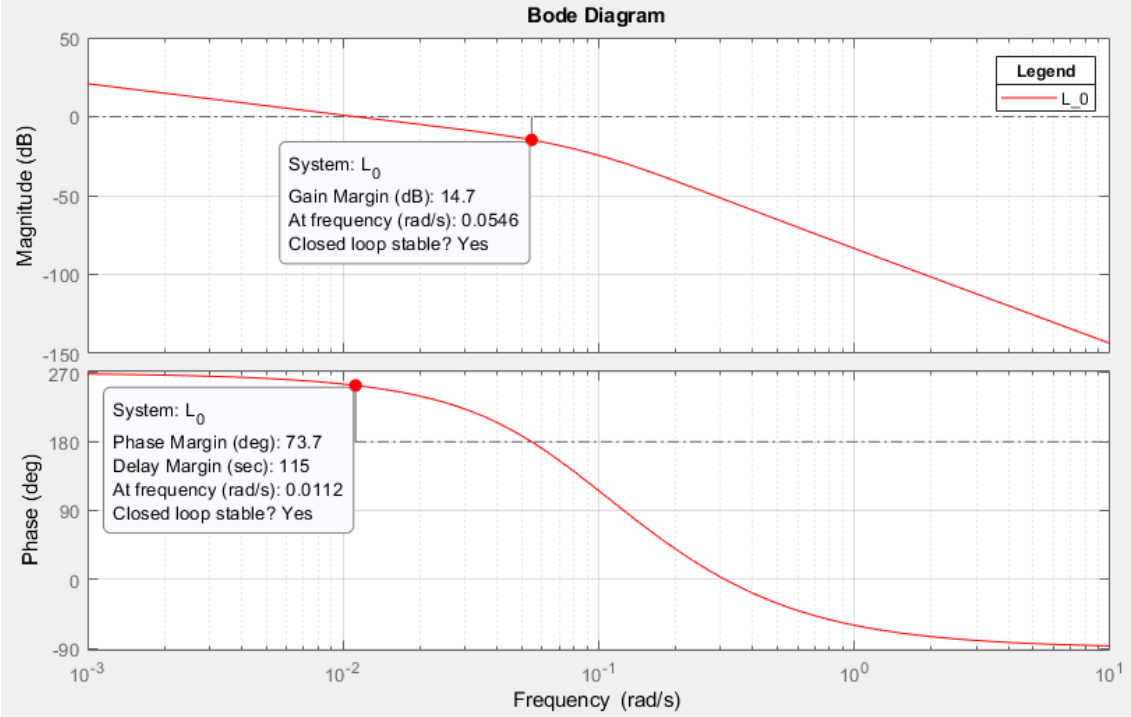

Figure 41: Open loop nominal bode plot showing gain and phase margins

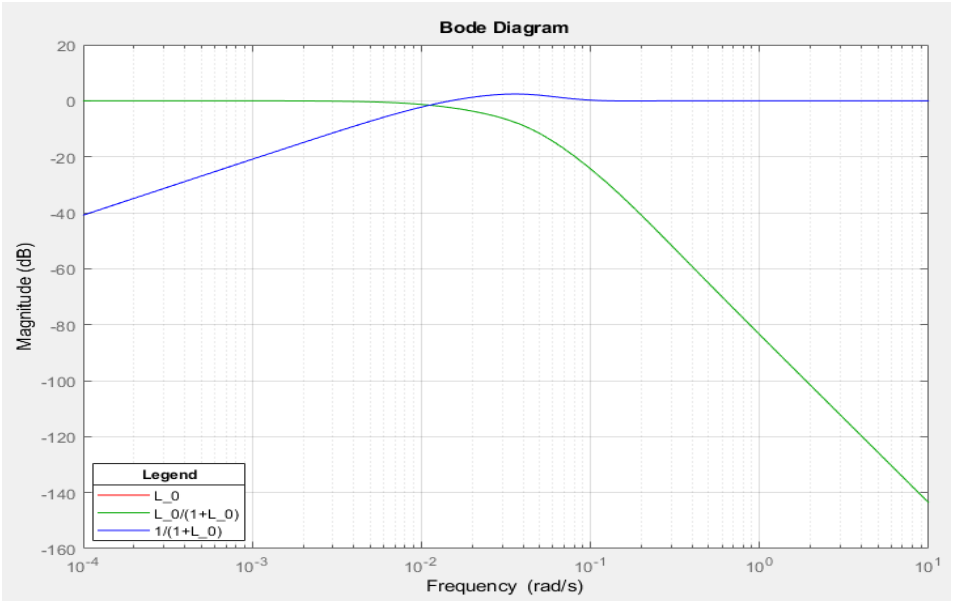

Figure 42: Controller design bode plot showing gain and phase margins

4.2.2 Attemperator 2 SISO controller design

Once the controller for Attemperator 3 was designed and implemented, a SISO controller was designed for Attemperator 2 valve using the QFT design methodology mentioned above and this design is summarised in Figure 43.

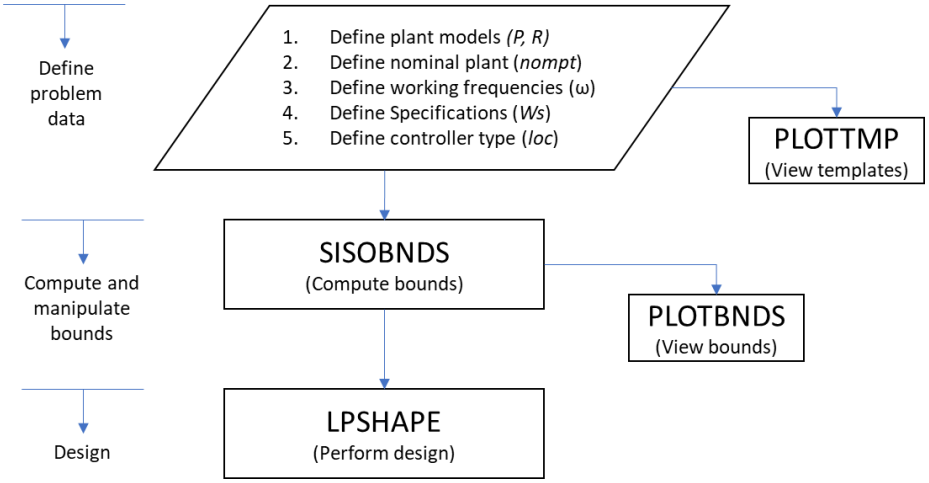

Figure 43: QFT design flow chart

Attemperator 2 valve regulates the Superheater 2 steam temperature, by injecting spray water at the inlet of the steam path, thus combining with the steam entering the superheater and cooling down the outlet steam. This dataset included a transient simulation of a 10% increase and decrease of attemperation 2 valve position as the input, and the corresponding Superheater 2 output steam temperature. Once the transients were completed for all MCR scenarios, data was imported to Matlab, where it was pre-processed before identifying the transfer functions for each plant system. The following describes the plant templates, bounds and loop shaping design for the Attemperator 2 valve controller in Matlab. Figure 44 illustrates the input (valve position (%)) and output (Superheater outlet steam temperature (°C)) signals which were pre-processed to remove offsets and unwanted data before the data object can be exported to the System ID toolbox.

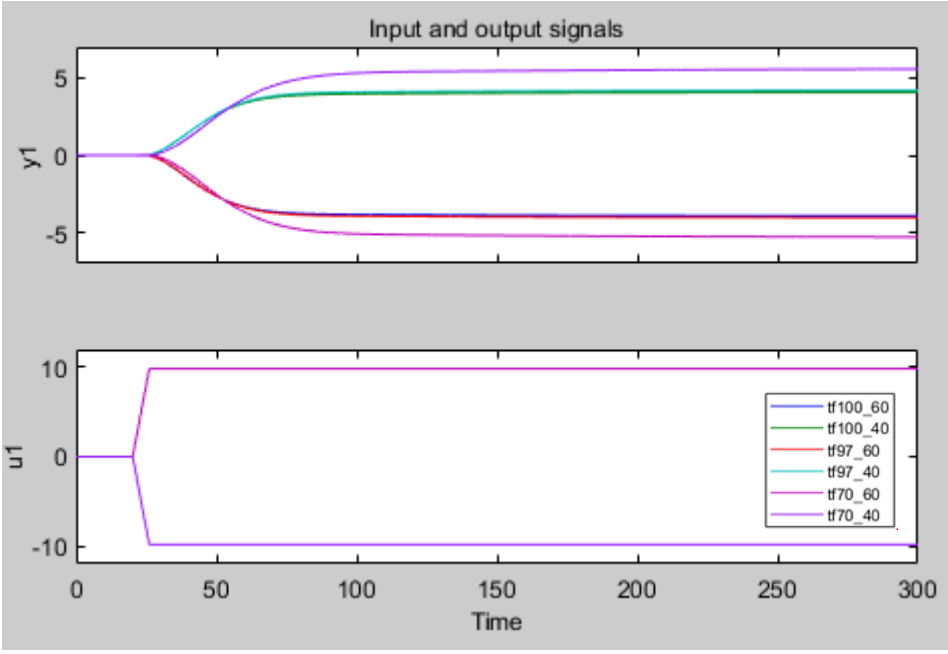

Figure 44: Time plot of input and output signals for Attemperator 2 SISO controller design

Comparing Figure 44 to Figure 35, for the same change in attemperator valve position, it is noted that change in output steam temperature for Superheater 2 is much smaller than for Superheater 3. This could be due to Superheater 2 having lower steam and flue gas temperatures, as well as smaller surface area for both steam and flue gas heat transfer. The transfer functions for the various plants were defined as:

Table 17: Transfer functions for 100%, 97% and 70% MCR in [°C/%]

MCR (%)	Transfer function for a 10% increase in valve position	Transfer function for a 10% decrease in valve position
100	$P_{100\_62}(s)=\frac{0.0081s-0.0033}{s^2+0.1757s+0.0085}$ (4.21)	$P_{100\_42}(s)=\frac{0.0075s-0.0032}{s^2+0.1691s+0.0077}$ (4.22)
97	$P_{97\_62}(s)=\frac{0.0082s-0.0032}{s^2+0.1703s+0.008}$ (4.23)	$P_{97\_42}(s)=\frac{0.0079s-0.0032}{s^2+0.1668s+0.0075}$ (4.24)
70	$P_{70\_62}(s)=\frac{0.01s-0.0025}{s^2+0.1293s+0.0048}$ (4.25)	$P_{70\_42}(s)=\frac{0.0095s-0.0024}{s^2+0.1235s+0.0043}$ (4.26)

From Figure 45, the design frequencies were chosen as:

$\omega=[0.003, 0.001, 0.01, 0.02, 0.03, 0.04, 0.06, 0.08, 0.1]\ rads/s$.

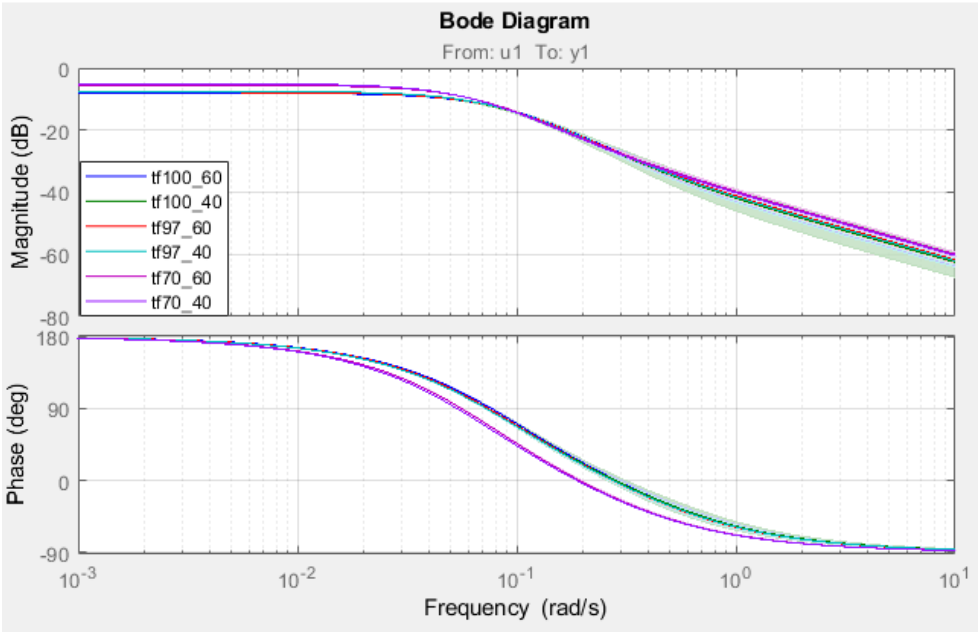

Figure 45: Magnitude (dB) and phase Bode plot showing confidence region for all plant sets

Figure 46 illustrates the zeros and poles map of the transfer functions, where the zeros lie on the right-hand plane.

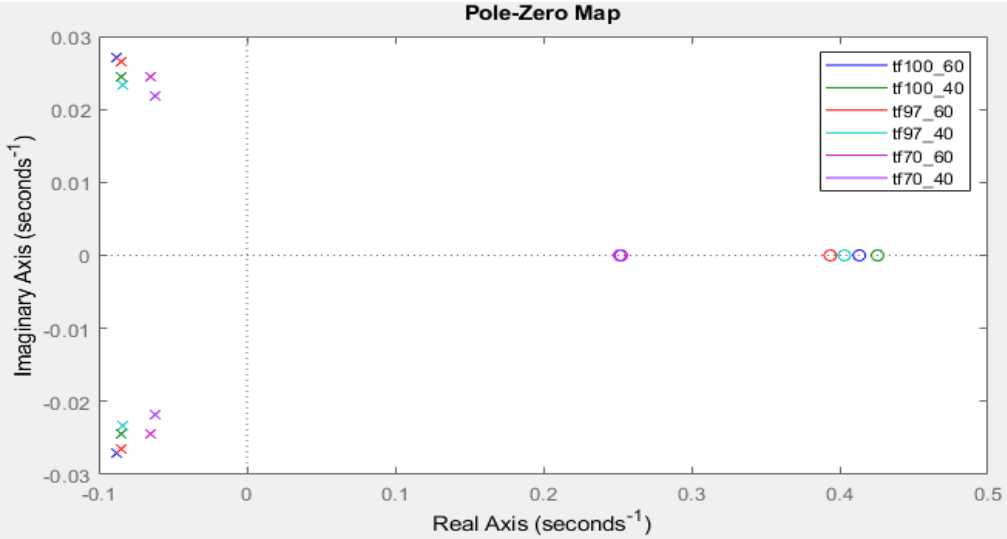

Figure 46: Zero's (o) and poles (x) for all plant sets[3]

Figure 47 represent the plant templates for each working frequency defined above. The open-loop gain for the plant templates for Superheater 2 appear to be about -4dB lower than that of Superheater 3 and more spread out when comparing Figure 47 to Figure 38.

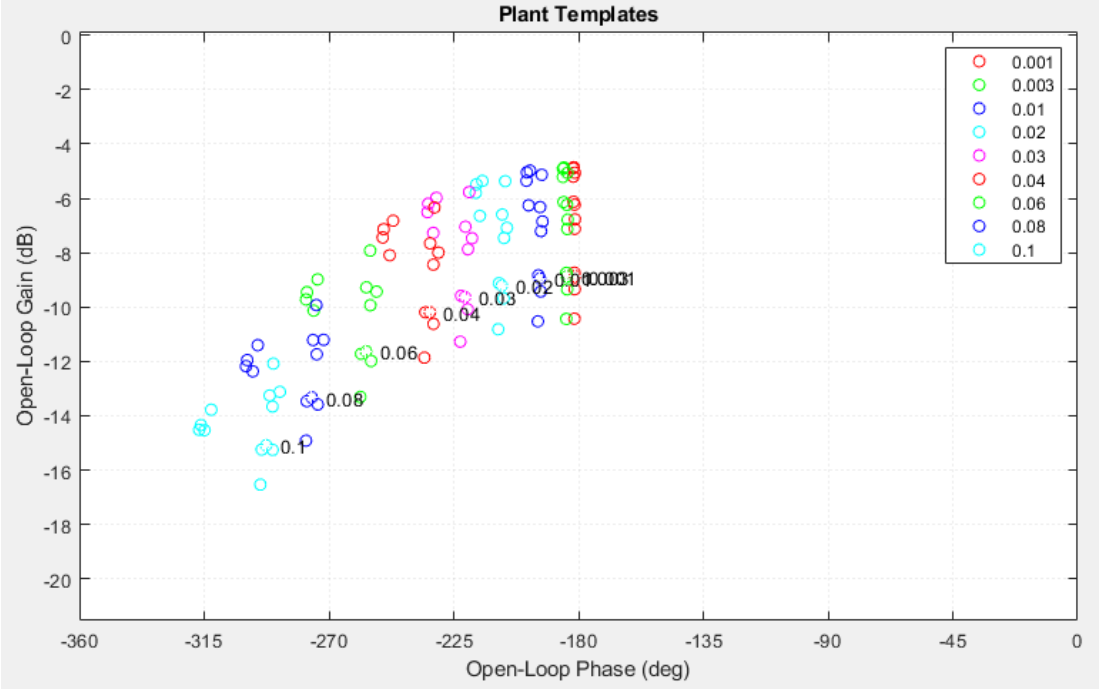

Figure 47: Plant templates for all frequencies

According to Figure 48, the Attemperator 2 valve controller was then designed with a sensitivity weight of -3dB for all frequencies (except $|T_2(j\omega)| \leq -20\text{dB},\ \omega \leq 0.001\text{rads/s}$), as $k = -0.02401$ and $z_1 = 0.04132$, resulting in the overall PI controller being calculated as:

[3] Imaginary axis scale is much smaller than real axis

$$G_{PI}(s) = K_P \cdot \left(1 + \frac{1}{T_i \cdot s}\right) = -0.58 \cdot \left(1 + \frac{1}{24.2s}\right) \tag{4.27}$$

The controller in equation (4.27) is comparable to the following settings on Plant A, although the gain is slightly lower:

$$G_{att2} = -0.9 \cdot \left(1 + \frac{1}{20s}\right) \tag{4.28}$$

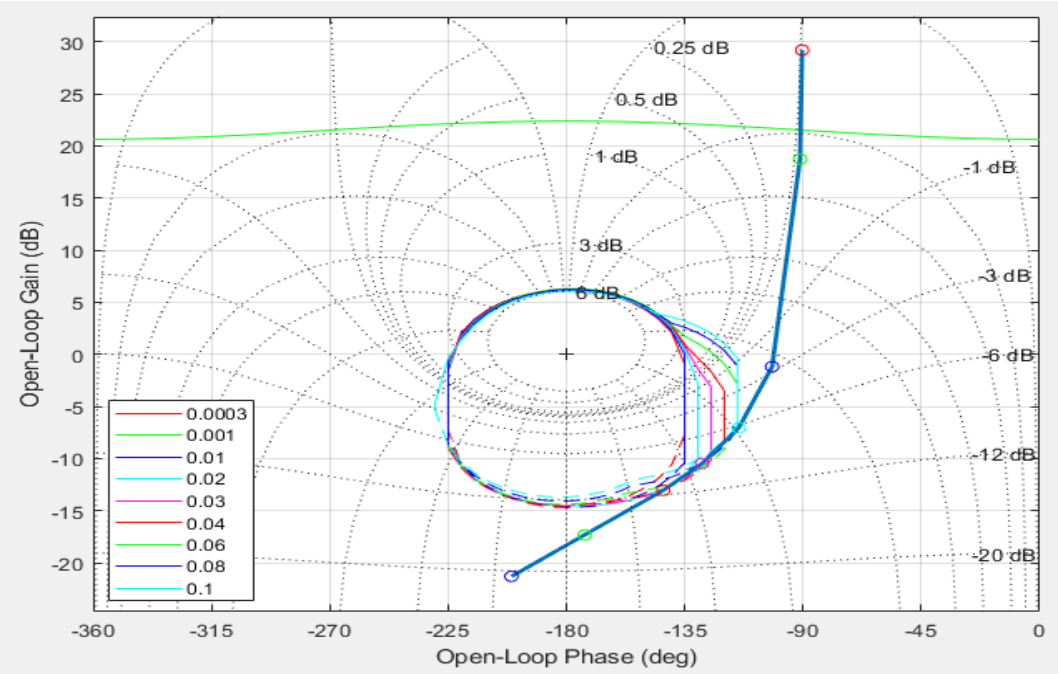

Figure 48: Loop shaping design for Attemperator 2 controller

The proportional gain for Superheater 2 (-0.58) PI controller is smaller than the gain designed for Superheater 3 (-0.65) due to the difference specifications used to design the controller. Although, there is a two second reset time difference between the two controllers.

Figure 49 shows the bode plot for systems L_o, $1/1+L_o$ and $L_o/1+L_o$. Figure 50 illustrates the peak response and stability margins for each system at its respective crossover frequency.

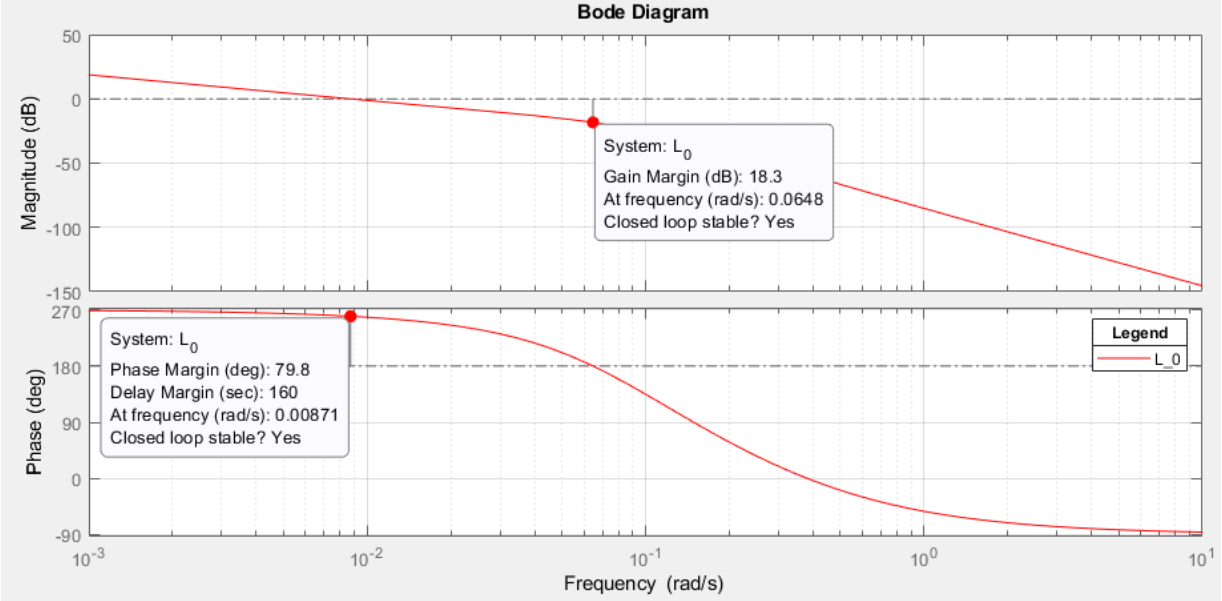

Figure 49: Open loop nominal bode plot showing gain and phase margins for Attemperator 2 controller

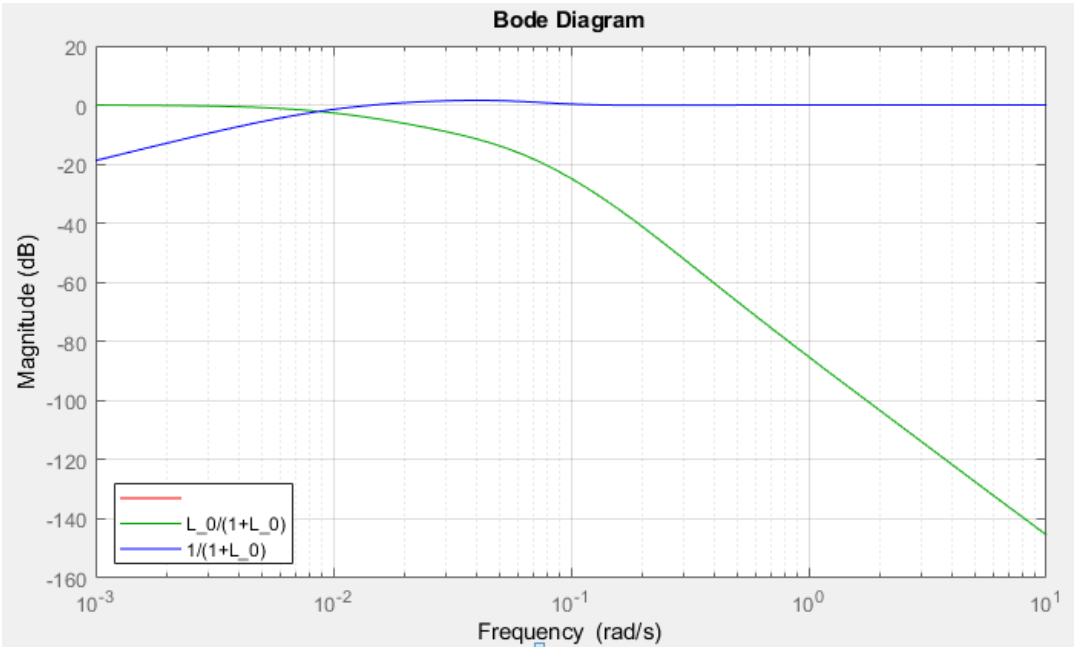

Figure 50: Controller design bode plot showing gain and phase margins

Noise amplification, resonances and unmodeled high frequency dynamics can be reduced by designing minimum bandwidth controllers [30].

5. Improved Control using a Multi-loop Control Structure

This chapter summarises various types of control methods and investigates the concept of two multi-loop control methods used to control the steam temperature at the final superheater at a constant setpoint while the steam and flue gas parameters at the inlet of the superheater vary. The first control technique uses two controllers designed in a cascade control structure around a single superheater section, where each controller has independent input measurements and the output of one controller manipulates the setpoint of the other controller. However, in a VPC arrangement, each controller is designed to control the outlet steam temperature around its local superheater section, unlike a cascade controller where both controllers control its local superheater outlet temperature via its local attemperator valve, i.e. in a Valve Position Controller (VPC) structure, the output of one superheater controller is the "measurement or process variable" for the other (2^{nd}) superheater controller. The second controller "process variable" is then compared to its desired valve position setpoint. The common result of these two types of control techniques is to manipulate a single final variable through multiple control loops.

5.1 Single Loop Attemperator Controller

The simplest method of controlling the main steam temperature is to measure the outlet steam temperature and compare it to a setpoint which then sends a signal to control the attemperation spray flow in order to keep the temperature constant, irrespective of the flow conditions as shown in Figure 51 [34]. However, this has its limitations as it only looks at a single temperature and tries to control it, regardless of any other temperature deviations occurring in other stages of the steam path.

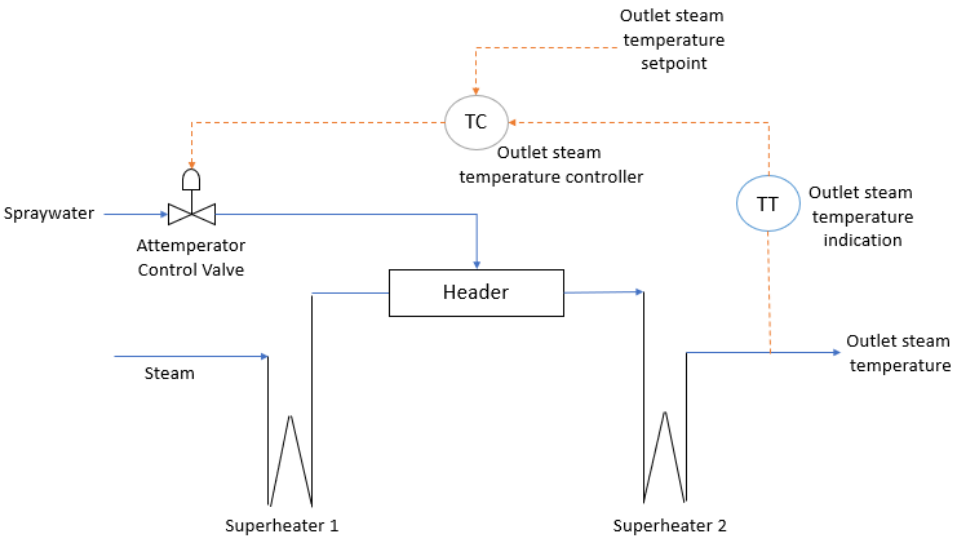

Figure 51: Single-loop temperature controller for outlet steam temperature

5.2 Feedforward/Feedback Control for Disturbance Rejection

The main requirement of control systems is to efficiently control any disturbances that affect the plant. In order for a corrective action to respond, the output steam temperature will need to deviate from its setpoint. Therefore, the addition of the feedforward control loop $\left[G_f(s)\right]$ onto the feedback control loop $\left[G(s)\right]$ results in a faster system response as the feedforward control loop corrects or compensates for any measured disturbances before the output steam temperature detects it. Each controller is tuned independently, and the design is initiated by selecting a feedforward component for the disturbance rejection, and a feedback controller for control of the output steam temperature.

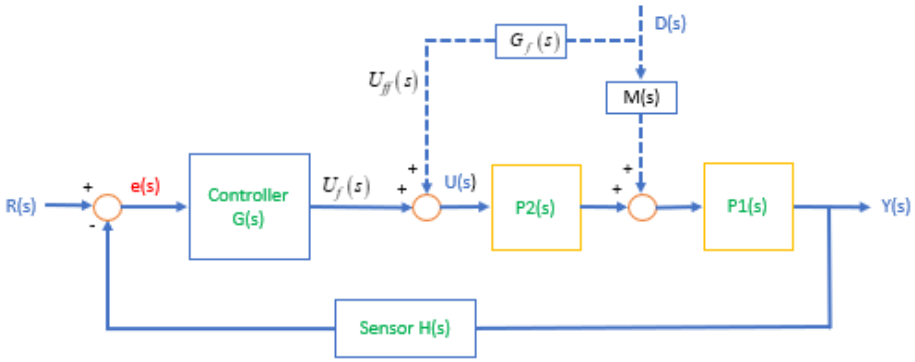

Figure 52: Feedforward-feedback control loop

5.3 Cascade Control

This section introduces a cascade control structure for controlling the attemperation valve in order to control the final outlet steam temperature. Shinskey [35] defines a cascade controller as a multi-loop structure which consists of an inner (secondary) and outer (primary) loop, resulting in the implementation of two controllers in a cascaded arrangement to control one *manipulated* process output variable, the output steam temperature, by manipulating the position of the attemperator valve.

There are two time lags associated with superheater temperature control [35]:

1. Any change in the firing rate has a delayed effect on the steam temperature heating rate.
2. The time it takes for the attemperation spray water and steam mixture to influence the final superheater outlet.

The second lag can be offset by implementing a cascaded attemperator controller, which is fast and can reduce the effects of valve gain uncertainty. The faster dynamic controller has the following advantages [35]:

1. Any disturbance and uncertainty that occurs within the secondary loop is immediately corrected by the secondary controller before it has any effect on the primary loop.
2. Any phase lag that exists within the secondary process is reduced by the secondary loop, which increases the response of the primary loop.
3. Any gain variations experienced within the secondary process is dealt with by its individual loop.

4. The secondary loop manipulates the thermo-fluid properties of the primary loop.

Cascaded PI controllers are conventionally used at power stations with the inner loop having a larger bandwidth control around the attemperator valve and superheater inlet temperature (regulating out valve and process uncertainty), while the outer control loop is around the superheater outlet temperature and provides a setpoint to the inner loop. By cascading PI controllers on a single superheater allows the inner loop to control the superheater inlet temperature, eliminating uncertainty in valve gain and inlet temperature variations.

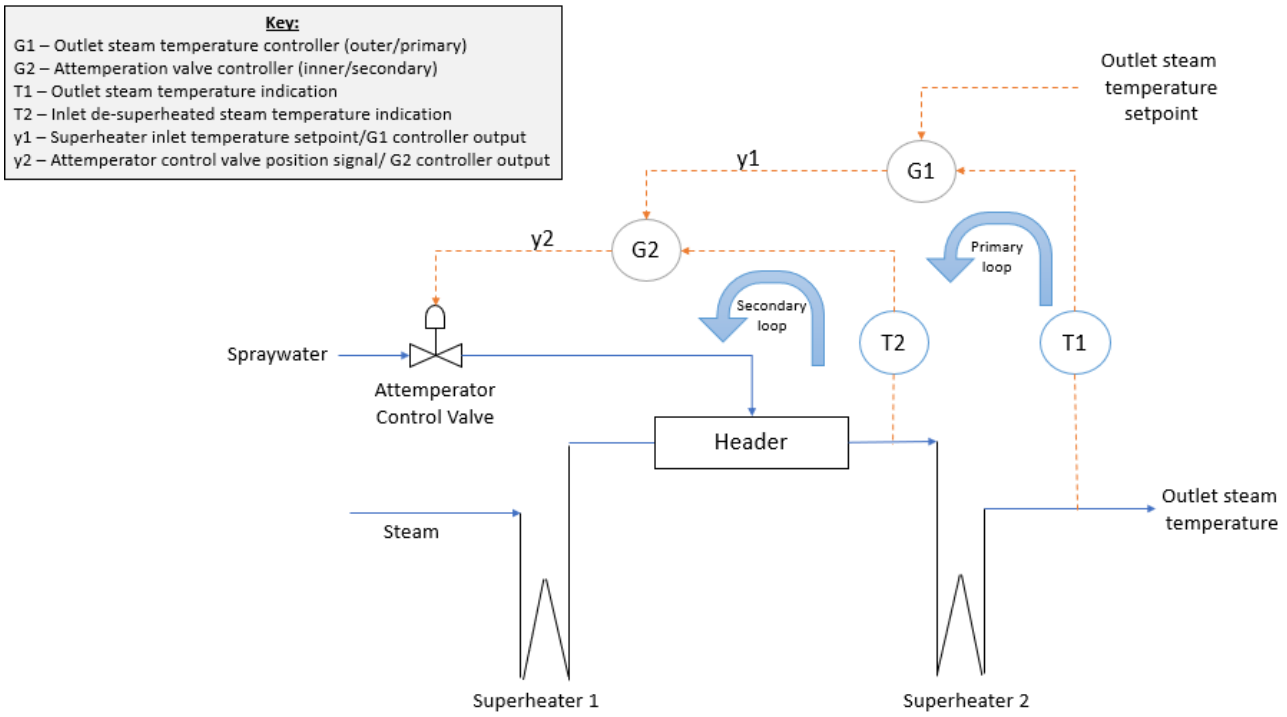

Figure 53: Cascade Controller superheater configuration

Figure 53 illustrates that the outer or primary controller (*G1*) generates a *setpoint (y1)* for the inner or secondary controller (*G2*). The secondary loop then compares the *setpoint* from the primary controller to the secondary controlled variable (*T2*: superheater inlet temperature) and adjusts the attemperation valve position accordingly, thus indirectly controlling the primary variable (*T1*: actual outlet steam temperature) at its setpoint. The *output* of the secondary controller (*y2*) manipulates the attemperator valve position, controlling the temperature of spray and steam mass flow mixture entering the superheater. The secondary variable has a slow coupling effect on the primary process, as the attemperated steam enters the superheater, therefore cooling down the outlet steam temperature. This type of control system is advantageous for applications with a time lag on the secondary process since the disturbance occurs in the secondary loop, therefore allowing the faster dynamic secondary loop to correct the disturbance before it influences the primary loop. This also reduces the sensitivity of the outlet steam temperature.

5.3.1 Methodology for Designing a Cascade Controller

Since the secondary control loop influences the primary control loop, the secondary loop PI controller was initially designed to cater for this effect, thereafter the primary loop PI controller was designed as explained below. The

cascade loop is designed using the following methodology and simulated in Flownex with the results shown in Figure 29.

1. Initially, the secondary PI controller (G_2) was designed by using the designed input temperature into the superheater pass as the setpoint and comparing this value to the actual process control variable. The secondary controller requires a faster response to deal with any upsets or disturbances in the secondary loop.
2. Once the secondary controller was designed, the primary controller (G_1) was then configured in a cascaded arrangement, with the output signal (*y1*) of the primary controller feeding into the secondary controller, forming its setpoint. The superheater output temperature was then connected to the process variable input of the controller.

5.4 Ziegler Nichols 2nd Tuning Method

The Ziegler Nichols rules can be used to determine the values for the controller parameters, K_P, K_I and K_D, which depends on the transient response of a system. They determine an initial or estimated set of PID controller parameters for an unknown plant. Ziegler and Nichols proposed two tuning methods for PID controllers, the open loop technique which involves an S-shaped reaction curve and the closed-loop technique which utilises an oscillation technique.

The Ziegler Nichols second method was investigated for research purposes, as it is as quick initial tuning method which was used to understand the controller component in Flownex, however a regular QFT design as explained in Section 4.1 is preferred. The following describes the tuning method used to determine the integral and gain parameters of a PI controller in Figure 25.

Ziegler Nichols 2nd Tuning Method (Oscillation Technique) [33]

This method is a closed-loop technique for tuning PID controllers.

- Table 14 assists in determining the type of controller to be designed.
    - The term K_P is required to reduce the rise time
    - The term K_I is required to eliminate steady-state error
    - The term K_D is required to decrease the overshoot and settling time
- Once the type of controller required (i.e. P, PI, PID, etc.) was determined, a PI controller was tuned.
- Start with a low gain value, K_P
- Slowly increase the gain until an oscillation occurs at steady-state. This gain then becomes the critical gain, K_{cr}

The following figure is a representation of a closed loop controller output which controls attemperator valve position illustrates the critical time constant, T_{cr}, which is the time it takes for one oscillation to occur.

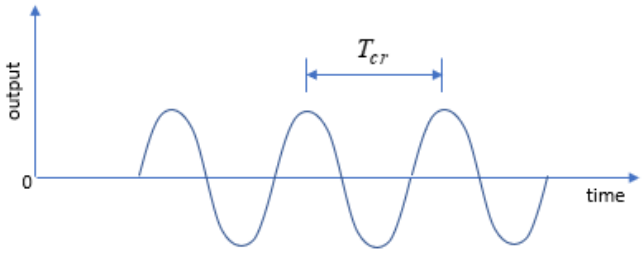

Figure 54: Closed loop controller output showing continuous oscillations [33]

- The following table was then used to estimate the gain and time constants for Attemperator 3 controller parameters:

Table 18: Ziegler Nichols gain estimator for the continuous oscillation technique [36]

Controller Type	K_P	T_i	T_d
P	$0.5K_{cr}$	∞	0
PI	$0.45K_{cr}$	$\frac{T_{cr}}{1.2}$	0
PID	$0.6K_{cr}$	$0.5T_{cr}$	$0.125T_{cr}$

Figure 55 represents the output for Plant B at which oscillations occur. The green signal represents the valve opening curve, blue represents the final outlet temperature, red represents Superheater 3 inlet temperature and purple represents the flue gas temperature at the inlet of Superheater 3.

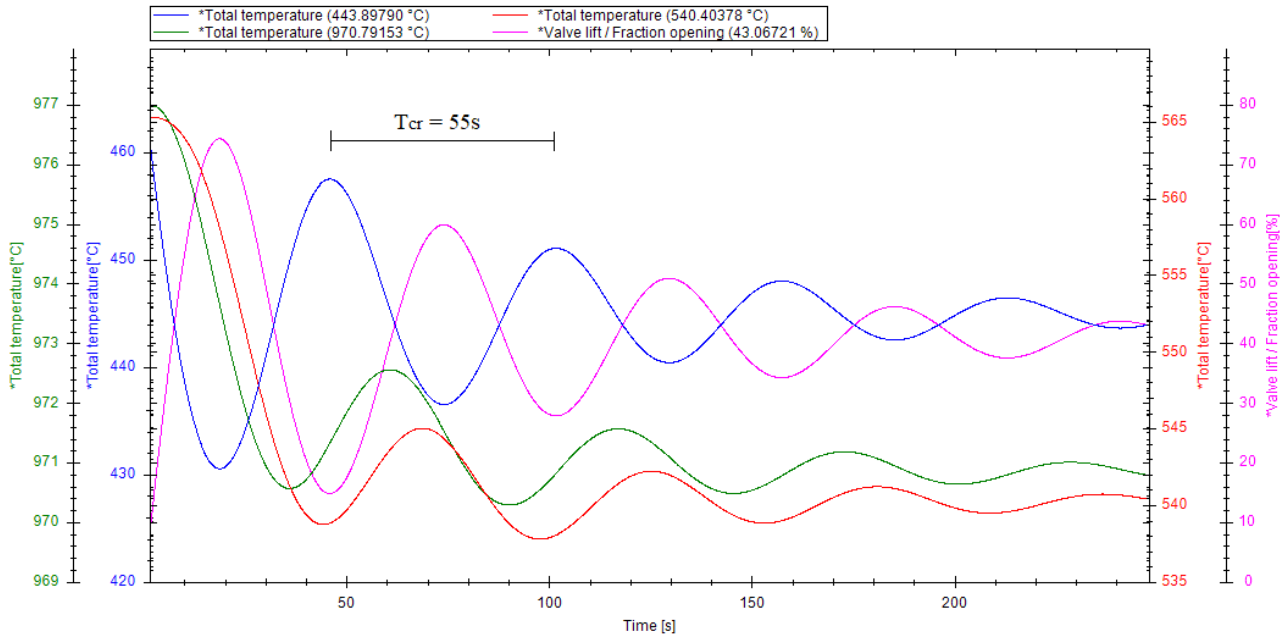

Figure 55: Closed loop controller output showing oscillations for Plant A

From Figure 55, where $K_{cr} = -5$ and $T_{cr} = 55s$, Table 18 was used to tune the gain and integral time constant for Attemperator 3 PI controller. Using the Ziegler Nichols second tuning method, the final PI controller was estimated to be

$$G_{ZN}(s) = -0.45\left(1 + \frac{1}{31.8s}\right) \tag{5.1}$$

Figure 56 illustrates the simulation of the Ziegler Nichols controller implemented on Plant B for Attemperator 3 valve.

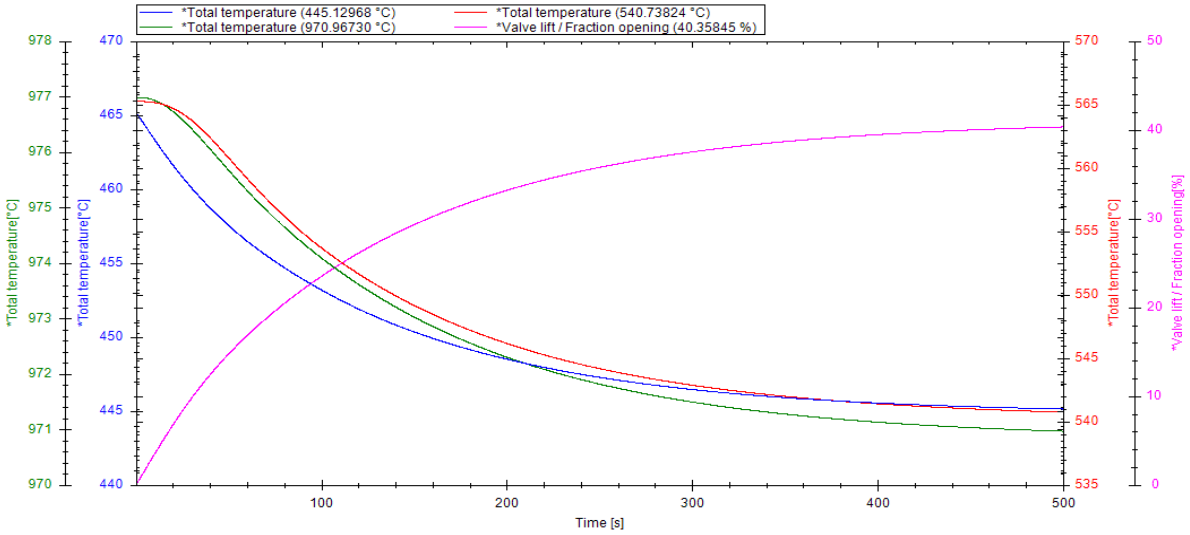

Figure 56: Simulation results for Ziegler Nichols controller

Although the Ziegler Nichols method was researched, uncertainties and other errors were not accounted for in this model and therefore a QFT designed controller is preferred. This method was therefore used for illustration and research purposes in order to understand the use of cascaded PI controllers in a steam generation boiler plant.

5.5 Current Control Philosophy on Plant A

5.5.1 Boiler Master Control

Boiler master control refers to the primary load demand signal interfacing with the turbine and boiler controls. The boiler demand determines the steam conditions (such as feed water mass flows and temperature) and is set according to the unit load demand (or required generated Megawatt output). The boiler master setpoint store is a switch that selects either the capabilities signal or boiler demand signal. This switch then sends a signal to control both the master air/fuel and master feed water setpoints.

The master air/fuel is a common setpoint for boiler firing. Primary air (PA) flow is a measure of the required fuel flow and is derived from the master fuel control. The required PA (which is dependent on load demand) is compared to the measured PA flow, and any resulting error is sent to the PA damper controller to adjust its position. The PA flow is proportional to the fuel mass flow, and therefore coal feeder speed. Hence, as the load demand changes, a signal is

sent to adjust the PA mass flow which then adjusts the coal feeder speed to supply enough coal and PA to the boiler in order to meet the demand. The fuel supplied is therefore directly proportional to the load demand.

Master feed water is the common setpoint to the boiler feed pump controllers, which supply feed water to the boiler, and adjusts the feed pumps discharge flow as the fuel demand setpoint changes. The master feed water setpoint is 'trimmed' or corrected by enthalpy. The corrected feed water demand then sends a signal to either control the scoop gearbox of the electrical feed pumps or the steam feed pump governor valves, depending on which feed pump is in service.

The master fuel and master feed water determine the mass flow and temperature setpoints of air-to-fuel ratio and feed water required to produce the set megawatt (MW) load demand.

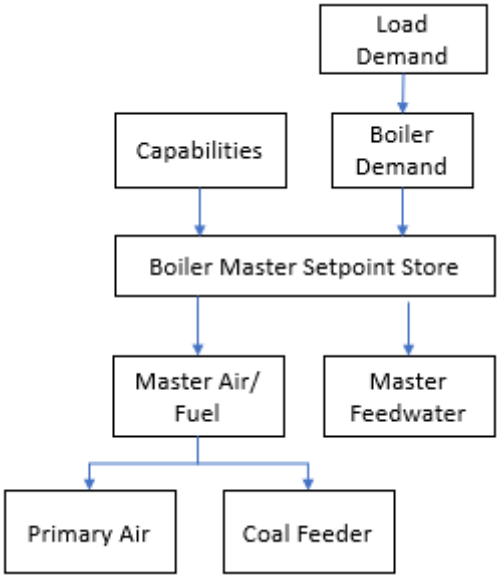

Figure 57: Boiler master control flow diagram

5.5.2 Attemperator Control Philosophy (Plant A)

The main steam outlet temperature is controlled at a design setpoint of 540°C by an attemperation control system which injects atomised feedwater through Attemperators 1, 2 and 3. The attemperation system works on a philosophy of first measuring the superheater outlet temperature and then spraying the atomised feed water should there be a deviation between the measured and setpoint temperatures. It is important that the correct steam temperature enters the superheater to ensure that the desired outlet temperature is achieved.

Superheater 4 steam outlet temperature is measured and compared to its design setpoint of 540°C. Any resulting error is summated with the load influenced fuel master control signal and the Superheater 4 inlet temperature feedback loop[4]. This derived signal is the 'input' to Attemperator 3 valve controller, while the output of the controller

[4] The pure integrator term 'I' in Figure 58 is a representation of the feedback loop and integrates the Superheater inlet error signal until the Superheater inlet setpoint is achieved, resulting in the error signal at the inlet equating to zero.

sends a signal to adjust the attemperator control valve. Spray water is then injected through Attemperators 3.1 – 3.4 to regulate the superheater 4 inlet temperature (see Figure 58), with the maximum temperature drop over Attemperator 3 being approximately 25°C. There is a time delay of approximately 2.5 minutes for the effect of attemperating at the inlet of superheater 4 to appear at the outlet.

If the main steam temperature continues to increase while Attemperator 3 valves are fully open and the final steam temperature is still above setpoint, Attemperator 2.1 – 2.4 spray valves start to open in order to decrease the temperature at Attemperator 3 inlet. This helps bring Attemperator 3 valve within its controllable range as the maximum temperature drop over Attemperator 2 is approximately 28°C.

The desired setpoint (SP in Figure 58) for Attemperator 2 is the differential temperature across Attemperator 3 summated with load influenced Superheater 4 inlet temperature measurement. This setpoint is then compared to the Superheater 3 steam outlet temperature. Any resulting error is summated with the fuel master control signal and Superheater 3 inlet temperature feedback loop. This derived signal is the 'input' to Attemperator 2 valve controller, while the output of the controller sends a signal to adjust the attemperator control valves. Spray water is then injected through Attemperators 2.1 – 2.4 to regulate the superheater 4 inlet temperature (see Figure 58). The time delay for the effect of attemperating at the inlet of superheater 3 to appear at the outlet of superheater 4 is approximately 6 minutes.

Although Attemperator 2 is used in conjunction with Attemperator 3 as a cascaded controller in order to control the final outlet temperature according to its setpoint as explained above, Attemperator 2 controller also acts as a local controller around Superheater 3. Should the temperature exiting Superheater 3 exceed its setpoint, Attemperator 2 valve is signalled to either open or close in order to regulate the temperatures surrounding this superheater within its controllable range. Although Eskom does not use valve position control for attemperation, it does use a multistage attemperation philosophy to co-ordinate multiple superheaters.

Should Attemperators 2 and 3 fail to control the temperature with their spray valves fully open, the differential temperature over Attemperator 2 forms a setpoint for enthalpy which sends a signal to the feed water controls to increase the feed water flow from the feed pump outlet to the boiler. This is however used as an emergency alternative as the 'additional' feed water enters the boiler at the economiser, resulting in a longer time delay before its effects can offset the temperature error in the convective pass of the boiler.

Attemperator 1.1 and 1.2 control valves serve as a safety circuit for large temperature increases and are generally not in control during normal operating conditions. They start to spray at approximately 400°C in order to protect the Separating vessels.

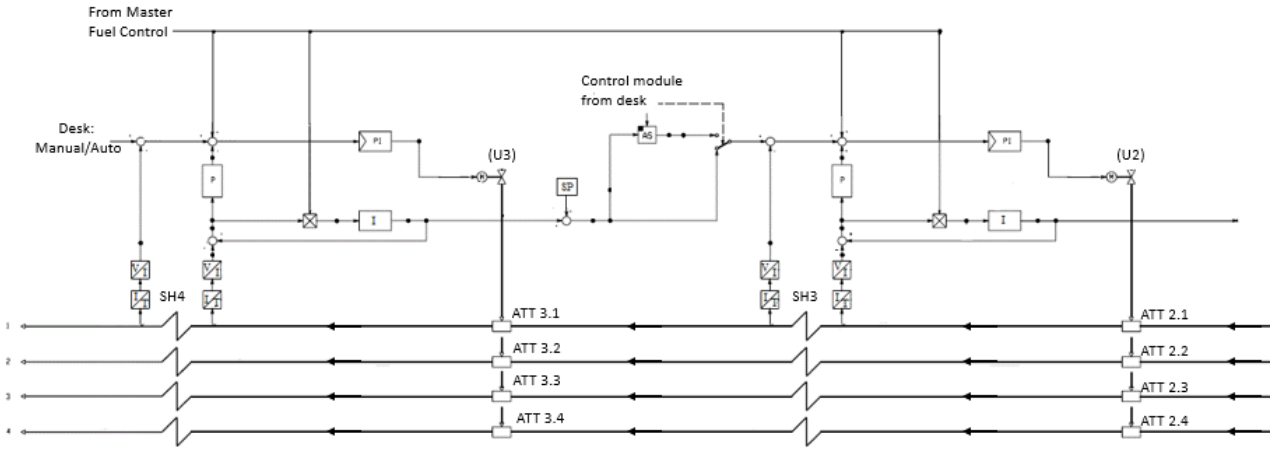

Figure 58: Current attemperator control philosophy at Plant A

5.6 Valve Position Control

Previous research [37] [38] has extensively proven the use of a cascade controller to effectively control the final steam outlet temperature of the superheater. A cascade controller has high bandwidth; however, it has a risk that the secondary loop could be designed to be too fast. But this is only required inside the bandwidth of $G_{1,}\ P_1$ and T_2. Therefore, by eliminating the effects of the fast-acting secondary loop controller, a valve position controller can be implemented as it cascades around two superheaters.

This section of the dissertation details a valve position controller (VPC) design which uses a similar approach to the SISO PI controller designed using the QFT technique. VPC is a multi-loop control technique used for controlling the output steam temperature. Shinskey [39] introduced the concept of valve position control for energy and efficiency optimisation in process control. This type of technique is mainly used in chemical process industries as it offers a simple and effective approach to solving various online optimisation issues. A valve position controller employs a slow effect on one control valve to manipulate its output variable at a desired setpoint. Shinskey first used this type of application on a distillation column to control the floating pressure, by keeping the cooling valve almost fully open and varying the pressure controller setpoint. VPC was also applied in a dual input process, such that one of the inputs is dynamically fast but heavily penalised, and the other input is dynamically slow and less expensive [36]. An example of this type of VPC application is the temperature control of exothermic reactors, where the use of the expensive refrigerant is minimised by adjusting the cooling water flow rate. The main objective of using VPC in a steam boiler power plant application is to compare this controller configuration to that of a SISO controller configuration which is currently being implemented on Plant A (described in Section 3.4.1).

It can be noted from Figure 59 that a VPC consists of two controllers (where the index of the controller $G(s)$ is compatible with the superheater attemperator number). $G_3(s)$ is the faster response controller that controls the process output variable while $G_2(s)$ "mid-ranges" $G_3(s)$. In the case of the power plant, the reference valve position may (for example) be set to 10% so that there is still control authority in both directions but spray water injection higher up in the flue gas pass is preferred. The control objective is to manipulate both controller variables upon a disturbance, where the controlled variable, $U_2(s)$ of $G_2(s)$, gradually manipulates the $G_3(s)$ control

variable, $U_3(s)$, to its desired steady state value (e.g. 10%) to accommodate for the changes in dynamics. Figure 59 represents a block diagram of a VPC system architecture used to test the technique in Flownex®, with the control objective to maintain the output steam temperature at its desired setpoint of 540°C.

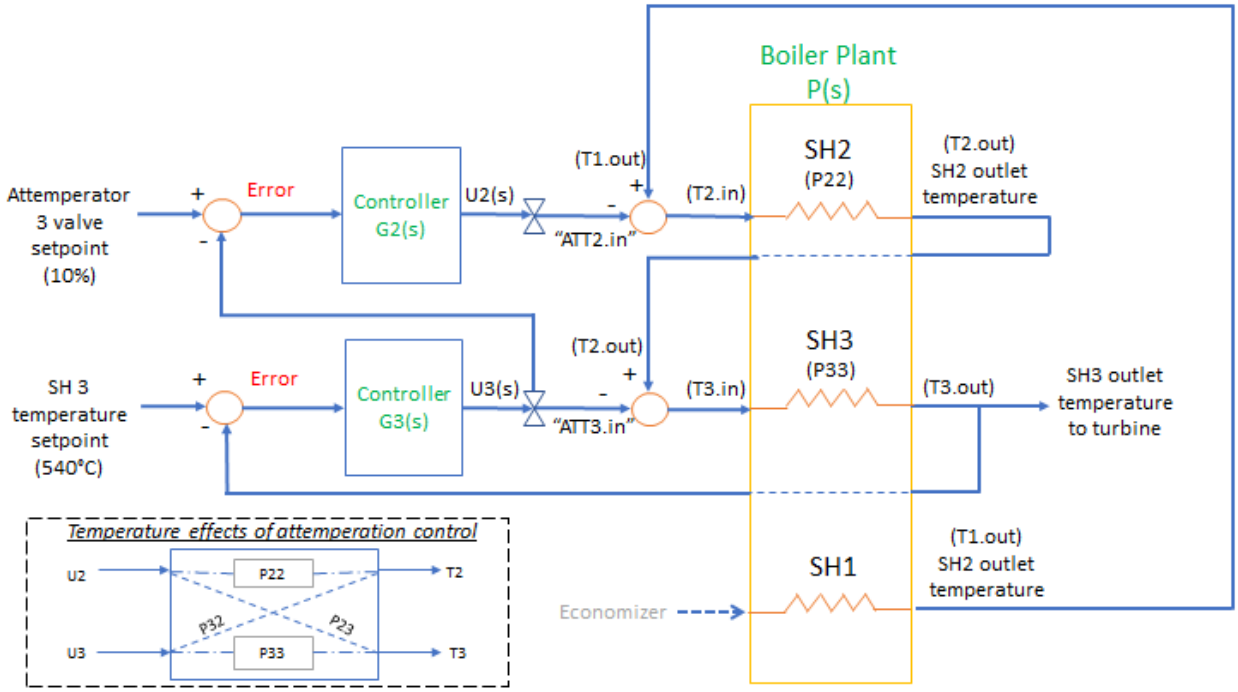

Figure 59: Valve position control system implemented on Plant B

Equation (5.2) summarises the normal transfer function from input control to output where the indices correspond to the input labels. P_{22} responds to $U_2(s)$ which influences the change of steam temperatures T_2. Similarly, P_{33} responds to $U_3(s)$ which influences steam temperature T_3. However, P_{23} and P_{32} are slow, low gain transfer functions, where $U_2(s)$ has a slow coupling effect on T_3 through steam flow and $U_3(s)$ a slow coupling effect on T_2 through the change in flue gas temperatures entering Reheater 2 and Superheater 2.

$$\begin{pmatrix} T_2 \\ T_3 \end{pmatrix} = \begin{pmatrix} P_{22} & P_{23} \\ P_{32} & P_{33} \end{pmatrix} \begin{pmatrix} U_2 \\ U_3 \end{pmatrix} \tag{5.2}$$

Using the QFT loop shaping method described in Section 3.3 above, the VPC controller (P_{22}) was designed. Since the same plant (Plant B) was used for the VPC example, Attemperator 3 controller was tuned independently as explained in Section 4.2.1, and the same controller used as in Equation (4.19), where

$$G_{att3.VPC}(s) = -0.65\left(1 + \frac{1}{26.93s}\right) \tag{5.3}$$

Thereafter $U_2(s)$ was tuned by increasing and decreasing the Attemperator 2 valve while the controller of $U_3(s)$ attempts to control the final outlet steam temperature. This is to account for the dynamics of the plant with respect to spray water temperatures and mass flow with steam. This data was then compiled and extracted from the Flownex model and exported to Matlab to begin the QFT process using the methodology explained in Section 4. Figure 60 illustrates the input data (u1) which represents Attemperator 2 valve position (%) and the output data (y1) which represents Attemperator 3 valve position (%).

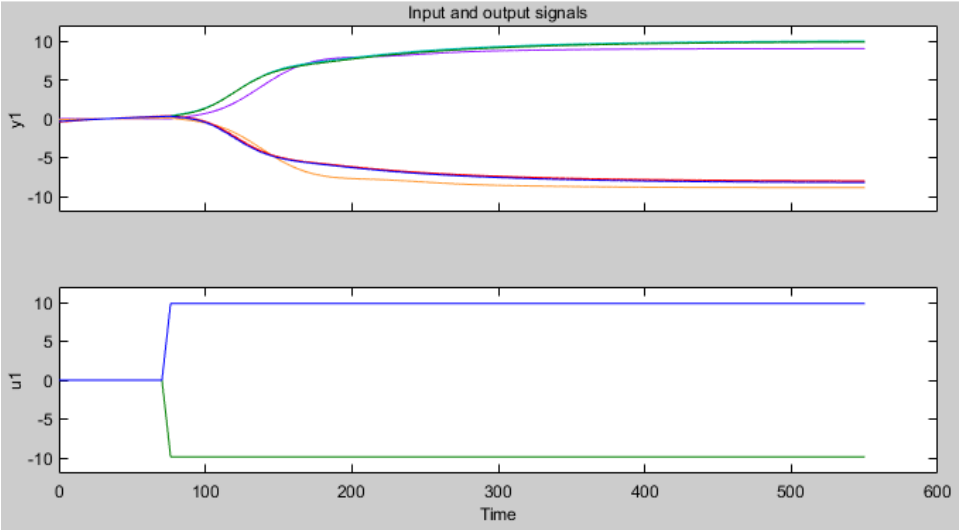

Figure 60: Input (u1) and Output (y1) signal for VPC controller

The transfer functions for the various plants for Attemperator 2 VPC valve using the System Identification toolbox as defined in Table 19.

Table 19: Transfer functions for 100%, 97% and 70% MCR (%/%)

MCR (%)	Transfer function for a 10% increase in valve position	Transfer function for a 10% decrease in valve position
100	$P_{100\_64}(s)=\frac{0.0153s-0.0013}{s^2+0.1245s+0.0016}$ (5.4)	$P_{100\_44}(s)=\frac{0.0046s-0.0013}{s^2+0.1059s+0.0013}$ (5.5)
97	$P_{97\_64}(s)=\frac{0.0155s-0.0012}{s^2+0.1147s+0.0015}$ (5.6)	$P_{97\_44}(s)=\frac{0.0036s-0.0012}{s^2+0.0961s+0.0012}$ (5.7)
70	$P_{70\_64}(s)=\frac{0.0101s-0.0008}{s^2+0.0566s+0.0009}$ (5.8)	$P_{70\_44}(s)=\frac{0.0098s-0.0008}{s^2+0.0575s+0.0009}$ (5.9)

Figure 61 represents the plant templates for each working frequency defined:

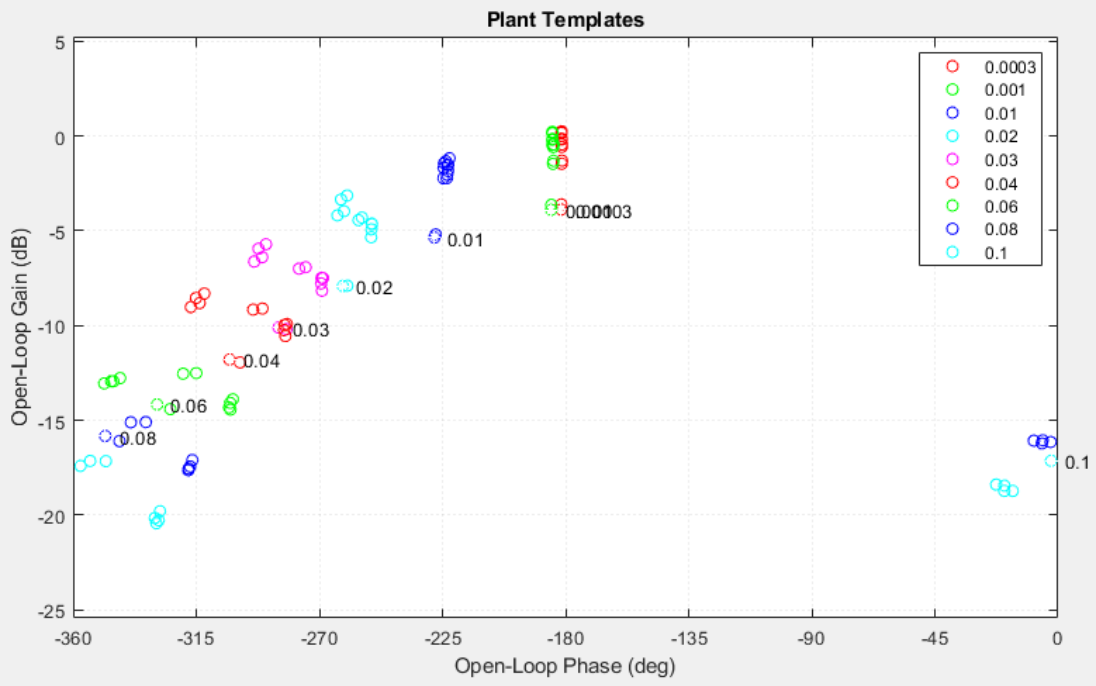

Figure 61: Plant templates for all frequencies

According to Figure 62, the Attemperator 2 valve controller was designed using the sensitivity weight described in equations (4.13) - (4.15) as gain $k = -0.01586$ and zero $z = 0.02227$. Equation (5.10) represents the PI controller that was designed for Attemperator 2 valve for the VPC technique:

$$G_{PI}(s) = K_P \cdot \left(1 + \frac{1}{T_i \cdot s}\right) = -0.712 \cdot \left(1 + \frac{1}{44.9s}\right) \tag{5.10}$$

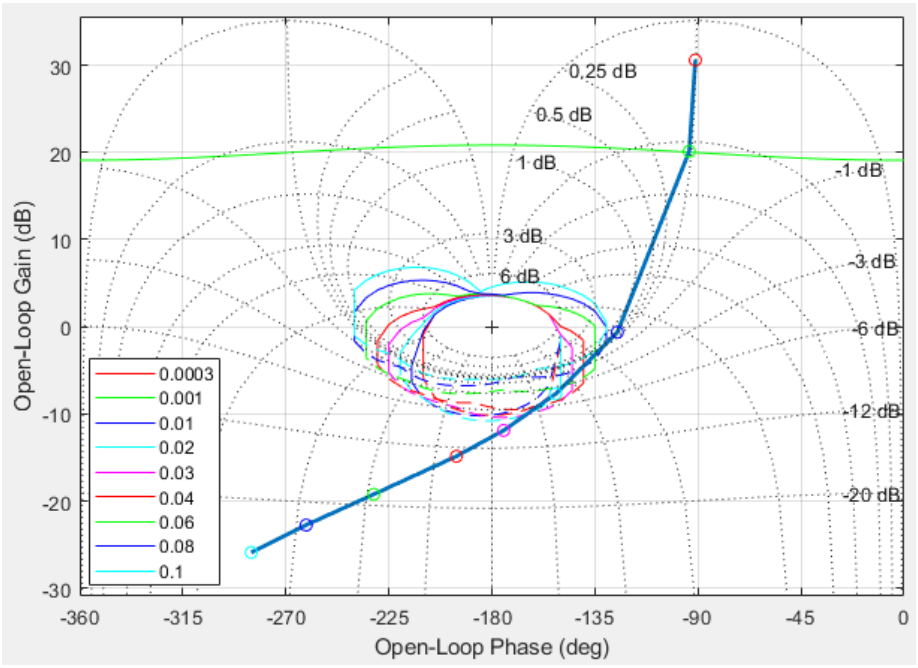

Figure 62: Controller design loop shape for Attemperator 2 VPC technique

By comparing the PI controller of Equation (5.10) with the PI controller SISO design of Attemperator 3 in Equation (5.3) and Attemperator 2 in Equation (4.27), it is noted that the Attemperator 2 controller for the VPC has a higher integral time than the SISO controllers. This is due to the VPC generally being an integral-only action controller [40][41]. Once both controllers were designed using QFT, the configuration of setting up a VPC is shown in Figure 30, where the output of controller $U_3(s)$ forms the setpoint (10%) for controller $U_2(s)$, forming a similar setup of a "cascaded controller arrangement". Using this arrangement attempts to minimise the valve position of Attemperator 3 valve at 10%, while controlling the final steam temperature mainly though Attemperator 2 valve. This allows for the Attemperator 3 valve to have a more control and flexibility over any disturbances directly influencing the heat transfer in Superheater 3 due to its faster dynamics. This provides a sufficient margin to control steam temperatures efficiently while avoiding excessive temperature increases from overheating metal temperatures during emergency upsets in the boiler. Spraying higher up in the boiler improves the total heat uptake in the boiler while spraying close to the turbine legs (i.e. boiler outlet) results in faster response.

6. Results and Discussion

6.1 Proposed control philosophy

Figure 63, Figure 64 and Figure 65 represents the Flownex® model for Plant B using a valve position controller arrangement which was simulated for a 20°C increase in flue gas temperature (disturbance) at 100%, 97% and 70% MCR operating conditions respectively. It can be noted from these figures that the purple line, which is the signal for $U_2(s)$, settles at around 68%, 65% and 48% open for each MCR and the red line, which is the $U_3(s)$ signal, settles at ~10% and the blue line is the final main steam temperature which is controlled to settle at 540°C, as per setpoint. Should the most-open valve, which is $U_2(s)$ in this case, exceed the setpoint of the VPC, $U_3(s)$, the VPC will override the demand signal in order to offset the change in disturbance. Therefore, as shown in the figures below, during a disturbance, both attemperator control valves start to open to reduce the effects that the increased flue gas temperature has on the outlet steam temperature. However, $U_3(s)$ decreases back to setpoint (10%) to limit its flow as $U_2(s)$ accommodates for the increased steam temperature. By controlling $U_3(s)$ at 10% results in $U_2(s)$ being the most open valve.

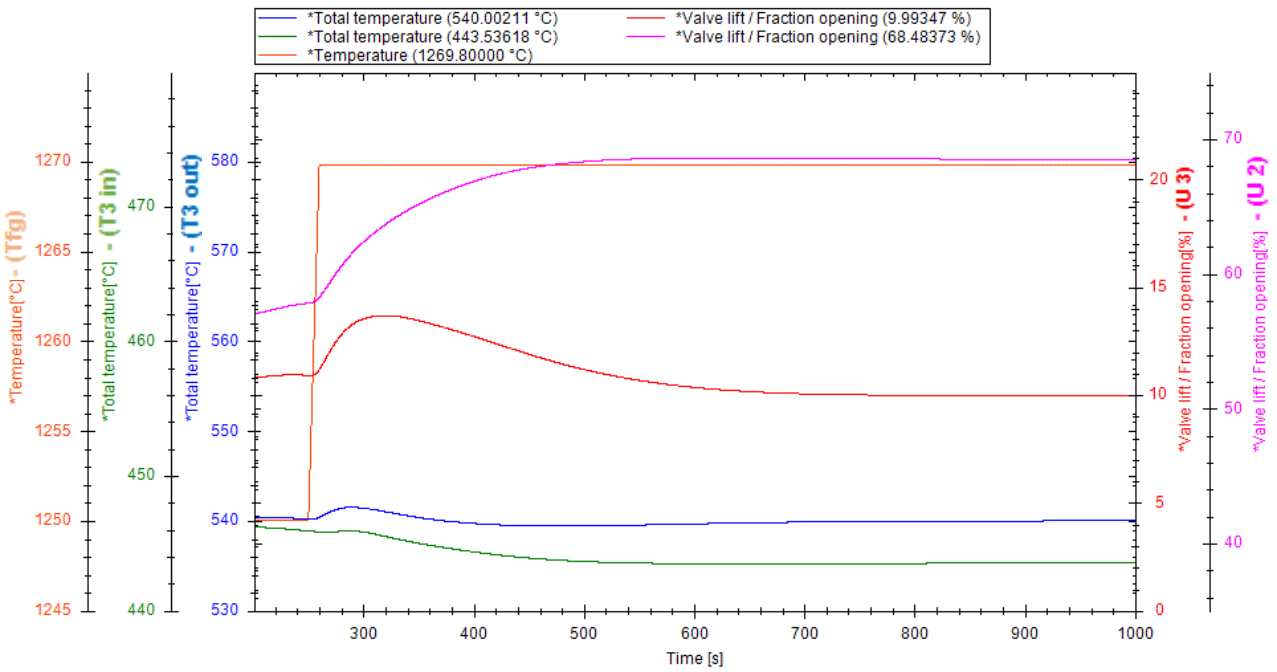

Figure 63: Flownex® simulation showing valve position control for 100% MCR

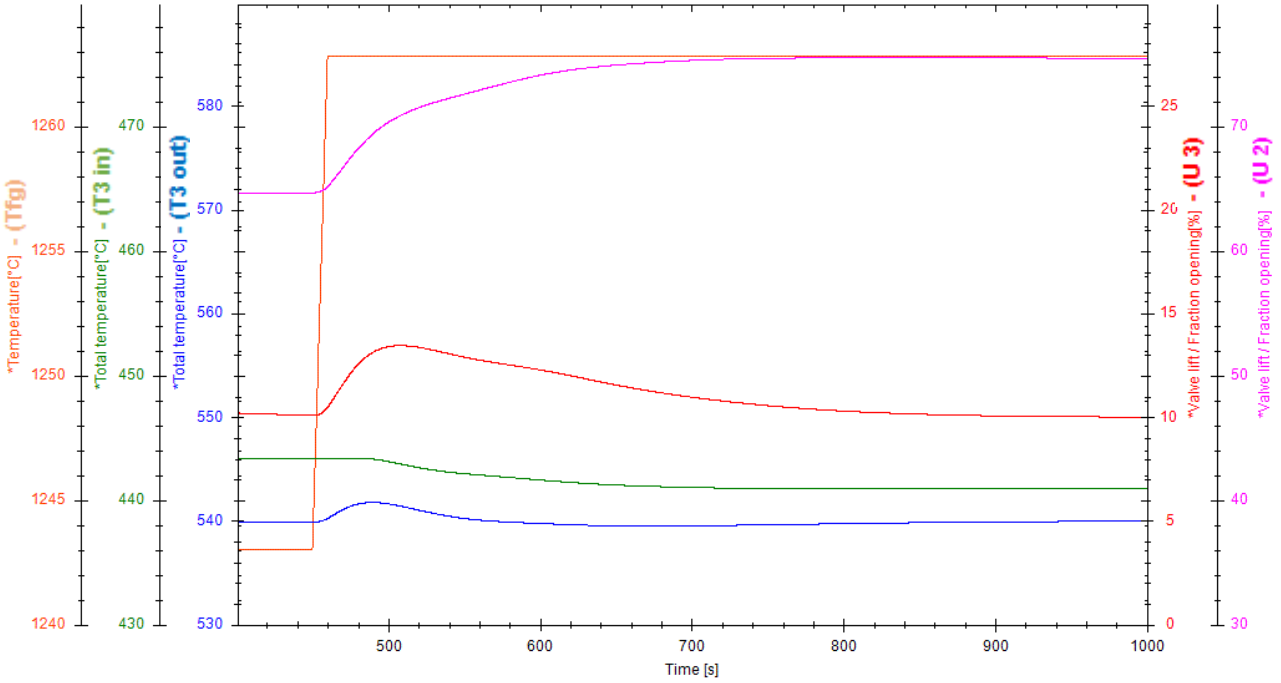

Figure 64: Flownex simulation showing valve position control for 97% MCR

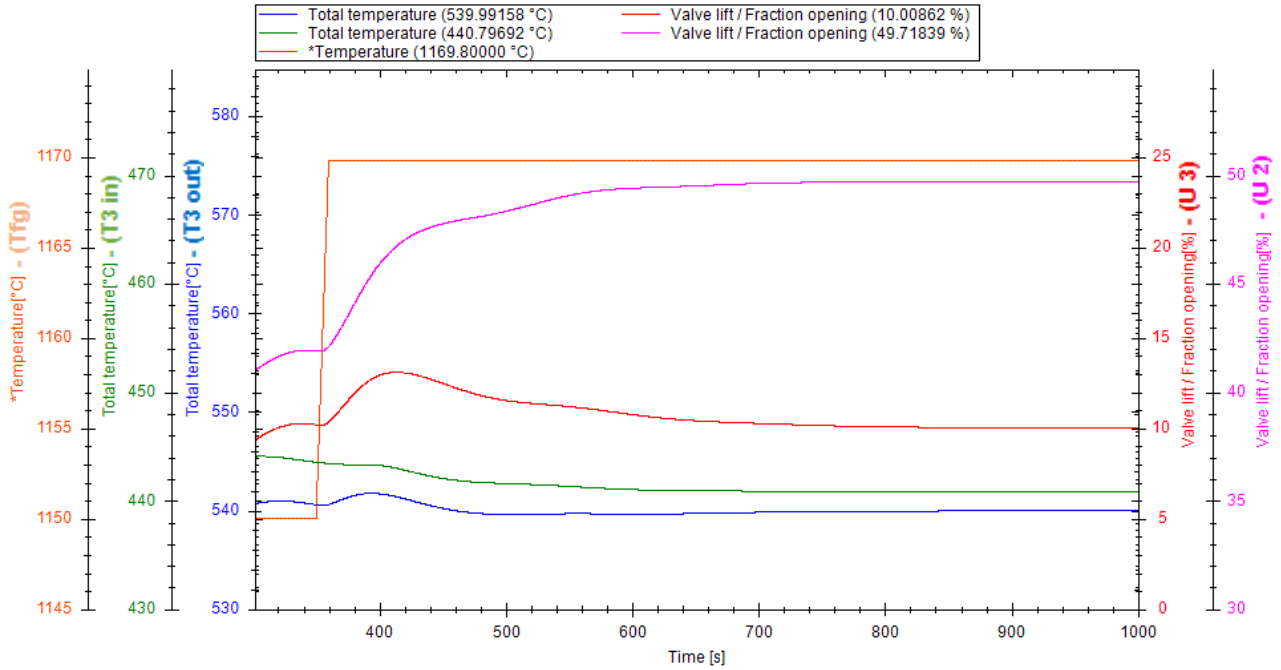

Figure 65: Flownex simulation showing valve position control for 70% MCR

By controlling the steam temperatures through attemperation at the inlet of superheater 2 for Plant B, increases the mass flow rate of the steam into Superheater 2, thus allowing cooler steam temperatures to enter Superheater 3 without being further cooled down by the Attemperator 3 spray water. This allows the hotter flue gas to enter the convective superheaters higher up in the boiler, thereby increasing the heat uptake in those superheaters. Table 20 illustrates the steady state heat uptake per superheater pass for the valve position and SISO PI controller application. It can be noted that the VPC arrangement is 1% more efficient compared to the SISO PI controller application by the

simple expedient of spraying the required amount of attemperator water as high up the flue gas pass as possible, increasing the total heat uptake (by approximately 4 MW in this example).

Table 20: Heat uptake (MW) for 100% and 70% MCR

	100% MCR		**70% MCR**	
	VPC	**SISO**	**VPC**	**SISO**
SH2	78.4	74.1	50.8	47.0
SH3	154.2	154.2	111.6	111.6
SH1	60.1	60.1	45.5	45.5

It is noted that at high loads, the steam temperature at the outlet of the platen superheater is lower due to the increase in steam mass flow rate at higher loads. The increased flow of steam results in there being more steam to cool the superheater tube walls. Since the heat transfer performance of the convective superheaters depends on the flue gas flow velocity, the heat transfer in these superheaters is high at higher loads, which results in a higher final outlet steam temperature due to the higher heat absorption [3].

7. Conclusion and Recommendations

7.1 Conclusion

The objective of this thesis was to analyse the dynamic behaviour of a convective pass in a once-through boiler and maintain the main steam temperature at its designed setpoint through advanced control strategies. Robust control of the main steam temperatures at the boiler outlet reduces the effects of having either excessively high steam temperatures entering the turbine, or moisture content at the last stages of the turbine. Both these effects negatively impact the boiler and turbine as it leads to creep and thermal fatigue in the boiler, while increasing the likelihood of blade erosion and failure in the turbine. Coal fired power plant are highly non-linear with operating conditions and parameters rapidly changing, therefore it is not possible to achieve efficient control when a boiler is modelled using a single operating point. It is therefore essential that the controller design methodology accounts for disturbances in conjunction with the uncertain boiler model.

This thesis mainly focused on the heat transfer between the flue gas and the steam through convection, conduction and radiation. The process was initiated by numerically modelling the convection pass in Mathcad using mass flow, temperature and pressures design data of a 600MW power plant. A high-level combustion process was modelled to calculate the temperature of the flue gas exiting the furnace into the convective pass as this temperature laid the foundation for heat transfer. Once the flue gas temperature entering the convective pass was known, the steam and flue gas heat transfer coefficients for convection and radiation were calculated. The convective heat transfer coefficient for steam was calculated using the Dittus Boelter correlation, while the flue gas was calculated using the Zukauskus correlation. Once the numerical model corresponded to the design data schedule, a dynamic thermo-fluid process was simplified and modelled using the simulation software package, Flownex. This process commenced by modelling a simplified one pass superheater heat exchanger and systematically developed into a full convection pass model, using the geometries and boundary conditions calculated in Mathcad. This final model was then used to validate the design of the robust control system for main steam temperatures. Two boiler configurations were modelled, namely Plant A and Plant B, where Plant B is a product of Plant A as both models use identical boundary conditions, although the configuration of the superheater layout varies. The purpose of Plant A was to validate the thermo-fluid design according to the design data which was numerically modelled. Plant B was modelled to implement the controllers designed for the attemperation system and prove the thermodynamic improvement of using advanced control strategies.

Some of the reasons for the importance of superheater main steam temperature control are the trade-offs and concerns about plant life, efficiency, stability during load changes and availability. These problems arise due to the complexity of the heat transfer process such as the dynamics are high order and load dependent, and the heating varies due to flue gas disturbances [6]. It is therefore necessary that advanced control strategies be tested in order to find the optimal solution for attemperation control in a once-through boiler. This would result in a reduction of thermal cycle fatigue in the superheaters, headers and the turbine.

This project investigated the application of various control strategies, such as cascade control and valve position control, with respect to controlling the main steam outlet temperatures of the convective pass of a coal fired once-through boiler. Robust controllers were required for these control strategies and were designed using Quantitative Feedback Theory. The main advantage of using QFT is that it accounts for model uncertainty which is common in coal fired boilers. Controllers designed using QFT are designed to meet specifications for every plant within the uncertainty

range and not just for a single plant with fixed parameters. Some of the uncertainties that were included in the design are load changes, errors in attemperation sensors and valve actuators, plant disturbances such as variations in steam and flue gas temperatures and mass flow rates and other unknown dynamics. The design methodology for the PI controllers which control the valve positions of both Attemperator 2 and Attemperator 3 is demonstrated in this thesis. The methodology initially concentrates on the single-input single-output (SISO) design around the individual attemperator systems by using the change in outlet steam temperature and valve position as the two design objectives. The variables were simulated in the final Flownex model for each load condition and the simulated transient data was exported to Matlab. The measured input-output data was then pre-processed and manipulated using System Identification to identify the continuous transfer functions for each operating load condition. Once the plant models with uncertainty were defined, the QFT design process commenced. This required selecting a nominal plant, calculating plant templates for each frequency specified, defining specifications and bounds for the system and finally loop shaping the controller to find the optimum design PI controller parameters.

Through literature review, various control strategies were researched around attemperation control for main steam temperatures. Valve position controllers are implemented for various processes such as at a chemical plant for exothermic reactor temperature control and distillation column to control the floating pressure. This thesis therefore researched the design and application of valve position controllers for the attemperation control system and compared the design to SISO PI controllers in order to investigate the improvement of the current attemperator control design at Plant A. The comparison proved that the valve position controller technique was 1% more efficient that the SISO design as the total heat uptake was around 4 MW higher. High flue gas temperatures increase the main steam outlet temperature which indirectly reduces thermal efficiency, therefore increasing the heat uptake between the flue gas and the steam in the boiler reduced the flue gas temperature leaving the boiler and improved efficiency. By cooling the flue gas earlier in the convective pass leads to poor thermodynamic efficiency as little heat is extracted from the flue gas at heat exchangers located further along the convective pass. By having a higher temperature differential results in higher heat uptake. Therefore, a co-flow arrangement of attemperating higher up in the boiler results in a higher heat transfer between the hot flue gas to the cooler steam, thereby increasing the efficiency of the boiler.

7.2 Recommendations

Through additional research, the following areas were identified as possible improvement areas and can be developed as future work.

1. The attemperation control philosophy for Plant A (explained in Section 5.5.2) shows that if Attemperator 3 control valve is fully open, the feedback bandwidth through Attemperator 2 is low. This can be improved by implementing the VPC technique on the current power generating plant. For example, the setpoint for Attemperator 3 controller can be set to 80% open to activate Attemperator 2 controller, therefore allowing Attemperator 3 to still have some control authority for fast transients.

2. The total correction factor for fuel is dependent on the furnace pressure deviation (between the actual pressure and the desire pressure), and the feed water control correction signal, Enthalpy. Enthalpy is a measure of steam quality after the evaporator and is formed by calculating the required steam temperature and pressure which is load dependent. Since the pressure remains fairly constant during normal operation,

any change in enthalpy will be a consequence of temperature changes only. Enthalpy is an important signal when it comes to adjusting the firing rate as this proportionally adjusts the master fuel and feedwater control signals. The controllers designed in this thesis focussed on controlling the main steam outlet temperature purely through attemperation control, thus ignoring the effects on enthalpy. It is recommended that enthalpy be included in future research as this signal assists in maintaining the spray water mass flow to within its controllable range. In addition to the accuracy of control, the idea of minimizing attemperator spray water consumption will be considered as this has a direct indication of the main steam flue gas temperatures.

3. The effect of over design on plant life and efficiency was not explicitly studied in this thesis. Although this thesis emphasised the improvement in using a VPC technique over a SISO controller when it came to efficiency, it is recommended that future work could include a Multiple Input Multiple Output (MIMO) controller. This multivariable controller can be implemented to improve control performance as it would act as the 'brain' of the attemperation system, taking into consideration all steam and flue gas inputs, outputs and setpoints such a mass flow rates, superheater inlet and outlet temperatures and pressures and load demand. This MIMO controller would then determine which is the best solution for correcting the error signal and will adjust that deviation by using either a specific local attemperator controller to regulate the temperature, or through the firing rate and feed water demand. The multivariable controller model can include steam temperature control around the reheater section of the convective pass.

8. References

[1] The Mathworks Inc, “System identification toolbox,” 2019. [Online]. Available: http://www.mathworks.com/products/sysid.html. [Accessed: 06-Dec-2019].

[2] R. K. Kapooria, S. Kumar, and K. S. Kasana, “An analysis of a thermal power plant working on a Rankine cycle : A theoretical investigation,” *Journal of Energy in Southern Africa* Nol. 19, no. 1, pp. 77–83, 2008.

[3] J. B. Kitto and S. C. Stultz, *Steam: its generation and use*, 41st ed. Ohio, United States of America: Babcock & Wilcox Company, 2005.

[4] G. Oluwande and A. R. Boucher, “Implementation of a multivariable modelbased predictive controller for superheater steam temperature and pressure control on a large coal-fired power plant,” *1999 European Control Conference*, ISBN: 978-3-9524173-5-5, pp. 816–820, 1999.

[5] W. J. Peet, (1989) “Superheater outlet steam temperature control,” Patent: 4,887,431.

[6] T. Molbak, “Advanced control of superheater steam temperatures - An evaluation based on practical applications,” *IFAC Proc. Vol.*, Vol. 30, no. 17, pp. 161–166, 1997.

[7] G. Prasad, E. Swidenbank, and B. W. Hogg, “A neutral net model-based multivariable long-range predictive control strategy applied in thermal power plant control,” *IEEE Trans. Energy Conservation*, Vol. 13, no. 2, pp. 176–182, 1998.

[8] J. B. Riggs, K. Curtner, and W. Foslien, “Comparison of two advanced steam temperature controllers for coal-fired boilers,” *Computing Chemical Engineering*, Vol. 19, no. 5, pp. 541–550, 1995.

[9] M. Menkina, “Possibility of robust temperature control of superheated steam of the through-flow boiler,” *Proc. 13th Int. Carpathian Control Conference*, pp. 474–479, 2012.

[10] L. A. Sanchez, F. G. Arroyo, and R. A. Villavicencio, “Dynamic matrix control of steam temperature in fossil power plants,” *IFAC Proc. Vol.*, vol. 28, no. 26, pp. 275–280, 1995.

[11] T. K. Sai and K. A. Reddy, “Design of fuzzy gain scheduler for superheater temperature control in power plant,” *2016 2nd Int. Conf. Control. Instrumentation, Energy Commun.*, pp. 521–525, 2016.

[12] W. F. Fuls, *MEC4118Z, System engineering in the power industry*. 2018.

[13] Eskom, "Eskom's generation plant mix" [Online]. Available: www.eskom.co.za/news/Pages/May15.aspx [Accessed: 10-Sept-2020].

[14] Eskom, “36-623: Consistent data set for eskom generating plant Rev 2,” 2016.

[15] P. Rousseau and W. Fuls, *Power plant systems analysis*. Cape Town, South Africa, 2018.

[16] Eskom, “360 View - Boiler arrangment.”, 2018.

[17] T. L. Bergman, A. S. Lavine, F. P. Incropera, and D. P. Dewitt, *Fundamentals of heat and mass transfer*, Seventh. United States of America: John WIley & Sons, Inc., 2007.

[18] P. Rousseau and R. Laubscher, *Power plant boilers - thermofluid processes and controls*. Cape Town, South Africa, 2019.

[19] Y. Zhang, Q. Li, and H. Zhou, *Theory and calculation of heat transfer in furnaces*. 2018.

[20] M-Tech Industrial, “Flownex library manual.” 2018.

[21] A. Zukauskas, A. Skrinska, J. V. Ziugzda, and V. Gnielinski, *Heat exchanger design handbook*. United States of America: Hemisphere Publishing Corporation, 2017.

[22] Y. A. Cengel and J. M. Cimbala, *Fluid mechanics: Fundamentals and applications*. New York: McGraw-Hill Companies, 2006.

[23] S. Kakac, *Boilers, Evaporators & condensers*. United States of America: John WIley & Sons, Inc., 1991.

[24] D. Taler and J. Taler, “Simplified analysis of radiation exchange in boiler superheaters,” *Heat Transfer*

Engineering, vol. 30, no. 8, pp. 601–609, 2009.

[25] P. Basu, C. Kefa, and L. Jestin, *Boilers and burners*. Springer, 2000.

[26] Eskom, “C-Schedule: Boiler design data,” 1974.

[27] M. Woite GmbH, “Material No.: 1.7380,” 2012. [Online]. Available: http://www.woite-edelstahl.com/17380en.html. [Accessed: 14-Jan-2020].

[28] M. Sidi and I. M. Horowitz, “Synthesis of feedback systems with large plant ignorance for prescribed time domain tolerances.,” vol. 6, no. 2, pp. 202–206, 1973.

[29] I. Horowitz, “Survey of quantitative feedback theory (QFT),” *Int. J. Robust Nonlinear Control*, Vol. 11, pp. 887–921, 2001.

[30] C. Borghesani, Y. Chait, and O. Yaniv, *The QFT frequency domain control design toolbox for use with Matlab*. 2003.

[31] E. Eitelberg, “Editorial,” *Int. J. Robust Nonlinear Control*, Vol. 11, no. 10, pp. 883–886, 2001.

[32] M. Garcia-Sanz, *Robust control engineering*. 2017.

[33] L. Wang, *PID control system design and automatic tuning using Matlab/Simulink.* John Wiley & Sons, 2020.

[34] D. Lindsley, *Power plant control and instrumentation*. United Kingdom: The Institute of Electrical Engineers, 2000.

[35] F. G. Shinskey, “Control systems — Cascade Loops,” *Process Control and Optimisation,* Vol. II pp. 148–156, Bela Liptak, 2006.

[36] C. C. Yu and W. L. Luyben, “Analysis of valve-position control for dual-input processes,” *Ind. Eng. Chem. Fundam.*, vol. 25, no. 3, pp. 344–350, 1986.

[37] R. Hýl and R. Wagnerová, “Design and implementation of a cascade control structure for superheated steam temperature control,” *2016 17th Int. Carpathian Control Conference*, pp. 253–258, 2016.

[38] X. Wei, M. Jingjing, J. Hongyan, and Y. Fei, “The main steam temperature cascade control of high order differential of feedback controller,” *2010 Int. Conference Intellectual System Design Engineering Applications*, vol. 2, pp. 683–687, 2010.

[39] F. G. Shinksey, *Process control systems*, 3rd ed. United States of America: McGraw-Hill Book Companies, 1979.

[40] F. G. Shinskey, *Process control and optimization Volume II*, 4th ed. United States of America: Taylor & Francis Group, 2006.

[41] B. J. Allison and S. Ogawa, “Design and tuning of valve position controllers with industrial applications,” vol. 1, pp. 3–16, 2003.

[42] D. Christiansen, D. G. Fink, R. K. Jurgen, *Electronics engineers' handbook*, 5th ed, United States of America: McGraw-Hill, Section 19, pp. 19.1-19.30, 2005

[43] S. Ozana and M. Pies, "Dynamical model of a power plant superheater," *WSEAS Transactions on Systems.,* Issue 7, Vol. 9, 2010

[44] M.S. Thopil, et. al., "A review of grid connected distribution generation using renewable sources in South Africa," *Energy Strategy Reviews,* pp. 88-97, 2018

[45] L. Waswa and B. Bekker, "Impact of PV small scale embedded generation on system demand profile," S*ASEC 2018 - 5th Southern African Solar Energy Conference,* 2018

Appendix A. Program code

Pre-processing data:

```
% Remove offset from outlet temperature
Out6_1 = Out100_60 - mean(Out100_60(1:150));
Out4_1 = Out100_40 - mean(Out100_40(1:150));
Out6_9 = Out97_60 - mean(Out97_60(1:150));
Out4_9 = Out97_40 - mean(Out97_40(1:150));
Out6_7 = Out70_60 - mean(Out70_60(1:150));
Out4_7 = Out70_40 - mean(Out70_40(1:150));
% Remove offset from inlet control valve
Cv6_1 = Vlv100_60 - mean(Vlv100_60(1:150));
Cv4_1 = Vlv100_40 - mean(Vlv100_40(1:150));
Cv6_9 = Vlv97_60 - mean(Vlv97_60(1:150));
Cv4_9 = Vlv97_40 - mean(Vlv97_40(1:150));
Cv6_7 = Vlv70_60 - mean(Vlv70_60(1:150));
Cv4_7 = Vlv70_40 - mean(Vlv70_40(1:150));
% Converting data for System ID toolbox
d6_1 = iddata(Out6_1,Cv6_1,0.1);
d4_1 = iddata(Out4_1,Cv4_1,0.1);
d6_9 = iddata(Out6_9,Cv6_9,0.1);
d4_9 = iddata(Out4_9,Cv4_9,0.1);
d6_7 = iddata(Out6_7,Cv6_7,0.1);
d4_7 = iddata(Out4_7,Cv4_7,0.1);
% Open System Identification Toolbox
systemIdentification
% Identify individual transfer function parameters
a = getpvec(tf100_60);
b = getpvec(tf100_40);
c = getpvec(tf97_60);
d = getpvec(tf97_40);
e = getpvec(tf70_60);
f = getpvec(tf70_40);
% Determine uncertainty within each transfer function parameter
[pvec,a_pvec] = getpvec(tf100_60);
[pvec,b_pvec] = getpvec(tf100_40);
[pvec,c_pvec] = getpvec(tf97_60);
[pvec,d_pvec] = getpvec(tf97_40);
[pvec,e_pvec] = getpvec(tf70_60);
```

```
[pvec,f_pvec] = getpvec(tf70_40);
% Categorise each plant with uncertainty and associate with a global variable
am = [a(1)+a_pvec(1);a(2)+a_pvec(2);a(3)+a_pvec(3);a(4)+a_pvec(4)];
aM = [a(1)-a_pvec(1);a(2)-a_pvec(2);a(3)-a_pvec(3);a(4)-a_pvec(4)];
bm = [b(1)+b_pvec(1);b(2)+b_pvec(2);b(3)+b_pvec(3);b(4)+b_pvec(4)];
bM = [b(1)-b_pvec(1);b(2)-b_pvec(2);b(3)-b_pvec(3);b(4)-b_pvec(4)];
cm = [c(1)+c_pvec(1);c(2)+a_pvec(2);c(3)+c_pvec(3);c(4)+c_pvec(4)];
cM = [c(1)-c_pvec(1);c(2)-c_pvec(2);c(3)-c_pvec(3);c(4)-c_pvec(4)];
dm = [d(1)+d_pvec(1);d(2)+d_pvec(2);d(3)+d_pvec(3);d(4)+d_pvec(4)];
dM = [d(1)-d_pvec(1);d(2)-d_pvec(2);d(3)-d_pvec(3);d(4)-d_pvec(4)];
em = [e(1)+e_pvec(1);e(2)+e_pvec(2);e(3)+e_pvec(3);e(4)+e_pvec(4)];
eM = [e(1)-e_pvec(1);e(2)-e_pvec(2);e(3)-e_pvec(3);e(4)-e_pvec(4)];
fm = [f(1)+f_pvec(1);f(2)+f_pvec(2);f(3)+f_pvec(3);f(4)+f_pvec(4)];
```

ATT3 VLV template

```
global am  bm  cm dm em fm; % Define global variables

disp('Computing plant templates ....')
drawnow

% Define plant transfer functions with uncertainty
P(1,1,1) = tf([am(1),am(2)], [1,am(3),am(4)]);
P(1,1,2) = tf([aM(1),aM(2)], [1,aM(3),aM(4)]);
P(1,1,3) = tf([bm(1),bm(2)], [1,bm(3),bm(4)]);
P(1,1,4) = tf([bM(1),bM(2)], [1,bM(3),bM(4)]);
P(1,1,5) = tf([cm(1),cm(2)], [1,cm(3),cm(4)]);
P(1,1,6) = tf([cM(1),cM(2)], [1,cM(3),cM(4)]);
P(1,1,7) = tf([dm(1),dm(2)], [1,dm(3),dm(4)]);
P(1,1,8) = tf([dM(1),dM(2)], [1,dM(3),dM(4)]);
P(1,1,9) = tf([em(1),em(2)], [1,em(3),em(4)]);
P(1,1,10) = tf([eM(1),eM(2)], [1,eM(3),eM(4)]);
P(1,1,11) = tf([fm(1),fm(2)], [1,fm(3),fm(4)]);
P(1,1,12) = tf([fM(1),fM(2)], [1,fM(3),fM(4)]);


nompt = 5;                                          % define nominal plant case

w = [0.001,0.01,0.02,0.03,0.04,0.06,0.08,0.1];  % working frequencies

disp(' ')
disp('plottmpl(w,P,nompt); %show templates')
drawnow
plottmpl(w,P,nompt), title('Plant Templates')    % plot template

%BOUNDS
disp(' ')
disp('Computing bounds...')
disp(' ')
disp('bdb1=sisobnds(1,w,W1,P,R,nompt); %margins')
drawnow
ws = 10.^([-20,6,6,6,6,6,6,6]/20);              % Define design specifications
R = 0;
```

```
bnd=sisobnds(2,w,ws,P,R,nompt); % Calculate the nominal bounds from the specs
disp('plotbnds(bdb1); %show bounds')
drawnow
plotbnds(bnd)                                   % Plot bounds

lpshape(w,bnd,P(1,1,5))                         % Perform design
grid
```